FACULTY OF CHEMISTRY
DEPARTMENT OF CHEMICAL ORGANIC TECHNOLOGY AND PETROCHEMISTRY

Doctoral dissertation

Bartłomiej Gaida

Bio-derived ionic liquids as precursors for sustainable functional materials

Ciecze jonowe pochodzenia naturalnego jako prekursory zrównoważonych materiałów funkcjonalnych

Supervisor: Prof Anna Chrobok

Auxiliary supervisor: PhD Alina Brzęczek-Szafran

Gliwice 2024

Acknowledgements

I would like to sincerely thank the supervisors of this work, ***Dr Alina Brzęczek-Szafran*** *and* ***Prof Anna Chrobok****, for their time, substantive care, knowledge, enormous development opportunities, faith in me, kindness, understanding and patience, without which this work would not have been created.*

I would like to thank my co-workers with all my heart, particularly ***Dr Karol Erfurt*** *and* ***Magdalena Gwóźdź****, but also* ***Dr Agnieszka Siewniak****,* ***Dr Piotr Latos****,* ***Dr Natalia Barteczko****,* ***Dr Monika Olesiejuk****,* ***Dr Anna Szelwicka****,* ***Dr Anna Maj****,* ***Justyna Więcławik****,* ***Anna Wolny****,* ***Angelika Mieszczanin,*** ***Dawid Janasik****,* ***Marcin Łuczyński*** *and* ***Lema Shumi****, for their support, help with everyday problems and, last but not least, for a friendly atmosphere at work.*

I would like to thank ***Dr Karolina Matuszek****, and* ***Prof Douglas R. MacFarlane*** *from Monash University in Australia for scientific cooperation, enabling me to complete my internship and positive contribution to my research.*

Finally, I would like to thank my brother ***Radosław Gaida****, for healthy competition in gaining chemical knowledge, my* ***Parents****,* ***Family****, my beloved* ***Ewelina Sobecko*** *and numerous* ***Friends****, notably* ***Marcin Górny****,* ***Maciej Olesiejuk****,* ***Marcin Pytlik****,* ***Patryk Janasik****,* ***Leszek Maj*** *and* ***Szymon Korusiewicz****, for motivation to work, help and support.*

I dedicate this work to my ***Grandma****, for her unsurpassed example of kindness, for her big heart and for following my achievements with incredible perseverance and interest.*

Podziękowania

Pragnę serdecznie podziękować promotorkom niniejszej pracy, ***Pani dr inż. Alinie Brzęczek-Szafran*** *oraz* ***Pani prof. dr hab. inż. Annie Chrobok****, za poświęcony czas, opiekę merytoryczną, przekazaną wiedzę, ogromne możliwości rozwoju, wiarę we mnie, życzliwość, wyrozumiałość i cierpliwość, bez których praca ta by nie powstała.*

Dziękuję z całego serca współpracownikom, w szczególności ***dr inż. Karolowi Erfurtowi*** *i* ***mgr inż. Magdalenie Gwóźdź****, ale także* ***dr inż. Agnieszce Siewniak****,* ***dr inż. Piotrowi Latosowi****,* ***dr inż. Natalii Barteczko****,* ***dr inż. Monice Olesiejuk****,* ***dr inż. Annie Szelwickiej****,* ***dr inż. Annie Maj****,* ***mgr inż. Justynie Więcławik****,* ***mgr inż. Annie Wolny****,* ***mgr Angelice Mieszczanin****,* ***mgr inż. Dawidowi Janasikowi****,* ***mgr inż. Marcinowi Łuczyńskiemu*** *oraz* ***mgr Lemie Deme****, za wsparcie, pomoc w codziennych problemach i co niemniej ważne przyjazną atmosferę w pracy.*

Chciałbym podziękować ***dr inż. Karolinie Matuszek*** *oraz* ***prof. dr Douglasowi R. MacFalaneowi*** *z Monash University w Australii, za współpracę naukową, umożliwienie odbycia stażu oraz pozytywny wkład w moje badania.*

Na koniec chciałbym podziękować bratu ***Radosławowi Gaidzie****, za zdrową rywalizację w zdobywaniu wiedzy chemicznej,* ***Rodzicom****,* ***Rodzinie****, ukochanej* ***Ewelinie Sobecko*** *oraz moim licznym* ***Przyjaciołom****, a zwłaszcza* ***Marcinowi Górnemu****,* ***Maciejowi Olesiejukowi****,* ***Marcinowi Pytlikowi****,* ***Patrykowi Janasikowi****,* ***Leszkowi Majowi*** *i* ***Szymonowi Korusiewiczowi****, za motywację do pracy, pomoc i wsparcie.*

Pracę tę dedykuję ***Babci****, za niedoścignionego przykład dobroci, za wielkie serce oraz śledzenie moich osiągnięć z niebywałą wytrwałością i zainteresowaniem.*

Table of Contents

1. List of abbreviations

AAILs – amino acid-based ionic liquids

bio-ILs – biomass-derived ionic liquids

CALB – Candida antarctica lipase B

ChILs – cholinium-based ionic liquids

CMC – critical micelle concentration

CV – cyclic voltammetry

DABCO – 1,4-diazobicyclo[2.2.2]octane

DESs – deep eutectic solvents

DSC – differential scanning calorimetry

EA – ethyl acetate / elemental analysis

HILs – herbicidal ionic liquids

ILs – ionic liquids

LCCs – liquid coordination complexes

LSV – linear sweep voltammetry

Man – D-mannitol

MeOH - methanol

MG – methyl α-D-glucopyranoside

MWCNTs – multi-walled carbon nanotubes

ORR – oxygen reaction reduction

PCMs – phase change materials

PE – petroleum ether

PEGDA – poly(ethyleneglycol) diacrylate

PILs – protic ionic liquids / polymeric ionic liquids

PTCs – phase transfer catalysts

RRDE – rotating ring-disc electrode

SWCNTs – single-walled carbon nanotubes

T_c – crystallization temperature

T_d – decomposition temperature

TES – thermal energy storage

T_g – glass transition temperature

TGA – thermogravimetric analysis

T_m – melting point

TSILs – task-specific ionic liquids

VOCs – volatile organic solvents

XRD – X-ray diffraction

ZIFs – zeolitic imidazolate frameworks

ΔH_c – crystallization enthalpy

ΔH_f – fusion enthalpy / melting enthalpy

2. Introduction and the research goal

The primary goal of this doctoral thesis was to explore the synthesis, properties, and applications of ionic liquids derived from renewable raw materials, specifically sugars and their derivatives. Sugars are an inexpensive and readily available resource, rich in hydroxyl functional groups, which dictates their distinctive properties, such as high solubility in polar solvents, chirality, structural diversity, biodegradability and biocompatibility. The transformation of sugars and their derivatives into ionic compounds yields materials which combine the properties of both sugars and ionic liquids. Such transformations can lead to compounds with unique task-specific characteristics, even though they often involve complex and multi-stage procedures.

Low-melting ionic compounds were described for the first time in the early 19th century and have developed significantly since then. Initially, they emerged as an alternative to toxic volatile organic solvents (VOCs) used in synthesis, due to their unique properties, such as low vapor pressure, high thermal and chemical stability, and persistence in the liquid phase over a wide temperature range. However, at the beginning of the 21st century, there were justified concerns about the ecotoxicity and bioaccumulation potential of ionic liquids. Therefore, there has been great interest in the development of biomass-derived ionic liquids with low environmental impact. Ionic liquids obtained from natural raw materials often have much higher biocompatibility and lower toxicity than their fossil fuel-derived counterparts, as well as present significant biodegradability. Apart from the bio-derived origin of the precursors, their transformation into the desired product in accordance with the principles of "green chemistry" is recently highly desired.

Carbohydrates, with their abundance, low cost, chirality, and biorenewable character, are one of the most promising raw materials. While the well-established

knowledge of sugar chemistry supports these efforts, carbohydrates transformation into ionic liquids can be challenging in terms of number of synthetic steps and purification procedures. Therefore, recent efforts have focused on the development of simple and economical procedures. The research described within this doctoral thesis was divided into three main chapters:

- Carbohydrate-based ionic liquids as phase change materials
- Carbohydrate-based ionic liquids as precursors for *N*-doped carbon materials
- Carbohydrate-based ionic liquids as surface active agents.

The work in particular includes the following research:

- Research on the synthesis of salts and ionic liquids based D-glucose modified at the terminal position
- Research on the synthesis of salts and ionic liquids based on D-glucose modified at the anomeric position
- Research on the synthesis of salts and ionic liquids based on D-mannitol modified at the α and ω positions (1 and 6)
- Analysis of the physical properties of the obtained ionic compounds
- Comparison of the properties of analogous salts and ionic liquids with protected and deprotected hydroxyl groups
- Research on the application of the obtained ionic compounds as phase change materials, precursors of *N*-doped carbon materials and surface active agents

3. Literature review

3.1. History and definition of ionic liquids

Liquids composed entirely of ions possess unique properties, which distinguishes them from molecular liquids. Liquid salts offer ability to dissolve substances, which are insoluble in conventional solvents, liquid state in a wide temperature range, low vapor pressure, nonflammability, ionic conductivity and tunability resulting from enormous possible cation/anion combinations as well as high chemical and thermal stability.[1]

At the end of 19th century, studies on low-melting salts sporadically appeared in the literature[2], but the breakthrough was the preparation of ethylammonium nitrate described by Paul Walden in 1914.[3] Therefore, liquid salts have a history spanning over a century, but due the pioneering work of Angell and others in the 1960s covering the electrochemical studies of chloroaluminate species, they began to emerge from the realm of scientific curiosity.[4–6] The era of the compounds known these days as ionic liquids (ILs) originated in the 1970s establishing so-called first generation of ILs. First generation ILs, is a of group of air and moisture sensitive materials, which includes e.g. dialkylimidazolium and alkylpyridinium chloroaluminates.[7,8]

The second generation of ILs was introduced at the beginning of the 1990s in response to the need for compounds with tunable and targeted physical and chemical characteristics. Wilkes and Zaworotko[9], simultaneously with Cooper and O'Sullivan[10], reported the first room temperature air and water stable ILs. These were obtained by introducing specific anions, such as nitrate ($[NO_3]^-$), nitrite ($[NO_2]^-$), tetrafluoroborate ($[BF_4]^-$), sulfate ($[SO_4]^-$), acetate ($[CH_3COO]^-$), triflate ($[OTf]^-$) and mesylate ($[OMs]^-$) to well-known dialkylimidazolium and alkylpyridinium cations. This development

enabled the creation of new functional materials with the flexibility to independently modify the properties of both the cation and the anion while preserving the core attributes of an IL. Owing to their interesting properties, ILs were recognized as ideal solvents and media for use in electrochemistry, organic chemistry and catalysis, with a special focus on green chemistry.[11–14]

At the beginning of the 21st century, IL research broadened its scope to encompass the toxicological, chemical, and biological aspects of ionic compounds, moving beyond a sole focus on their physical properties. Consequently, the third generation of ILs emerged, resulting in task-specific ionic liquids (TSILs).[15] TSILs allowed the design of compounds with targeted biological properties, paving the way for ILs with antimicrobial, anti-inflammatory or anesthetic activity, using biologically active ions.[16] This innovation has improved the applications of ILs in fields of biomedicine and pharmaceuticals. An example of third generation ILs is the combination of the lidocaine cation, which has anesthetic properties, and the ibuprofenate anion with anti-inflammatory properties.

According to the established definition, ILs are salts composed of organic cation and inorganic or organic anion, which melt below 100 °C.[1] The significant potential of those liquids, along with the restrictive definition limiting melting points to below 100 °C, probably directed research away from higher melting point materials within these families of salts, which melt above 100 °C.[17] Therefore, the melting temperature limit is recently considered unnecessary, as other ionic compounds melting above 100 °C exhibit analogous properties. The fourth generation of ionic liquids was described by MacFarlane *et al.*[18] These materials can contain both ionic and neutral components and often possess properties similar to conventional ILs. The fourth generation includes deep eutectic solvents (DESs)[19,20], liquid coordination complexes (LCCs)[21–24], solvate ionic liquids[25–28] or concentrated salt-water systems[29]. These systems have unique

characteristics, often different from what is expected, and go beyond the standard definition of an IL, broadening application possibilities.

3.2. Structure and classification of ionic liquids

The term ionic liquids has permanently replaced the previously used name "molten salts", which also includes high-melting inorganic salts such as sodium chloride, that melts at 801 °C.[30] Many ionic liquids exist in a liquid state already at room temperature, originating from the presence of bulky organic cations in their structures, often with a low symmetry. This results in larger distances between the ions and a lower degree of crystal lattice order, which translates directly into weaker coulombic interactions and lower melting temperatures compared to traditional inorganic salts.[13,31,32]

A widely adopted method for classifying ILs involves examining the structure of the cation and anion. Taking into account the structure of the cation, or rather the atom at which the positive charge is located, ammonium, sulfonium, oxonium and phosphonium ILs, can be distinguished.[13] In the case of ammonium salts, an additional division due to the hybridization of the nitrogen atom can be considered.[12,33] There are ILs with sp^3 hybridization, where the molecule has a tetrahedral shape, such as in tetraalkylammonium, piperidinium, pyrrolidinium or morpholinium salts. On the other hand, there are ILs with sp^2 hybridization, where the molecule around the nitrogen atom is flat and the cation is aromatic, such as in: imidazolium, triazolium, pyridinium and quinoline salts.

Looking at the structure of an anion, differentiation between organic and inorganic anions is possible. Inorganic anions can be divided into simple and complex. Examples of simple anions are halides (Cl^-, Br^-, F^-, I^-), nitrates ($[NO_3]^-$, $[NO_2]^-$) and sulfates ($[SO_4]^{2-}$,

[HSO_4]$^-$). Complex anions include single-core anions: tetrafluoroborate ([BF_4]$^-$), hexafluorophosphate ([PF_6]$^-$) or multi-core anions, mainly chloroaluminate ([Al_2Cl_7]$^-$, [Al_3Cl_{10}]$^-$). In turn, among the organic anions, the most popular are formates, acetates, fluoroacetates, lactates, saccharinates and salicylates. Frequently used organic anions also include bis(trifluoromethylsulfonyl)imide anion ([NTf_2]$^-$), trifluoromethanesulfonic acid anion ([OTf]$^-$) and dicyanamide anion ([$N(CN)_2$]$^-$).[32,34–37]

Other criteria for the division of ILs consider more detailed differences in the structure. For example, ILs in which a hydrogen atom is attached to a positively charged atom in a cation are called protic ionic liquids (PILs). When the central atom with a positive charge is not connected to any hydrogen atom, such ILs are called aprotic ionic liquids (AILs).[38–40]

In addition to ILs with single charged cations, systems with several charged atoms can be designed. Dicationic ILs, tricationic ILs and polycationic ILs, such as polymeric ionic liquids (PILs) have been reported.[41–43] To obtain (PILs), ionic monomers are used, i.e. ILs having active centers in the form of reactive chemical groups or unsaturated bonds capable of polymerization. The most popular are those with vinylpyridinium and vinylimidazolium cations.[44]

3.3. Bio-derived ionic liquids

The initial enthusiasm for ILs experienced a downturn as considerations shifted toward the economic and environmental implications tied to their production and usage. Due to the high chemical stability and often notable solubility in water, concerns emerged regarding possible release of ILs into the environment, where they could persist and accumulate over an extended period.[45] Despite these challenges, recent years have

witnessed substantial advancements in IL research, and ongoing efforts to expand their applications underscore their evident industrial potential. Several processes, exemplified by technologies such as BASIL™, HycaPure™ Hg, SILP catalyzed hydroformylation or ISOALKY™ use ILs successfully.[46] Furthermore, economies of scale have contributed to price reduction for certain ILs, coupled with notable improvements in their ecotoxicology and biodegradability.[47] The latter one was significantly contributed by the progress in the development of biomass-derived ILs (bio-ILs), originating from naturally occurring compounds such as amino acids, carbohydrates, carboxylic acids, or choline.[48] These bio-ILs exhibit lower toxicity and enhanced biocompatibility compared to their fossil fuel-derived counterparts, as comprehensively reviewed by Gomes *et al*.[49] and Hulsbosch *et al*.[50].

3.4. Carbohydrate-based ionic liquids

Since 2003, when Handy *et al*.[51] first introduced the synthesis of an imidazolium IL using fructose as a precursor, the family of carbohydrate-derived ILs has expanded significantly. Although the final IL reported by Handy did not contain the carbohydrate moiety in its structure, this transformation marked the first use of sugar as a renewable starting material for IL preparation. One year later, the first carbohydrate-derived IL was synthesized, transforming D-glucopyranoside into the corresponding cation.[52] Thereafter, a wide range of ILs based on carbohydrates and their derivatives have been developed, including glucose[53–60], galactose[61–63], fructose[51], ribose[61], xylose[62,64], arabinose[65], isomannide[66–68], glucosamine[69,70], isosorbide[71,72], ribitol[73], and mannitol[54]. The synthesis and applications of carbohydrate-derived ILs have been comprehensively reviewed by the author of this thesis in collaboration with his supervisor[48] and other groups (Chiappe *et al*.[74], Kaur and Chopra[75], Jopp[76], Reddy *et al*.[77] and Zullo *et al*.[78]). In the next

chapter, the most common synthetic pathways for obtaining sugar-based ILs will be briefly presented.

3.5. Synthetic methods for preparing carbohydrate-based ionic liquids

Carbohydrates can be converted into cations or anions using standard reactions commonly employed in carbohydrate chemistry. However, most of the research on sugar-based ILs has focused on transformation of carbohydrates into cations. The most promising synthetic route in terms of the number of required steps involves using carbohydrate-derived anions such as gluconate, glucuronate, or galacturonate.[79–82]

The synthesis of ILs in which the parent carbohydrate structure was retained in the cation will be discussed first, starting from cyclic precursors and then linear ones. The transformation of carbohydrate into an anionic moiety will be presented later, following the same order.

Cyclic carbohydrates are usually modified at either terminal or anomeric position, because of the high reactivity of hydroxyl groups in these positions and well-established synthetic procedures. For modification at the terminal position, unprotected carbohydrates can be used as well as carbohydrates in the form of a glucoside. Such intermediates are prone to nucleophilic substitution at the terminal position (–OH is substituted by a good leaving group e.g. –Br, –I, –OTf), followed by quaternization with aliphatic or aromatic tertiary amines[79,83], such as *N*-alkyl- or *N*-aryl-imidazole[58–61,84], pyridine[85] or 1,4-diazobicyclo[2.2.2]octane (DABCO)[63], to produce ionic compounds. Some synthetic strategies require protection of the hydroxyl groups by etherification or acetylation to facilitate later purification, wherein alteration of the polarity of the carbohydrate moiety is desired. The physiochemical properties of the as-prepared ILs and salts can be further tuned via anion exchange.

Jayachandra *et al*.[61] used D-galactose as a starting material to synthesize a series of carbohydrate ILs with various anions (**Figure 1**). The authors protected the secondary hydroxyl groups of D-galactose with acetone in the presence of $ZnCl_2$ and H_2SO_4, while the remaining primary –OH group was substituted with iodide. After purification *via* column chromatography, the isolated derivative was quaternized with *N*-methylimidazole. Various lithium and sodium salts have been used for anion metathesis, resulting in ILs with $[BF_4]^-$, $[PF_6]^-$, $[OTf]^-$, or $[NTf_2]^-$ anions. A similar procedure was applied to produce analogous ILs from D-ribose.

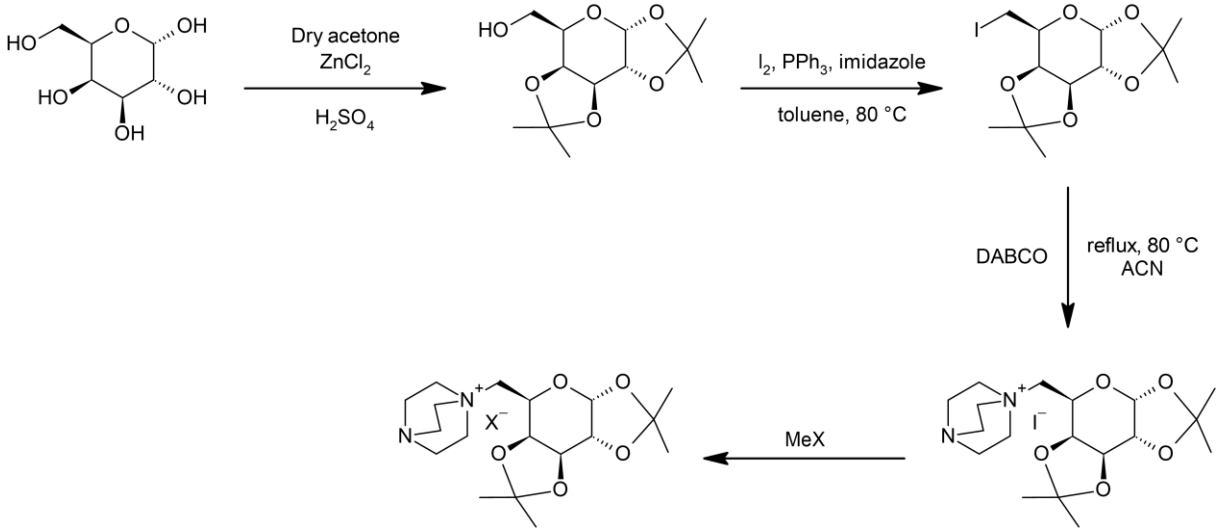

Figure 1. Synthesis of carbohydrate-based ionic liquids (ILs) via modification of D-galactose at terminal position. Adapted from [48].

Kaur *et al*.[63] applied the same procedure to modify D-galactose where they replaced *N*-methylimidazole with DABCO in the quaternization step. After anion metathesis, a series of ILs was produced containing $[BF_4]^-$, $[PF_6]^-$, $[BrCH_2CH_2SO_3]^-$, $[OTf]^-$, or $[SbF_6]^-$ anions. The overall yield for this four-step synthesis was 32–35%, with individual step yields ranging from 65% to 82%. Our group also synthesized ILs following this procedure using methyl-α-D-glucopyranoside as the starting material, omitting the protection step,

which increased overall ILs yields to 44–65% and allowed to retain the hydrogen-bond-rich structure.[79,83]

Jopp *et al*.[58] developed even more effective procedure, in which the terminal –OH group was substituted with iodide and quaternized with *N*-methylimidazole, producing iodide salt in two steps with the overall yield of 92%. Furthermore, the authors exchanged the I^- anion with the $[OH]^-$ anion using Amberlite IRN-78 ion exchange resin, to produce ILs *via* a simple acid-base reaction using D-glucuronic acid, L-arginine, *trans*-cinnamic acid and caprylic acid for the neutralization. It is worth noting that the IL obtained in the reaction with D-glucuronic acid contained a carbohydrate moiety in both the cation and the anion. A year later a series of analogous ILs quaternized with *N*-ethyl-, butyl- or octyl-imidazole was obtained.[59] This time the metathesis reaction was performed to exchange I^- anion to $[BF_4]^-$, $[OAc]^-$, $[OMs]^-$, $[OTf]^-$ and $[NTf_2]^-$. This work was further developed and ILs with different *N*-substituted imidazoles were obtained (including vinyl, phenyl, benzyl and mesityl). In addition octyl- and phenyl-β-D-glucopyranosides were used as starting materials.[60] Finally, the same group used *N*-vinyl imidazole derivative (1-(methyl-*α*-D-glucopyranosid-6-yl)-3-vinylimidazolium iodide) as a monomer to produce ionic hydrogels via radical polymerization with poly(ethyleneglycol) diacrylate (PEGDA) as a cross-linker.[84]

Reiß *et al*.[85] investigated various functionalization possibilities in ILs derived from pentoses (D-ribose, D-lyxose, D-xylose, D-arabinose) and hexoses (D-glucopyranose). Typically, the pentoses were peracetylated, followed by substitution of a thiophenyl group at the anomeric center. This site was then further reduced using tributyltin hydride to yield the corresponding 1-deoxypentose. In the next step, the acetyl groups were deprotected, and the primary –OH group was tritylated to facilitate the transformation of the remaining secondary hydroxyl groups into methyl, ethyl, propyl, or allyl ethers. Finally, the unprotected –OH group at C5 was converted

into a triflate moiety and quaternized with pyridine. Similarly, methyl, allyl, and phenyl β-D-glucosides were employed in a similar synthetic procedure, although acetylation and reduction at the anomeric positions were omitted. The overall yields for pentose-based ILs were 25–32% over eight steps, while hexose-based ILs were synthesized with the yield of 31–56% in five steps.

A second approach focuses on modifying the carbohydrate unit at the anomeric position (**Figure 2**). The Chrobok group has applied this method to study the glycosylation of D-glucopyranose with halogenoalcohols (such as bromoethanol, chloroethanol, 3-chloropropanol, or 3-chloro-1,2-propanediol), yielding glycosides with 50% to 78% yield after purification by column chromatography.[56,79,86–89] The glycosides were further quaternized with amines to produce halide salts, which were applied as task-specific ILs after metathesis with specific anions, such as bis(trifluoromethanesulfonyl)imide ($[NTf_2]^-$)[56,79], 4-chloro-2-methylphenoxyacetate ($[MCPA]^-$), 2,4-dichlorophenoxyacetate ($[2,4\text{-}D]^-$)[86], dicyanamide ($[N(CN)_2]^-$)[79], or amino acid anions[87]. Furthermore, triazoles were synthesized by glycosylation of D-xylose with propargyl alcohol, followed by a click reaction and subsequent *N*-alkylation.[90] Another synthetic pathway involved selective bromination at the anomeric position with HBr, allowing the resulting halide to be further converted into azide[91] or quaternized[57].

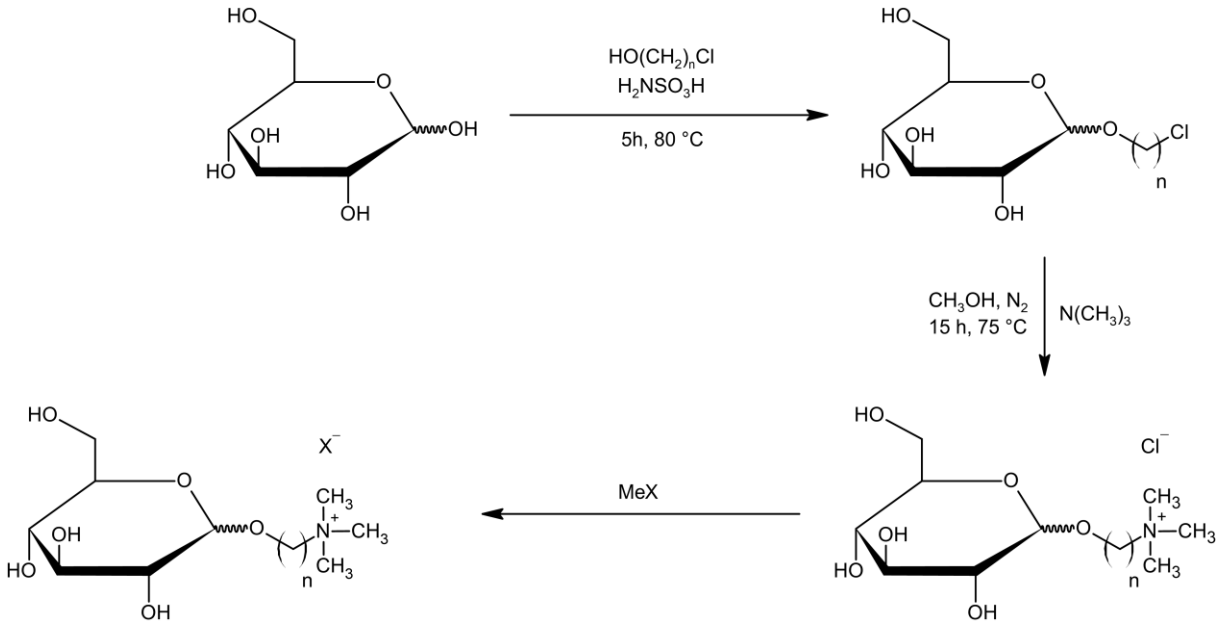

Figure 2. Synthesis of ILs with carbohydrate-based cation via modification of D-glucose at anomeric position. Adapted from [48].

Another example of cyclic glucose derivatization into a cation was developed by Jopp *et al.*[69,70], who synthesized ILs from glucosamine, which is obtained *via* depolymerization of chitin and chitosan. Glucosamine is a good building block for the sugar-derived ILs, as the N atom is already attached to the precursor at the C2 position and thus the quaternization can be performed with alkylating agents. First, the group synthesized methyl-2-dimethylamino-β-D-glucopyranoside in a three-step procedure from glucosamine, which was then quaternized with methyl iodide or methyl triflate, producing salts with overall yields ranging from 37 to 44%. The salt with iodide anion was further used in the metathesis reaction to give a series of ionic compounds bearing $[BF_4]^-$, $[PF_6]^-$, $[OMs]^-$, $[CF_3COO]^-$, $[N(CN)_2]^-$, $[N(FSO_2)_2]^-$, and $[NTf_2]^-$ anions.

Billeci *et al.*[92,93] pioneered preparation of ILs using glucono-δ-lactone as a precursor (**Figure 3**). A linear gluconamide derivative was formed by the reaction of glucono-δ-lactone with either *N*,*N*-dimethylethylenediamine or *N*,*N*-dimethylpropylenediamine. The significant advancement of this method is the simplified purification protocol, which

omits column chromatography in favor of washing the product with an ethanol/ethyl acetate mixture, resulting in a 93% yield. The final ILs were obtained after quaternization of the corresponding amines with various alkyl halides such as 1-bromo/1-iodobutane, 1-bromooctane, 1-bromododecane, or 1-bromo-2-ethylhexane, with reported yields ranging from 83% to 97%. Anion metathesis was performed if applicable. These synthetic protocols for carbohydrate-based ILs adhere to the Principles of Green Chemistry[94], with atom economies of 100% in most cases and mass efficiencies/optimum efficiencies ranging from 69% to 96%.

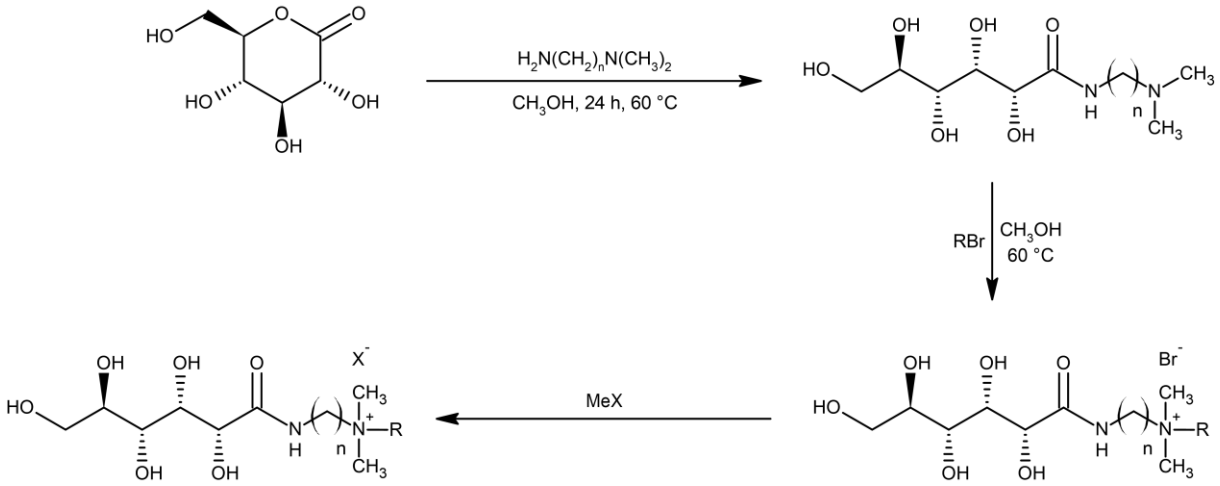

Figure 3. Synthesis of ILs with carbohydrate-based cation via modification of glucono-δ-lactone. Adapted from [48].

In the following section possible transformations of carbohydrates and their derivatives into anionic moieties are presented.

In 2017 Gatard *et al.*[95] demonstrated a conversion of cyclic sugars (e.g. D-xylose) into anions (**Figure 4**). The synthetic procedure involved the peracetylation of D-xylose, followed by the reaction with the corresponding ester (ethyl glycolate, methyl 6-hydroxyhexanoate or methyl 4-(hydroxymethyl)benzoate in the presence of $BF_3 \cdot Et_2O$. The resulting compounds were then deacetylated and neutralized

with tetrabutylammonium, tetrahexylammonium, or tetrabutylphosphonium hydroxide, producing the corresponding ILs. This method provides flexibility in tuning the physiochemical properties through possible modifications of the carbohydrate unit, similar to the procedures that convert sugars into cations.

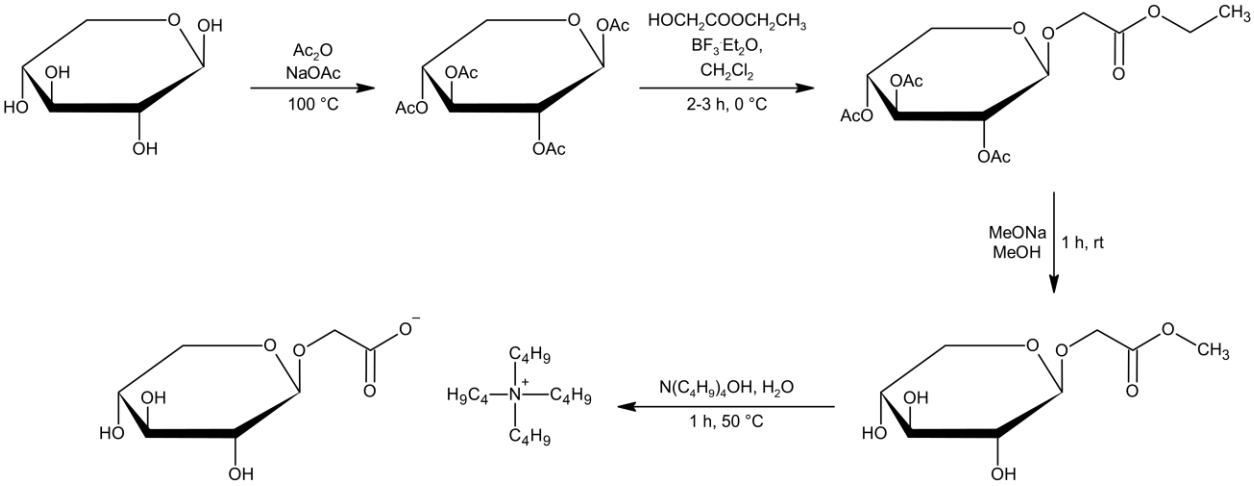

Figure 4. Synthesis of ILs with carbohydrate-based anion via modification of D-xylose at the anomeric position. Adapted from [48].

The last strategy described here is the most promising in terms of the number of synthetic steps (**Figure 5**). However, this simple synthetic procedure is limited to sugar acids. It requires formation of the hydroxide of the desired cation using an ion exchange resin. Hydroxides utilized in carbohydrate-derived IL syntheses so far were prepared from *N,N,N′,N′*-tetramethylguanidine, tetraalkylammonium, tetraalkylphosphonium, or alkylimidazolium halides[79–81,96], which were further neutralized with commercially available linear or cyclic sugar acids (e.g., gluconic, glucuronic, or galacturonic acid). The synthesis of ILs with carbohydrate anions has a similar complexity to the preparation of extensively applied cholinium-based ILs (that is, 2 steps: ion exchange, followed by neutralization), yet it has been explored to a much lesser extent.[97–100]

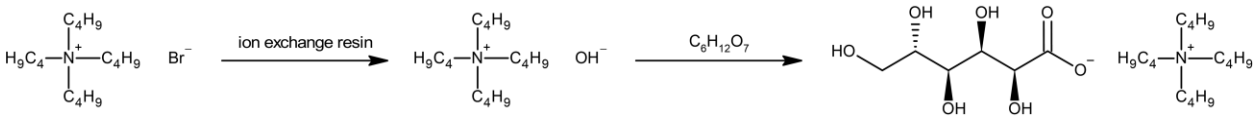

Figure 5. Synthesis of ILs with carbohydrate-based anion. Adapted from [48].

3.6. Characterization and properties of carbohydrate-based ionic liquids

The structure of carbohydrate-derived IL or salt significantly affects its potential environmental effect and physiochemical properties. These attributes result from (i) the presence of carbohydrate moieties in cation, anion or both and/or (ii) functionalization which can involve the incorporation of alkyl chains of various lengths, alkyl spacers between carbohydrate moieties and quaternary ammonium groups, protected or free hydroxyl groups, or quaternization with different amines. Herein, more than 100 carbohydrate-derived ILs and salts were compared to provide a comprehensive overview of the structure–property relationships and discussed how specific motifs in the structure influence biodegradability, toxicity, and thermal properties. Importantly, such comparisons can guide the future design of sugar-rich systems for targeted applications. The structures of the discussed ILs are presented in **Figure 6**.

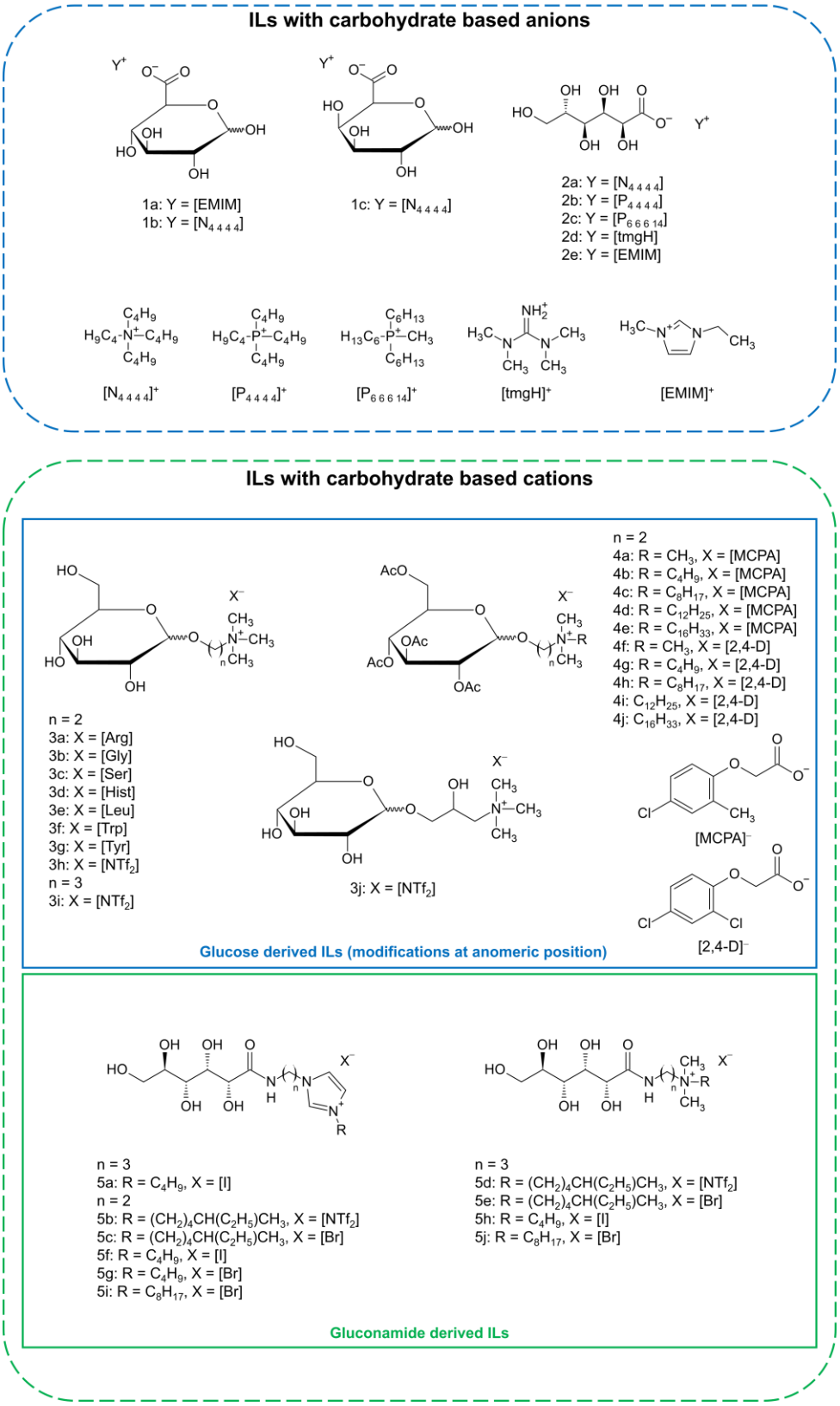

Figure 6. Structures of carbohydrate-derived ILs. Adapted from [48].

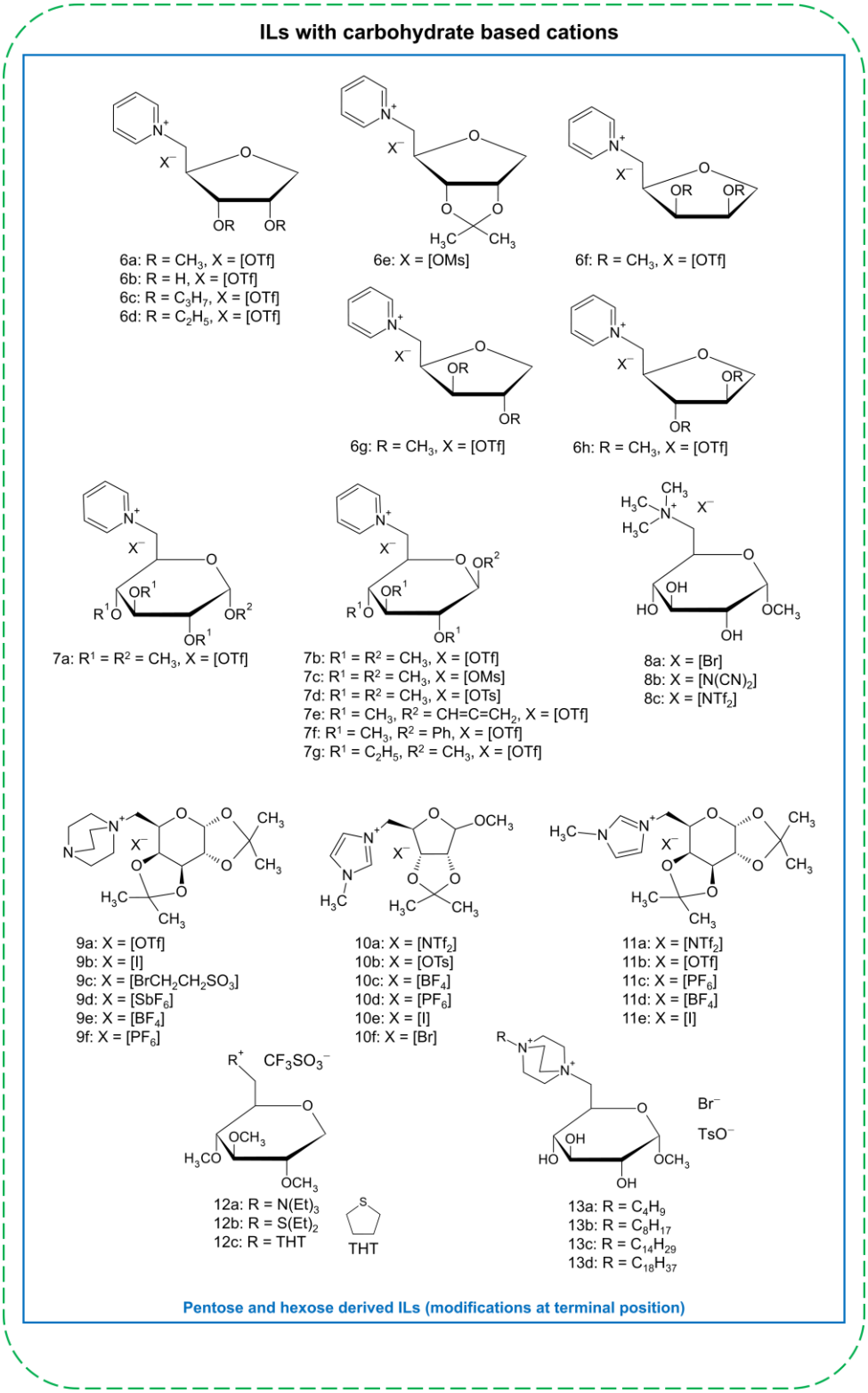

Figure 6. Structures of carbohydrate-derived ILs – continuation.

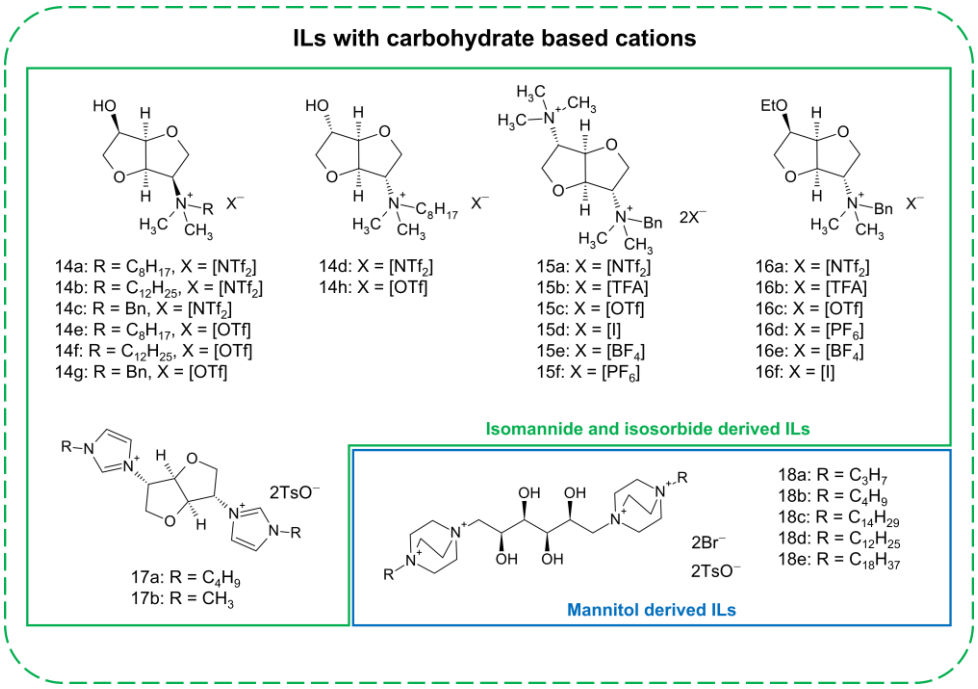

Figure 6. Structures of carbohydrate-derived ILs – continuation.

3.6.1. Biodegradation/toxicity

The major challenges currently faced in IL syntheses are related to the employment of "green" synthetic techniques and the reduction of the ecological impact of the products. Many ILs are water-soluble, raising concerns about their environmental effects in case of leakage or wastewater discharge, which could lead to water or soil pollution.[101,102] According to Earle *et al.*[103], some ILs can be distilled at low pressure , suggesting that atmospheric contamination cannot be completely ignored, particularly when ILs are used at elevated temperatures. Using natural and biorenewable building blocks (i.e., organic acids, amino acids, or choline) frequently leads to biodegradable ILs.[45,47] However, some of these compounds still resist complete biodegradation.[104] Additionally, as reviewed by Jordan and Gathergood[47], the biodegradability of the ILs is significantly influenced by their chemical structures. Unbranched alkyl chains containing ester, formyl,

carboxylic, or hydroxyl groups support biodegradation processes because they are readily hydrolyzed or oxidized.

Ionic liquids with sugar moieties as natural building blocks are rich in hydroxyl groups, which have been shown to enhance IL biodegradability, despite limited research in this area. Ferlin *et al*.[80], investigated a series of tetrabutylammonium ILs containing anions derived from natural organic acids, and demonstrated that ILs derived from D-glucuronic (**1b**) and D-galacturonic (**1c**) acids show higher biodegradability than analogous ILs derived from L-lactic, L-tartaric, malonic, succinic, L-malonic, and pyruvic acids. Furthermore, all bio-derived ILs investigated exhibited higher biodegradability in the Closed Bottle test (OECD 301D) in comparison to common tetrabutylammonium bromide salt and tetrabutylammonium hydroxide. Nevertheless, the biodegradability of carbohydrate ILs is related to the length of the alkyl chain in the cation, if employed. In a series of quaternary ammonium salts based on D-glucose cation, that include alkyl chains of different length (–CH_3, –$C_{12}H_{25}$, –$C_{16}H_{33}$, **4a**, **4b**, **4c**, respectively), the derivative with the shortest alkyl chain (**4a**) was found to be readily biodegradable (74–83%), while **4b** with the –$C_{12}H_{25}$ nearly met the ready biodegradability criterion (60%), reaching 57%.[88] In contrast, ILs with the –$C_{16}H_{33}$ substituent (**4c**) showed a longer lag phase of 10 days before beginning to degrade, not reaching a plateau within the experiment duration.

Combining carbohydrates with other bio-derived molecules such as amino acids, has also produced readily biodegradable ILs (**3a–g**), capable of decomposing in activated sludge within 5–6 days.[87] This findings demonstrate the potential of carbohydrate-derived ILs as alternatives to the cholinium based ILs (ChILs), which are known for high biodegradability.[47] Despite cholinium amino acid-based ILs (AAILs) exhibit lower viscosity and can be easily prepared, a "green" synthetic pathway for obtaining sugar-derived ILs has also been reported recently.[92] Moreover, carbohydrates possess hydrogen bond-rich structures, making them advantageous for specific applications.

When evaluating the environmental impact of ILs, it is crucial to consider their toxicity and that of their metabolites on living organisms. ILs derived from naturally occurring compounds are expected to be less toxic, with ChILs standing out as particularly promising in this regard.[105–107] In addition to ChILs, carbohydrates have also attracted attention as starting materials for synthesizing non-toxic and biocompatible ILs. Carbohydrate-derived ILs typically exhibit very low (eco)toxicity towards bacteria, fungi[80], human cancer cells[93], mouse cells[85,108], rat cells[88], and zebrafish eggs[93], highlighting their high biocompatibility.

Among the examined tetrabutylammonium ILs combined with natural organic acids (D-glucuronic (**1b**), D-galacturonic (**1c**), L-lactic, L-tartaric, malonic, succinic, L-malic, and pyruvic acids), those derived from carbohydrates were found to be the least toxic.[80] Interestingly, functionalization of conventional imidazolium ILs with sugar moieties reduced their toxicity or even eliminated it.[93,108] Hong *et al*.[108] further confirmed the positive influence of carbohydrate units on decrease in toxicity by introducing sugar moieties into PILs. A polymer containing quaternary ammonium salts and pendent sugar units revealed a notable cytotoxic activity reduction against mouse fibroblast cells (L929) compared to traditional PILs.

However, Reiß *et al*.[85] observed that IL toxicity depends on concentration, investigating a series of pentose- (**6a–h**) and D-glucopyranose-based ILs (**7a–g**). At 0.1 M concentration, almost all of the investigated ILs showed no cell viability; however, at 10 mM concentration, some differences were observed. Specifically, among pentoses-derived ILs, those based on ribose were the least toxic. Additionally, glucose-derived ILs showed differences in toxicity between α- and β-anomers (**7a** and **7b**, respectively), with the α-anomer-based IL showing higher toxicity against mouse cells than the β-anomer-based IL.

IL cytotoxicity can be also affected by the length of the carbon chain. Erfurt et al.[88] examined glucose-based ILs modified at the anomeric position with various alkyl substituents (**4a–c**). Derivatives with the shortest alkyl chain (**4a**) showed the lowest cytotoxicity against rat leukemia cells, with no effect on cell viability up to 0.584 mM concentration. For derivatives **4b** and **4c,** the EC50 values were sufficiently lower: 0.085 for **4b** and 0.010 mM for **4c**, indicating an increase in cytotoxicity in the following order, **4a** < **4b** < **4c**. These results confirm that higher cytotoxicity corresponds to the higher hydrophobicity of the IL. Surprisingly, replacing the Br^- anion with the $[NTf_2]^-$ anion in **4c** had little impact on toxicity. Comparatively, dimethyl-phenyl-ammonium chloride showed similar trends in cytotoxicity relative to hydrophobicity. However, replacing the phenyl ring with hydrophilic D-glucose significantly reduced the cytotoxicity.[109]

Considering the influence of cations and anions on toxicity, ILs with cationic sugar moieties showed toxicity largely dependent on the anion. For D-glucopyranose-derived ILs (**7b–d**), replacing $[OTf]^-$ (**7b**) or $[OTs]^-$ (**7d**) anions with $[OMs]^-$ (**7c**) anions significantly reduced toxicity. Conversely, for ILs with carbohydrate moieties in the anion, the toxicity was primarily influenced by the cation. Gluconate ILs combined with phosphonium cations (**2b**,**2c**) were more toxic than their ammonium (**2a**) or guanidinium (**2d**) analogues. Moreover, in agreement with previous reports, increasing the length of alkyl chains in a tetraalkylphosphonium cation resulted in increased toxicity.[110,111]

These findings illustrate that modifying conventional ILs with carbohydrate motifs can reduce toxicity, highlighting the potential of using carbohydrate units to develop biodegradable, non-toxic ILs, highly desirable for applications in chemistry, biology, and ecology.[16]

3.6.2. Thermal stability and melting point

The thermal properties of various ILs and salts play a crucial role in determining their potential applications. ILs are frequently considered to be thermally stable because of their high decomposition temperatures (T_d). However, data on these properties are typically obtained through ramped-temperature thermogravimetric analysis (TGA), and as shown by Del Sesto *et al.*[112], this method can significantly overestimate stability, sometimes by hundreds of degrees, due to rapid temperature increase. The long-term stability of ILs can be more accurately assessed using isothermal TGA (static TGA) with measurements conducted over several hours. The T_d values obtained using this method are considerably lower than those from ramped-temperature TGA.[113] Nevertheless, such experiments have not yet been conducted for carbohydrate-derived ILs, but they would be valuable for understanding the potential caramelization of saccharides, which may also occur in sugar-based ILs.[114]

The thermal properties of carbohydrate ILs, such as the decomposition temperature (Td), the melting point (T_m), and the glass transition temperature (T_g), are influenced by various structural features. These include modifications to the cation, such as the length of the alkyl chain on the quaternary ammonium group or the alkyl spacer between the carbohydrate moiety and the quaternary ammonium group, as well as the presence of additional functional or protecting groups. The nature of both the cation and the anion also plays a significant role.

3.6.2.1. Anion

The type of anion in carbohydrate-derived ILs and salts as well as in their common imidazolium analogues corresponds to their nucleophilicity and basicity, significantly

affecting their thermal stability.[115] More nucleophilic and basic anions result in less stable ILs and salts. This trend is clear for glucose-derived salts investigated by our group, with Br^-, $[N(CN)_2]^-$, and $[NTf_2]^-$ anions (**8a**, **8b**, and **8c**, respectively), where their thermal stabilities increased in the order, **8c** > **8b** > **8a**, corresponding to decreasing anion nucleophilicity.[56,79]

This trend was also observed in the open chain gluconamide derivatives (**5b**, **5c**) investigated by Billeci et al.[93], where derivative **5b** with $[NTf_2]^-$ anion demonstrated higher thermal stability than **5c**, with Br^- anion. Interestingly, derivatives with longer alkyl spacers in their cations (**5d**, **5e**) exhibited the opposite trend. The typical trend was maintained for isosorbide (product of glucose hydrogenation to sorbitol, followed by dehydration) derivatives (**14a–d** and **14e–h**, with $[NTf_2]^-$ and $[OTf]^-$ anions, respectively) where the latter exhibited higher thermal stability.[72] In halide-based gluconamide derivatives (**5f** and **5g**, with I^- and Br^-, respectively), higher thermal stability was observed for the derivative with the I^- anion, along with the decreasing basicity of the halides ($F^- > Cl^- > Br^- > I^-$). However, some deviations from this trend may occur. For example, Kaur *et al*.[63] reported a series of chiral salts derived from D-galactopyranose and DABCO (**9a–f**), with T_d values between 180 °C and 250 °C, which increase in the following order, $[OTf]^- < I^- < [BrCH_2CH_2SO_3]^- < [SbF_6]^- < [BF_4]^- < [PF_6]^-$.

Interestingly, a series of amino acid/carbohydrate-based ILs (**3a–g**) studied in our group demonstrated the significant impact of the amino acid structure on T_d.[87] Among the anions investigated ($[Arg]^-$, $[Gly]^-$, $[Ser]^-$, $[His]^-$, $[Leu]^-$, $[Trp]^-$, and $[Tyr]^-$), the thermal stability of the salts increased with the elongation of the amino acid side chain, with the exception of $[Arg]^-$, which reduced the stability of **3a**.

Comparing the T_d values for derivatives where the carbohydrate moiety was transformed into an anion (e.g., cyclic glucuronate (**1b**) and open-chain gluconate (**2a**)), combined with a tetrabutylammonium cation, the latter exhibited higher thermal

stability (T_d = 136 °C and 162 °C, respectively). The derivative **2a** also showed a higher melting point and glass transition temperature than **1b**.[80,93] The same trend was observed for ILs with glucuronate and gluconate anions combined with $[EMIm]^+$ cations. Specifically, T_d for the derivative with the glucuronate anion (**1a**) was < 200 °C, while T_d for the gluconate anion derivative (**2e**) was > 250 °C.[79,81] This is likely due to the higher number of hydroxyl groups in the gluconate anion (five, compared to four in glucuronate) and the stronger H-bonding interactions.

The type of anion also affects the T_m of carbohydrate-derived ILs and salts. Kumar *et al*.[66] prepared a series of dicationic salts derived from isomannide (**15a–f**), where the T_m values ranged from 60 °C to 251 °C, increasing in the following anion order: $[NTf_2]^- < [TFA]^- < [OTf]^- < I^- < [BF_4]^- < [PF_6]^-$.

Certain carbohydrate salts with halide anions have exceptionally high T_m values, even higher than their analogues bearing $[BF_4]^-$ or $[PF_6]^-$ anions. In a series of chiral ammonium ILs and salts derived from isomannide (**16a–f**), the highest T_m value (170 °C) was observed for the derivative with the I^- anion (**16f**).[67] Derivatives with $[NTf_2]^-$ (**16a**) and $[TFA]^-$ (**16b**) anions were liquids at room temperature; however, changing the anion to $[OTf]^-$, $[PF_6]^-$, or $[BF_4]^-$ led to increases in their T_m values, to 80 °C, 95 °C, and 150 °C, respectively. This was also the case for D-ribose- (**10a–f**) and D-galactose-derived (**11a–e**) ILs and salts.[61,116] Specifically, D-ribose-based salts containing $[NTf_2]^-$, $[OTs]^-$, or $[BF_4]^-$ anions were liquids at room temperature, while for the derivatives with $[PF_6]^-$, I^-, or Br^- anions, T_m values rising in the following order: $[PF_6]^- < I^- < Br^-$ were observed. The corresponding D-galactose derivatives were all solids with significantly higher T_m values.

3.6.2.2. Cation

Both the origin and functionalization of an IL's cation can impact the thermal properties of the sugar-based ILs. Poletti *et al*.[53] studied the effects of modifications at the C6 position of methyl-α-D-glucopyranoside using trimethylamine (**12a**), diethyl sulfide (**12b**), or tetrahydrothiophene (**12c**). Compounds **12a** and **12c** were solids at room temperature, with T_m = 138 and 110 °C, respectively. Additionally, **12c** showed an exothermic crystallization peak at 52.6 °C, whereas **12b**, neither crystallized nor melted but formed a glass upon cooling to -53 °C. The thermal stability of these ILs increased in the order: **12b** < **12c** < **12a**.

Reiß *et al*.[85] developed a series of pentose- (**6a–h**) and D-glucopyranose-based ILs (**7a–g**) which displayed significant differences in thermal properties. Although direct comparisons are difficult to make because they have different functionalization at the anomeric centers, comparison of pentose-derived ILs with glucoside-derived ILs possessing the same anions and protection of hydroxyl groups reveals that the pentose-derived ILs were mostly liquids at room temperature, while glucoside-derived ILs were mostly solids under the same conditions. Pentose-derived ILs also had higher T_d values (297–345 °C), relative to glucoside-derived ILs (T_d = 205–250 °C). Among the pentose-derived ILs, thermal stability increases in the following order: D-lyxose < L-arabinose < D-xylose ≈ D-ribose. More exact comparisons can be made among glucoside-based products, where differences in thermal properties were reported for α- and β-anomers. For example, the methyl-α-D-glucopyranoside-derived IL with $[OTf]^-$ anion (**7a**) had a T_m of 95–100 °C, while the β-anomer (**7b**) was a liquid at room temperature.

Carbohydrate moieties transformed into anions and combined with common alkylimidazolium, tetraalkylammonium, tetraalkylphosphonium,

or *N*,*N*,*N*′,*N*′-tetramethylguanidium cations, demonstrated thermal stabilities inconsistent with traditional ILs having non-carbohydrate-derived anions.[79,80,93,113] In a series of gluconate-based ILs with phosphonium, ammonium, or guanidium cations (**2a–d**), thermal stability depended on the cation type, increasing in the order: $[tmgH]^+ < [P_{4444}]^+ < [N_{4444}]^+ < [P_{66614}]^+$.[93] Moreover, comparison of T_d values for **2b** and **2c**, shows that T_d can be enhanced by elongation of the alkyl chain. It is worth underlying that the derivative **2c** with the $[P_{6\ 6\ 6\ 14}]^+$ cation, exhibits even higher T_d than **2a** with the $[N_{4\ 4\ 4\ 4}]^+$ cation. Moreover, for glucuronate-based ILs (**1a**, **1b**), the imidazolium salt (**1a**) showed higher thermal stability than the corresponding ammonium salt (**1b**) ($[N_{4\ 4\ 4\ 4}]^+ < [EMIm]^+$).[79] This trend was also verified when imidazole was used as the functionalization moiety in a salt with a gluconamide-based cation (**5a**), which demonstrated higher thermal stability than the corresponding ammonium-based cation salt (**5h**).[93]

3.6.2.3. Length of the Carbon Chain

The length of the carbon chain is another factor influencing the thermal properties of carbohydrate-derived ILs and salts. This includes the carbon chain on the quaternary ammonium group and the spacer between the carbohydrate moiety and the quaternary ammonium group.

According to Arellano et al.[117] investigating traditional imidazolium ILs, increasing the alkyl chain length strengthens Van der Waals intermolecular interactions which affects the molecular organization within the sample, leading to increased thermal stability.[118] In contrast, increased chain lengths can also decrease the electrostatic interactions, thus causing lower thermal stability.[119] Moreover, it was shown that longer alkyl chain lengths in piperidinium ILs may increase the stability of the corresponding

carbocations and carbon radicals, making them better leaving groups and thereby promoting decomposition.[120]

In a series of herbicidal ILs (HILs) derived from D-glucose, containing 4-chloro-2-methylphenoxyacetate anions and alkyl substituents at the ammonium head ranging from $–CH_3$ to $–C_{16}H_{33}$ (**4d–h**), no obvious trend in thermal stability was observed.[86] However, the order of thermal stability ($C_1 < C_8 < C_4 < C_{16} < C_{12}$) aligned well with a similar group of HILs containing 2,4-dichlorophenoxyacetate anions (**4i–m**), with the exception of derivative **4j** (having C_4 substituent), which showed the lowest stability.

Comparison of T_d values of isosorbide-derived ILs with C_8 and C_{12} alkyl chains (**14a**, **14e**, and **14b**, **14f**, respectively) indicates that alkyl chain length had minimal influence on the thermal stability of this type of IL.[72]

A more distinct impact of the alkyl chain length on the ammonium head is evident in the melting point data for the investigated salts. For instance, in the dicationic mannitol salts (**18a–e**), a systematic increase of T_m was observed along with elongation of the chain length from $–C_3H_7$ to $–C_{18}H_{37}$.[54] Additionally, the isomannide-based salt with a $–C_4H_9$ alkyl chain (**17a**) had higher melting point than its corresponding derivative with a methyl substituent (**17b**), which was an oil.[68] There is an observable, yet less profound influence of the alkyl chain length, which was also demonstrated for α-D-glucopyranoside derivatives functionalized with DABCO amine and quaternized with C_4 to C_{18} alkyl chains (**13a–d**).[54]

The protection of hydroxyl groups by etherification provides a similar effect, as demonstrated by glucose derivatives **7b** and **7g**, where hydroxyl groups were methylated or ethylated, respectively.[85] Specifically, **7b** remained a liquid at room temperature, while **7g** had a T_m of 118–120 °C.

The nature of the alkyl spacer between the carbohydrate moiety and the quaternary ammonium group also influences the thermal stability depending on whether the spacer is linear or branched. In a series of glucono-based derivatives, branching of the alkyl chain resulted in decreased T_d values (**5c**, **5i**, **5e**, and **5j**).[93] Additionally, the thermal stability of glucose derivatives with the $[NTf_2]^-$ anion and modified at the C1 position with ethoxy or propoxy chains (**3h**, **3i**), showed a slight increase in stability with chain elongation (ΔT_d = 2 °C).[56] This trend was also observed for glucono-based derivatives **5c** and **5e,** with ethyl and propyl linkers, respectively, combined with Br^- anions.[93] However, the opposite trend (decrease of thermal stability with lengthening of the alkyl spacer) was reported for corresponding derivatives combined with I^- and $[NTf_2]^-$ anions (**5f**, **5h** and **5b**, **5d**, respectively). Despite the opposite trend reported for derivatives with $[NTf_2]^-$ anions, the effect of lengthening the alkyl chain was minor (ΔT_d = 3 °C), as demonstrated by comparing glucose derivatives **3h** and **3i**.[56] For halide derivatives with I^- (**5f, 5h**) and Br^- (**5c, 5e**) anions, the effect is more pronounced (ΔT_d = 12 °C and ΔT_d = 27 °C, respectively).[93]

In conclusion, conventional ILs typically exhibit higher thermal stabilities than most carbohydrate-derived ILs, likely due to the easier degradation of carbohydrate motifs at elevated temperatures.

Most ILs with hexose in the cation have T_d values between 150 and 250 °C; however, additional stability can be achieved when combining sugar cation with the $[NTf_2]^-$ anion. On the other hand, some pentose-derived ILs reveal a higher thermal stability of 296 to 345 °C.[85] To compare, the conventional ILs with 1-ethyl-3-methylimidazolium cation and anions such as: Cl^-, Br^-, I^-, $[OTf]^-$, $[OMs]^-$, $[N(CN)_2]^-$, $[C(CN)_3]^-$, $[BF_4]^-$, $[PF_6]^-$, $[AsF_6]^-$, $[NTf_2]^-$, $[Beti]^-$, $[EtSO_4]^-$ revealed T_d ranging from 282 to 462 °C [116], while ILs containing the 1-butylpyridinium cation combined with: Br^-, $[BF_4]^-$, $[PF_6]^-$, $[NO_3]^-$, $[OTf]^-$, $[N(CN)_2]^-$, $[HSO_4]^-$, $[H_2PO_4]^-$ revealed T_d ranging from 239 to 392 °C [120]. Substituting the anion

in the IL with the 1-ethyl-3-methylimidazolium cation into either gluconate or glucuronate results in significantly lower thermal stabilities, up to 250 °C.[79,81,115] These examples show that certain pentose-based ILs can operate within similar temperature ranges as many conventional ILs, with the added benefit of being less toxic.

3.7. Applications of carbohydrate-based ionic liquids

In the past years, extensive research on the applications of ionic liquids has been conducted, and their use in various fields has already been well documented.[121] The chiral nature and hydrogen-bonding capabilities of carbohydrate-based ILs make them particularly promising for catalytic applications. Additionally, their lower toxicity and higher biocompatibility offer a sustainable alternative to conventional ILs, potentially reducing the ecological impact of industrial processes. These unique properties have also expanded their potential in biomedical and ecological applications. This chapter will discuss applications previously explored in [48], as well as novel applications that extend beyond this review, to provide a comprehensive overview of the versatile trends in the field of carbohydrate-based ILs applications.

3.7.1. Organocatalysts/chiral catalysts

Carbohydrates belong to the natural chiral pool, so their IL derivatives have been studied as sustainable chiral solvents for applications in catalysis and material synthesis. A particular characteristic of ionic liquids, which also applies to sugar-derived ones, is that ILs often can serve dual roles as both solvent and catalyst in organic reactions (chiral or achiral).

The Chrobok group demonstrated that catalytic amounts of carbohydrate ILs can enhance Diels–Alder reactions, achieving complete conversion and a high ratio of endo:exo isomers (13.0-13.1) within minutes.[56] Remarkably, glucose-based ILs exhibited catalytic activity comparable to $Yb(OTf)_3$, a highly active metal catalyst for such reactions. The abundant hydroxyl groups in the cationic carbohydrate units positively influenced both reaction kinetics and selectivity, as confirmed by comparative studies with ILs having fewer hydroxyl groups. Jopp *et al*.[69] reported the first glucosamine-based ILs, which were also tested in the Diels-Alder model reaction between cyclohexadiene and diethyl maleate. However, in this case, the product yield was much lower (30%, with endo:exo = 12.3), probably due to the higher rigidity of glucosamine-based ILs compared to D-glucose-based ILs used by Chrobok *et al*.[56]

The Chrobok group[88] also explored glucose-derived ILs modified with long alkyl chains on the quaternary ammonium group as phase transfer catalysts (PTCs) in the synthesis of 2-chloro-1,3-butadiene (chloroprene) using a two-phase system. The influence of alkyl chain length of ammonium bromides on the conversion of 3,4-dichloro-1-butene was described, with the highest activity reported for IL bearing a C12 alkyl chain. The elaborated method, employing carbohydrate ILs as PTCs allowed chloroprene formation with a high yield of >99% and 100% selectivity at room temperature in 1 h.

Garg and Reddy[122] used D-ribose-based IL as a catalyst in the efficient synthesis of functionalized dihydropyrano coumarins *via* condensation reaction. A wide range of products substituted with aromatic and aliphatic aldehydes was prepared under mild conditions with good to excellent yields ranging from 76 to 92%. Moreover, the reusability of the catalyst up to 5 times was tested and no significant loss of activity was reported.

Kaur and Chopra[63] investigated D-galactose- and DABCO-based ILs as chiral recognition agents for the enantiodifferentiation of sodium salts of Mosher's acid. Moreover, chiral iodide salt was used as an organocatalyst in the asymmetric reduction of aromatic prochiral ketones. Secondary alcohols were obtained in moderate to high yields, although only low-to-moderate enantiomeric excess was achieved (5–17%).

Carbohydrate-derived ILs have very good solubility in water, which can facilitate the separation of water-insoluble reaction products and the regeneration of the IL for the next reaction cycle. ILs based on carbohydrates and amino acids were successfully utilized as catalysts for the Knoevenagel condensation reaction, where conversion values of 67–94% were achieved following reaction times as short as 15 min under exceptionally mild conditions using water as the solvent.[87] Moreover, AAILs have been intensively studied in the absorption of greenhouse gases due to the available amino group, suitable for efficient CO_2, NO_x, and SO_x capture. So far AAILs with common imidazolium[123,124], tetraalkylphosphonium[125], and tetraalkylammonium[126] cations as well as biocompatible cholinium[127] have been shown as promising liquid absorbents. Nevertheless, this promising, sustainable approach still remains unexplored for carbohydrate based AAILs.

The work done by Yuan et al.[57] is an example, where sugar-based IL was used as both a catalyst and a solvent. Chiral glucose-containing pyridinium ILs was applied in a one-step asymmetric synthesis of Tröger's base compounds, which are used in supramolecular chemistry, DNA recognition, gas separation, medicine, or as promising catalysts in asymmetric reactions. The products were generated with high enantioselectivity (up to 84%) and efficiency (up to 83%).

In previous cases carbohydrate derived ILs were the only catalysts in the reaction environment, but they can also be a constituent of the catalytic system, improving its catalytic activity, selectivity or both. Zhou *et al*.[128] showed that carbohydrate-derived

ILs can be successfully used as ligands for Pd-catalyzed homo-coupling reactions of arylboronic acids. The carbohydrate moiety in the ligand was proven to be crucial for improving the catalytic activity of the resulting catalysts and arylboronic acids were obtained with high yields (85-99%).

Another example of synthesis and application of Pd(II) complexes containing glucose-based ligands is the work done by Jopp *et al.*[129]. 11 acyl-protected glucosyl imidazolium iodides served as precursors and 15 complexes have been synthesized, then utilized as catalysts in a model Suzuki-Miyaura reaction. Reaction between bromobenzene and 4-toluneboronic acid has been investigated, and a highly reactive complex leading to >99% yield at 0.005 mol% catalytic loading has been reported.

Chrobok *et al.*[83] studied the performance of the biocatalyst consisting of the Candida antarctica lipase B (CALB) and multi-walled carbon nanotubes (MWCNTs) modified by D-glucose-based ionic liquids for the synthesis of n-butyl acrylate *via* esterification of acrylic acid and n-butanol. For the most promising carbohydrate-based IL, a 99% yield of n-butyl acrylate was achieved in 24 h. The presented catalytic system was cross-verified and benchmarked against the commercially available biocatalysts, clearly revealing the outperformance of the novel formula. A year later, Lehman and Jopp[59] used D-glucose based IL as a support for Novozym 435 (commercially available immobilized CALB) in the same reaction. However, in this work, the maximum yield was 67% for n-butyl acrylate. In another work[130], the same authors optimized the reaction parameters for various substrates, while the catalyst remained unchanged. Different alcohols and reaction conditions were extensively screened, yielding 17 acrylate and 2 methacrylate esters at room temperature with complete or nearly complete conversion reported for most of the products.

3.7.2. Biomedicine and ecology

The increasing interest in the biological activity of ILs has driven significant advancements in their applications within biomedicine and ecology, leading to the development of biomaterials and drugs utilizing ILs.[16] A considerable aspect of this newly emerging field is the establishment of a third generation of ILs, employing biodegradable and natural ions with known biological activities. Although choline and amino acid-based ILs have dominated the biomedical research, sugar-based ILs have the potential to become the next essential contributor. The antimicrobial activity and generally low toxicity of sugar-based ionic liquids have attracted considerable attention, leading to recent growth in the number of reports on their environmental impact, including toxicological aspects[80,85,93,108] and biodegradability[80,87].

For example, Chen *et al*.[131] demonstrated that pyridinium-based polymeric ILs (PILs) with pendent sugar units exhibited enhanced binding affinity and antibacterial activity against Gram-negative *E. coli*. Additionally, they developed hybrid nanocomposites based on PILs containing pendent sugar units with Fe_3O_4 nanoparticles, showing potential as antibacterial agents for water treatment.[108] Incorporating carbohydrate moieties into PILs has significantly reduced cytotoxicity towards mammalian cells while enhancing antibacterial efficacy compared to unmodified PILs. In 2009, polycationic carbohydrate-derived salts were found to have promising antibacterial and antifungal activities, particularly as gels for topical disinfection.[54]

Moreover, Billeci *et al*.[93] demonstrated that glucono-based ILs could induce moderate or low antiproliferative effects and are safe for human erythrocytes in toxicity tests involving three different cancer cell lines and fish embryos. Toxic effects were detected only when unusually highly concentrated solutions were analyzed. Their research also showed that functionalizing conventional imidazolium ILs with sugar

moieties reduces toxicity, which could lead to the development of safer aromatic ILs and sugar-based IL systems for biomedical use.

While investigating novel composites for biomedical engineering, Krukiewicz *et al*.[132] developed a polymer material, co-doped with a biodegradable, D-glucopyranoside-derived IL with conductive properties. Electrodeposition of poly(3,4-ethylenedioxythiophene) (PEDOT) in the presence of a carbohydrate IL (which also acts as an electrolyte) resulted in the formation of highly corrugated and structured polymer films with increased biocompatibility relative to undoped polymers. Thus, such composites represent promising candidates for applications as neural interfaces or tissue scaffolds.

Moreover, sugar-based ILs demonstrate herbicidal activity (as HILs) when combined with specific anions.[86] Pernak *et al*. in collaboration with the Chrobok group, have reported that such ionic systems exhibit negligible vapor pressure, and their structures can be modified to control their water solubility, thus limiting their mobility in the environment.

3.7.3. Solvents (biomass conversion, extraction and absorption)

Ionic liquids are traditionally known to act as reaction media in chemical transformations because of their low volatility and high solubility for many organic compounds. However, their utility extends beyond this, as they can also be employed as absorbents, extractants and dissolution media for biomass processing.

This is particularly important in the context of reducing the reliance on fossil fuels by valorizing renewable biomass. In such processes, wastes from food production or forestry can be repurposed to produce ILs, which are then used as recyclable solvents.

The concept of a closed-loop biorefinery has recently been introduced, where biomass is processed using ILs derived from the same or similar biomass feedstock.[50] Given this potential, the development of sugar-based ILs is advantageous for breaking down hard-to-dissolve polysaccharides, particularly due to their lower toxicity compared to conventional solvents used for biopolymer dissolution.

Javed et al.[133] used *N,N*-diethyl-*N,N*-dimethylammonium gluconate, prepared by simple neutralization of diethyl dimethyl ammonium hydroxide with gluconic acid, to extract cellulose from oil palm lignocellulosic biomass. By using this sugar-derived IL, 52% wt. of cellulose was extracted from the crude biomass, without any pretreatment, within 30 min at 25 °C. While conventional ILs have been extensively researched for polysaccharide dissolution, sugar-based ILs have only recently begun to attract attention for this purpose.[134] Although these ILs typically exhibit high viscosities, newly developed glucono-based derivatives with viscosities as low as 106.3 mPa·s makes them an attractive solvent, with high hydrogen-bonding abilities and low environmental impact.

Moreover, taking advantage of the strong coordinating abilities of hydroxyl groups, the potential use of this type of ILs as extractants should be explored. Recently, Billeci et al.[96] investigated gluconate-based ammonium and phosphonium salts as gelators to produce sugar-based gels with a thick network of hydrogen bonds, further used for desulfurization of fuels. Reported systems were able to remove approximately 70–80% of benzothiophene and dibenzothiophene, which are generally considered as refractory compounds in desulfurization.

Reddy *et al*.[116,135] studied hydrophobic D-galactose-based ILs in Pb^{2+} and Cd^{2+} removal from aqueous solutions. Various batch parameters such as pH, IL dose, contact time, initial metal ion concentration and temperature were considered, showing

that the carbohydrate IL can remove up to 374.9 $mg \cdot g^{-1}$ of Pb^{2+} and 84.5 $mg \cdot g^{-1}$ of Cd^{2+} under optimal conditions.

Sugar-based ILs were also recently applied in the synthesis of hydrogels. Jopp *et al*.[84] used ionic vinyl imidazolium carbohydrate monomer and cross linkers such as *N,N'*-methylenebis(acrylamide) or poly(ethylene glycol) diacrylate to prepare cationic hydrogels. These hydrogels are hydrophilic, three-dimensional cross-linked polymers capable of reversibly absorbing significant amounts of water while maintaining their structure.[136]

3.7.4. Energy conversion and storage

Although conventional ILs have been widely studied in the context of their potential applications in electrochemistry, with a special focus on use as electrolytes, carbohydrate-based ILs have barely been investigated with regard to this approach.[137]

Billeci et al.[92] exploited the coordinating properties of sugar-based ILs, reporting a thermochromic system that employed glucono-based ILs ligands to coordinate cobalt(II). The solution changed color from pink to blue upon heating/cooling in the range of 20–60 °C due to the change in the coordination geometry of the Co^{2+} ion with the hydroxyl groups present in the sugar moiety. This system was further incorporated into a polymer film and maintained its performance. Such stimuli-responsive "smart" systems have potential for energy storage applications like window glazing, because they use solar radiation energy with increased efficiency.

Ionic liquids have also been proposed as precursors for nitrogen-doped carbon materials, which are highly valued for their excellent electrical conductivity and chemical,

mechanical, and thermal stability. These materials have become desirable for energy conversion and storage, gas separation, and catalysis applications.[138]

The research conducted by our group has shown that carbohydrate-based ILs can serve as versatile precursors for *N*-doped carbon, providing the carbon source, nitrogen dopant, and acting as pore-generating agent.[79] By carefully designing these ILs at the molecular level, it is possible to finely tune the properties of the resulting carbon materials, optimizing factors such as yield, porosity, and nitrogen content. The metal-free, nitrogen-doped carbon materials produced from these ILs have exhibited electrocatalytic activity in oxygen reduction reactions, underscoring their potential in energy-related applications.

The manufacture of ILs using abundant, inexpensive and renewable carbohydrates represents a promising strategy to tackle the challenge of sustainable chemical production that addresses the challenges related to depletion of fossil sources. Sugar-based ILs can be synthesized using various pathways, which have become more and more attractive from economic and sustainability perspectives. Although the purification of suitable intermediates is a bottleneck of carbohydrate IL synthesis, recently reported procedures that replace the column chromatography purification step with simple extraction using green organic solvents are examples of successful advancements toward development of green chemicals.

When considering applications that take advantage of the versatile features of carbohydrate-derived ILs, these derivatives can be used as alternatives to cholinium or amino acid derivatives, which are currently more commonly used in the synthesis of bio-ILs. The advantageous features of carbohydrate-derived ILs include their hydrogen bond-rich structure which endows these ionic liquids with high coordinating ability and solubility in polar solvents. Moreover, the chirality, low toxicity, and high biodegradable potential of carbohydrate ILs make them attractive targets of research

for catalytic, biomedical, and ecological applications. Overall, the spectrum of possible applications for sugar-based ILs has broadened considerably to the point that they now demonstrate potential as solvents, extractants, or materials for energy conversion and storage.

One of the most attractive features of ILs is that their properties can be tuned by selecting the specific cations, anions, side chains, or task-specific functional groups. The family of carbohydrate ILs and salts has only begun to be investigated, so there is a need to report more data describing the influence of structure on their (eco)toxicological properties. Overall, it will allow for more targeted design regarding this class of bio-ILs.

In the following sections, the study on the properties and applications of novel sugar-based ionic liquids as phase change materials (chapter 4.1.), *N*-doped carbon materials precursors (chapter 4.2.) and surface active agents (chapter 4.3.) will be provided.

4. Results and discussion

4.1. Carbohydrate-based ionic liquids as phase change materials

4.1.1. Introduction

In an era defined by the growth of electricity consumption, the need for sustainable solutions and energy-efficient technologies has intensified like never before. The seamless storage and conversion of renewable energy resources stand as key strategies to bridge the growing gap between electric energy supply and demand.[139] Phase change materials (PCMs) have emerged as a potential remedy for this problem. Possessing the unique ability to store thermal energy in the form of latent heat during phase transitions and liberating the stored energy upon reversed the transition.[140] PCMs date back to the 1970s, predominantly focusing on solid ↔ liquid transitions, characterized by minimal volume change and substantial transition enthalpy (for melting, it is denoted as the fusion enthalpy (ΔH_f)).[141] Recent attention has directed towards PCMs with melting points spanning intermediate temperature range (100 – 220 °C) for the efficient exploitation of renewable resources such as solar and wind energy. PCMs not only allow for storage and reuse of thermal energy, but can also be used in the next generation thermal batteries (Carnot battery), which are able to convert heat into electricity.[142] Within this temperature spectrum, a variety of candidates including sugar alcohols[143], inorganic salt hydrates[144,145], organic salts and ionic liquids[146–149], fatty acid diamides[150,151] and polymers[152] have been studied. However, many of these candidates have to be excluded from practical consideration due to inherent drawbacks, such as corrosivity, flammability, phase separation, supercooling, low volumetric energy

storage or poor cycling stability.[153] The pursuit of novel organic phase change materials is driven by economic needs and the urgency of environmental conservation.

Striking to formulate PCMs with melting points between 100 and 220 ° C, this work has been guided by two distinct groups of materials: sugar alcohols and ionic liquids. Primarily, sugar alcohols, which exhibit the highest capacity for latent heat storage (>200 J g^{-1}), surpassing all other organic materials that melt below 220 °C. Sugar alcohols such as erythritol[154–160], galactitol (D-dulcitol)[154,157], D-mannitol[154,155,157–159,161], myo-inositol[154,157,158,162], adonitol[155], arabinitol[155,158], sorbitol[154–156,159] and xylitol[154,155,160,163,164] have been investigated as potential PCMs, so far. Of paramount importance is the biorenewable character of sugar alcohols that makes them sustainable materials, key to the transition to net zero.[165] On the other hand, sugar alcohols suffer from poor thermal stability and significant supercooling (usually once melted, they are not able to recrystallize). Sugar alcohols own extraordinarily high ΔH_f values (**Table 1**). This phenomenon finds its origins in the abundance of hydroxyl groups within their molecular structure, which facilitates the formation of extensive hydrogen bonding networks in the solid state. The disruption of these hydrogen bonds upon phase transition significantly contributes to the observed ΔH_f values.[154–161,163,164,166]

Table 1. Thermal properties of sugar alcohols.

Sugar alcohol	T_m [°C]	ΔH_f [J g^{-1}]	T_c [°C]	ΔH_c [J g^{-1}]	T_m - T_c	Ref.
Sugar alcohols able to crystallise						
erythritol	119	334	17	171	102	[154]
D-galactitol	187	351	117	232	70	[154]
D-mannitol	166	277	114	228	52	[154]
myo-inositol	225	262	181	199	44	[154]
Sugar alcohols unable to crystallise						
adonitol	100	250	n.a.	n.a.	n.a.	[155]
arabinitol	103	280	n.a.	n.a.	n.a.	[155]
sorbitol	99	184	n.a.	n.a.	n.a.	[154]
xylitol	93	231	n.a.	n.a.	n.a.	[154]

Various strategies have been employed to adjust and enhance the crystallization behavior of sugar alcohols. These approaches include the formation of binary sugar alcohol eutectic mixtures[154,155,167,168], the fabrication of composite materials involving sugar alcohols and polymers[169–171], porous carbonaceous materials[172,173], zeolitic imidazolate frameworks (ZIFs)[174,175], inorganic porous materials[176,177], encapsulation of sugar alcohols[178–180], and enhancement of crystallization by adding metal powders such as copper or aluminum[181]. Additionally, chemical modification of sugar alcohols stands out as another method explored to refine their properties and this field was scarcely explored.

Currently, only one research group has described the chemical modification of sugar alcohols to obtain materials for thermal energy storage. Sari *et al.* synthesized fatty acid (stearic, palmitic, myristic, and lauric acid) hexaesters of D-galactitol/D-mannitol to increase the cycling stability of sugar alcohols.[182,183] Nevertheless, in terms of application, particularly with respect to melting temperature, the investigated esters with T_m in the range of 32 – 65 °C, offer alternatives more closely aligned with fatty acids (T_m of palmitic acid = 63 °C, ΔH_f = 214 J g^{-1}; T_m of stearic acid: = 69 °C, ΔH_f = 235 J g^{-1}) than with sugar alcohols (T_m of D-galactitol = 186 °C; T_m of D-mannitol = 166 °C).

More recently, low melting organic salts and ionic liquids have been recognized as compelling candidates for PCMs. Many organic salts including ionic liquids possess properties valuable for phase change materials and their application in thermal energy storage (TES) such as thermal stability, high specific heat storage capacity, inherent nonflammability, and negligible vapor pressure. A further dimension to their potential lies in the structural modifications related to the diversity of cations and anions combinations, which allows fine tuning of their physiochemical characteristics.

Among organic salts that can be utilized as PCMs in the range of 100 to 220 °C are compounds containing imidazolium[184–190], pyrazolium[146], pyridinium[148],

arylphosphonium[191], cholinium[192,193] or guanidinium[147,192] cations and counter ions such as bromide (Br^-), tetrafluoroborate ($[BF_4]^-$), hexafluorophosphate ($[PF_6]^-$), bis(trifluoromethane)sulfonimide ($[NTf_2]^-$), mesylate ($[OMs]^-$), tosylate ($[Tos]^-$), tartarate ($[Tart]^-$) and dihydrogen phosphate ($[DHP]^-$) (**Table 2**).[166] Most of the investigated ionic liquids and organic salts show melting enthalpies, lower than 130 J g^{-1}, however, there are some outstanding exceptions, such as geminal dicationic ILs with ΔH_f reaching up to 159 J g^{-1} for $[C_4(C_2H_4Im)_2]Br_2$ (T_m = 135 °C).[190] Moreover, few organic salts have gained considerable attention due to their biorenewable character, such as guanidinium mesylate (T_m = 208 °C, ΔH_f = 190 J g^{-1}) and cholinium tartarate (T_m = 151 °C, ΔH_f = 129 J g^{-1}).

Table 2. Thermal properties of organic salts with T_m in the range of 100 – 220 °C. Reproduced with permission.[166] Copyright 2021, Royal Society of Chemistry.

Compound	T_m [°C]	ΔH_f [J g^{-1}]	Ref.
[Gdm][OMs]	208	190	192
[Ch][Tart]	151	129	192
[Pzy][OMs]	168	160	147
$[C_2H_3O_2MIm]Br$	177	104	187
$[C_2H_3O_2MMIMm]Br$	148	58	187
$[C_4(C_2H_4Im)_2]Br_2$	135	159	190
$[C_4(C_2H_5O_2Im)_2]Br_2$	209	118	190
$[C_4(C_2H_5Im)_2]Br_2$	131	102	190
$[C_4(C_2H_5OIm)_2]Br_2$	103	127	190
$[C_4(C_2H_2NIm)_2]Br_2$	212	126	190
$[C_4(MIm)_2]Br_2$	135	116	189
$[C_4(MIm)_2][PF_6]_2$	111	85	189
[Ch][DHP]	123	6	193
[Ch][Tos]	105	69	193
$[PPh_4][NTf_2]$	135	52	191
$[PPh_3$-*o*-Ph-O-Ph$][NTf_2]$	164	71	191
$[PPh_3$-*p*-Ph-O-Ph$][NTf_2]$	102	47	191
$[C_2(MIm)_2]Br_2$	208	116	188
$[C_2(MIm)_2][BF_4]_2$	145	94	188
$[C_2(MIm)_2][PF_6]_2$	191	109	188
$[C_2(MIm)_2][NTf_2]_2$	140	74	188
$[C_4$(Thia)]Br	135	113	194

4.1.2. Goal of the research

Taking advantage of the hydroxyl-group-rich structure of sugars and the expertise of the Chrobok's group in the synthesis of carbohydrate-based ionic liquids and salts[79,87], the goal of the thesis was to transform sugar derivatives into organic salts tailored for sustainable thermal energy storage. Sugars, which also possess multiple hydroxyl groups, similarly to sugar alcohols, have never been studied as PCMs before. Thus far, carbohydrates have only been found solely as PCM additives.[195,196] The goal of this work was to investigate and better understand the structure-property relationship in the obtained ionic sugar derivatives and evaluate their potential in thermal energy storage. Melting points of sugars are in the intermediate temperature range and it is expected that they will have high enthalpies of fusion. Yet, the potential of chemical modifications of both sugar alcohols and carbohydrates to tune their thermal properties (supercooling in specific), remain a little exploited area in the PCM domain. Therefore, synthesis of bio-derived PCMs with low supercooling, good cycling stability, high heat of fusion and T_m values in the intermediate temperature range (100-220 °C) is still a challenge.

4.1.3. Glucose-derived organic salts as phase change materials

Saccharides are among the most prevalent organic compounds in nature, with glucose emerging as the most abundant monosaccharide. It serves as a fundamental building block for polysaccharides such as starch, cellulose, and glycogen, which is widely distributed in biomass (animals, fungi, and bacteria). Glucose is also a constituent of various disaccharides such as sucrose, maltose present in many plants, including fruits or lactose, a by-product of the dairy industry. Corn-derived starch stands

out as the primary raw material utilized in the enzymatic hydrolysis process for commercial glucose production.[197] Glucose is produced ether in the liquid form – glucose and glucose-fructose syrup or in anhydrous and monohydrate crystalline form. Majority of the glucose is used in the food industry, while the largest nonfood use is as a raw material for the production of fuel-grade ethanol. Glucose itself is a biorenewable and affordable precursor for multiple valuable chemicals, which is used successfully in many industrial processes and the pharmaceutical industry, gradually replacing raw materials of petrochemical origin.[198–201]

4.1.4. Synthesis of glucose-derived organic salts

To prepare sugar-based phase change materials, glucose derivative – methyl α-D-glucopyranoside (MG) was chosen as a model compound. MG was transformed into two series of salts, with free hydroxyl groups in the cation ([Glu][X]) or methylated hydroxyl groups ([TMGlu][X]) (**Figure 7**).[202] Each series contained 4 compounds with different anions. Based on preliminary screening and literature review, anions such as: Br^-, $[NO_3]^-$, $[OMs]^-$ and $[BF_4]^-$ were chosen.

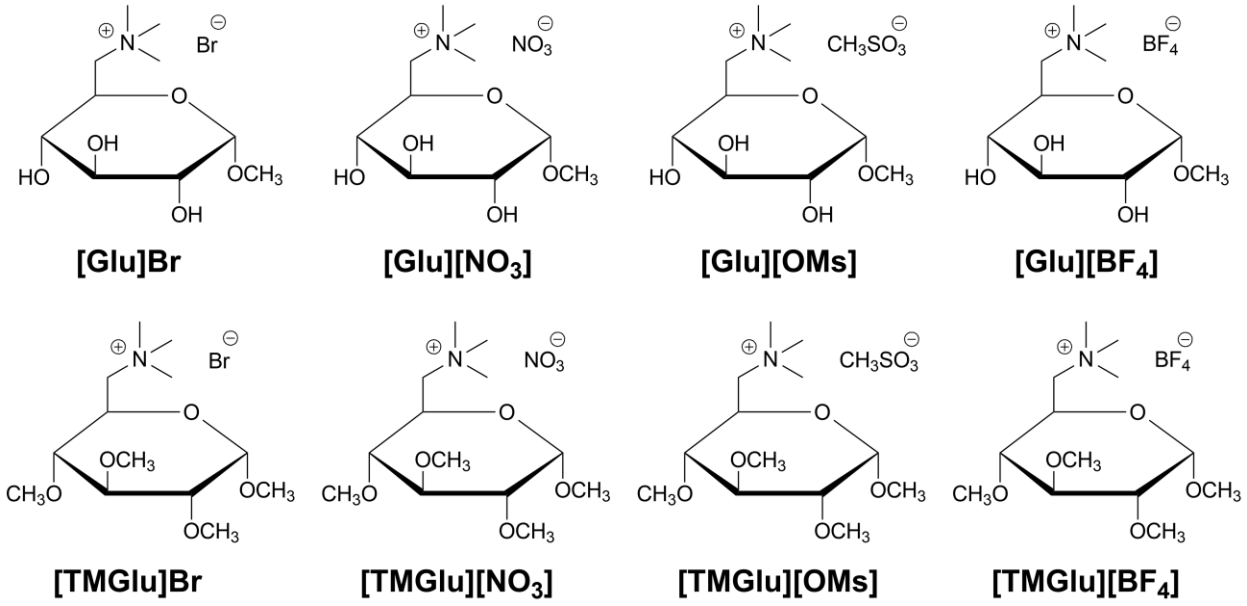

Figure 7. Sugar-based organic salts derived from methyl α-D-glucopyranoside (MG). Adapted from [202].

[Glu][X] series was obtained by the bromination of methyl α-D-glucopyranoside with tetrabromomethane in the presence of triphenylphosphine *via* the Appel halogenation reaction using pyridine used as a solvent (**Figure 8**). Methyl 6-bromo-6-deoxy-α-D-glucopyranoside (**1**) was purified by two-step column chromatography (1. CH_2Cl_2 to CH_2Cl_2:MeOH 9:1, 2. EA:MeOH 9:1). Afterwards, the methyl 6-bromo-6-deoxy-α-D-glucopyranoside was quaternized with a 33% wt. ethanolic solution of trimethylamine in an autoclave, yielding [Glu]Br (**2**) with the yield of 73%. Anion metathesis was carried out with the corresponding silver salts i.e. commercially available $AgNO_3$, AgOMs (synthesized from Ag_2O and methanesulfonic acid (MsOH)), and *in situ* formed $AgBF_4$ (from Ag_2O and HBF_4 48% wt. in H_2O). For the anion metathesis, the [Glu]Br was dissolved in MeOH and mixed with the corresponding silver salts. The products were obtained after filtration and condensation of the filtrates, to yield respectively [Glu][NO_3] (**5**), [Glu][OMs] (**6**) and [Glu][BF_4] (**7**). Anion metathesis was achieved with high yields of 95%, 88% and 98% respectively. An alternative pathway to obtain ionic compounds from methyl α-D-glucopyranoside through 6-iodo-6-deoxy-

α-D-glucopyranoside (**3**) was developed by Jopp *et al.*[58] This method was adopted in this work and modified to obtain [Glu]I (**4**). In this procedure, methyl α-D-glucopyranoside and imidazole were dissolved in THF. Subsequently, triphenylphosphine and iodine were added. The reaction mixture was stirred under reflux. The product was purified by column chromatography (CH_3Cl to CH_3Cl:MeOH 12:1). This procedure eliminated the use of highly toxic pyridine as a solvent and offered a significantly higher product yield of 93%. Most of all, it simplified the purification procedure to single column chromatography. Quaternization with trimethyl amine afforded [Glu]I (**4**) (Y = 87%) which was used for anion metathesis instead of [Glu]Br.

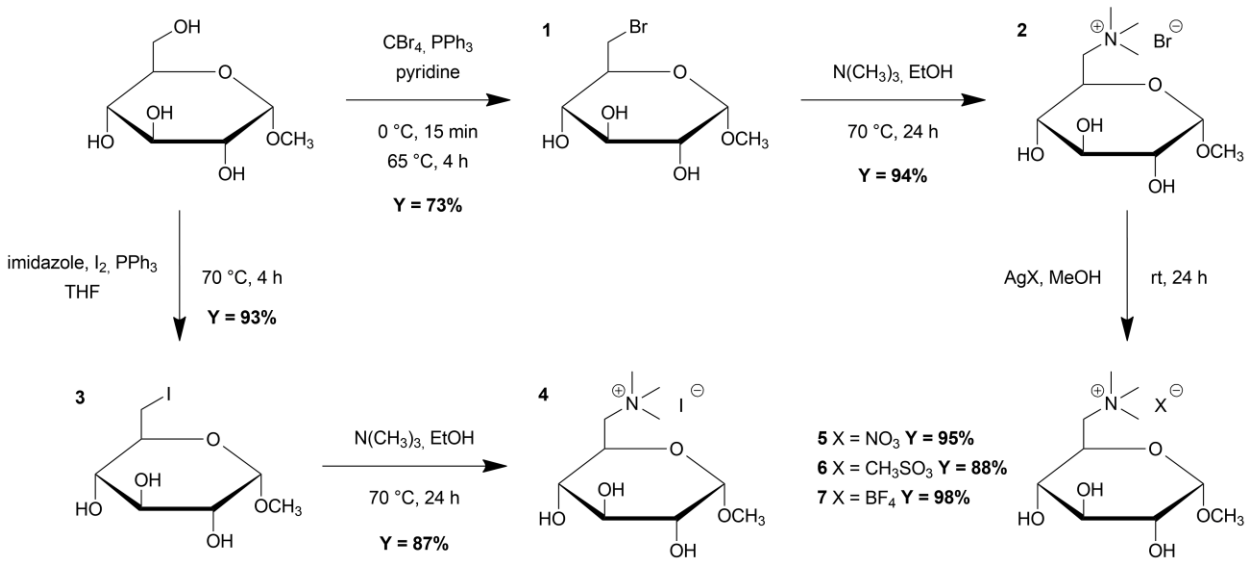

Figure 8. Synthetic procedure for [Glu][X] series preparation. Adapted from [202].

To investigate the importance of hydrogen bonds in the synthesized salts on their thermal properties, the analogue series [TMGlu][X] with methylated –OH groups was obtained (**Figure 9**). Methyl 2,3,4-*O*-methyl-α-D-glucopyranoside (**8**) was synthesized according to procedure described by Reiß *et al.*[85], followed by bromination with CBr_4, in the presence of triphenylphosphine to get methyl 2,3,4-*O*-methyl-6-bromo-α-D-

glucopyranoside (**11**). Subsequent quaternization with trimethylamine 33% wt. ethanolic solution, according to the analogous procedure that was applied for the synthesis of [Glu][X] series, yielded ionic derivative [TMGlu]Br (**12**). Nevertheless, the protection of the –OH groups simplified the purification procedure – it allowed the purification of methyl 2,3,4-*O*-methyl-6-bromo-*α*-D-glucopyranoside (**11**) with column chromatography in a single eluent system (PE:EA 3:1 to EA) instead of two, used for the purification of methyl 6-bromo-6-deoxy-*α*-D-glucopyranoside (CH_2Cl_2 to CH_2Cl_2:MeOH 9:1 and EA:MeOH 9:1). On the other hand, after quaternization, an additional purification procedure had to be applied for [TMGlu]Br. The post-rection mixture was condensed on a rotary evaporator and washed with ethyl acetate. The resulting precipitate was filtered off and further purified *via* flesh column chromatography using MeOH as an eluent. Anion metathesis was carried according to the same procedure applied for [Glu]Br. [TMGlu][NO_3] (**13**), [TMGlu][OMs] (**14**) and [TMGlu][BF_4] (**15**) were obtained with yields of 97%, 87% and 94%, respectively.

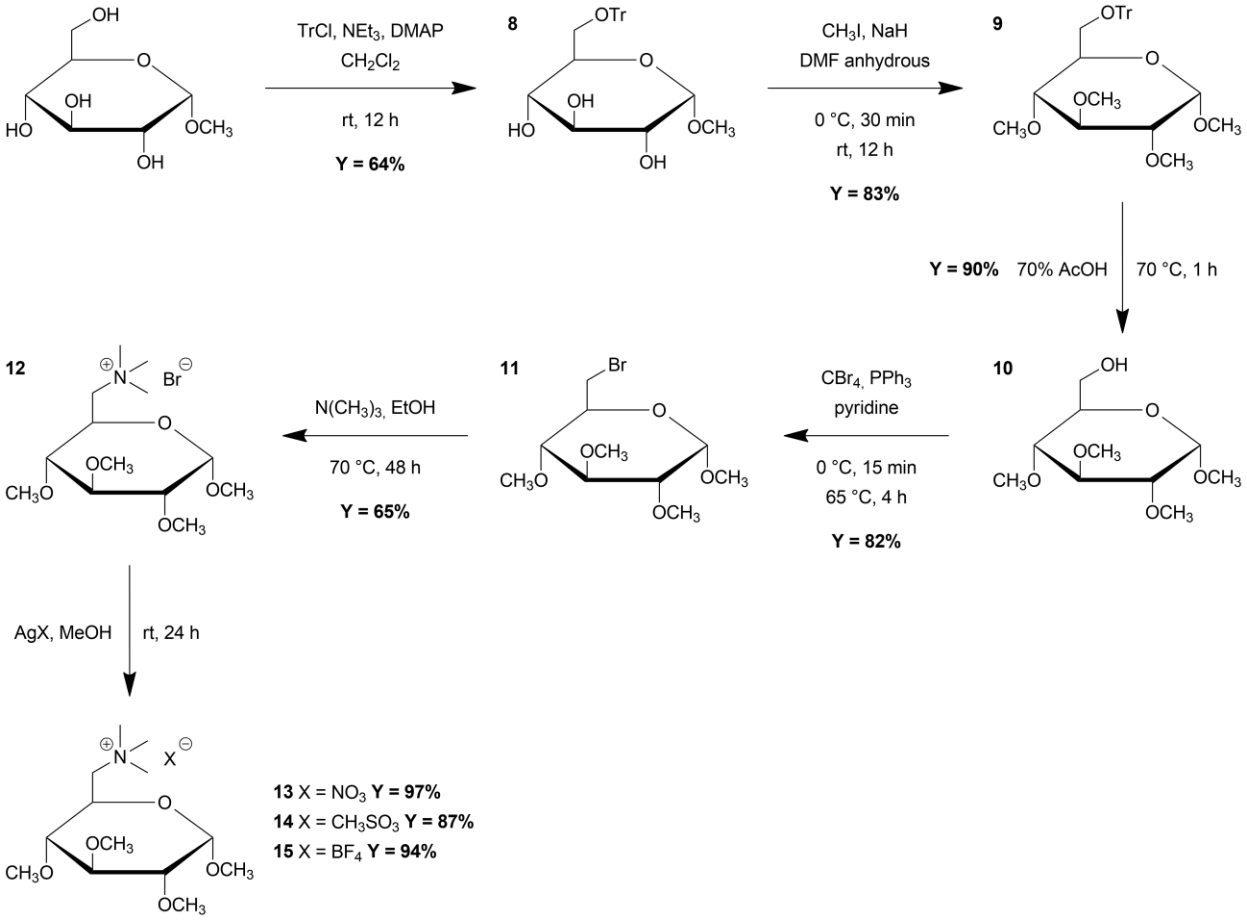

Figure 9. Synthetic procedure for [TMGlu][X] series preparation. Adapted from [202].

4.1.5. Thermal properties of glucose-based ionic compounds

The thermal properties of non-ionic precursor (methyl α-D-glucopyranoside (MG)), [Glu][X] and [TMGlu][X] series were investigated using differential scanning calorimetry (DSC). Primary interest was centered on melting temperature (T_m), enthalpy of fusion (ΔH_f), crystallization temperature (T_c) and enthalpy of crystallization (ΔH_c) to evaluate the potential of the salts for TES. The decomposition onset was determined by thermogravimetric analysis (TGA). All the data have been summarized in **Table 3**.

Table 3. Physical properties of methyl-α-D-glucopyranoside (MG), glucose-based ionic compounds. (cc) – cold crystallization. Adapted from [202].

Compound	T_m [°C]±2°C	ΔH_f [J g^{-1}]±5%	T_c [°C]±2°C	ΔH_c [J g^{-1}]±5%	T_d [°C]
MG	168	178	-	-	185
[Glu]Br	233	109	-	-	246
[Glu][NO_3]	163	88	84	76	267
[Glu][OMs]	152	59	86	59	221
[Glu][BF_4]	99	48	-	-	180
[TMGlu]Br	155	65	104 (cc)	35	168
[TMGlu][NO_3]	116	30	-	-	182
[TMGlu][OMs]	135	49	73 (cc)	33	250
[TMGlu][BF_4]	147	66	103	46	171

The model compound MG displayed a melting point of 168 °C (T_d = 185 °C) and exhibited substantial ΔH_f of 178 J g^{-1}. However, once it was melted during the initial heating cycle, it failed to undergo recrystallization (**Figure 10**).

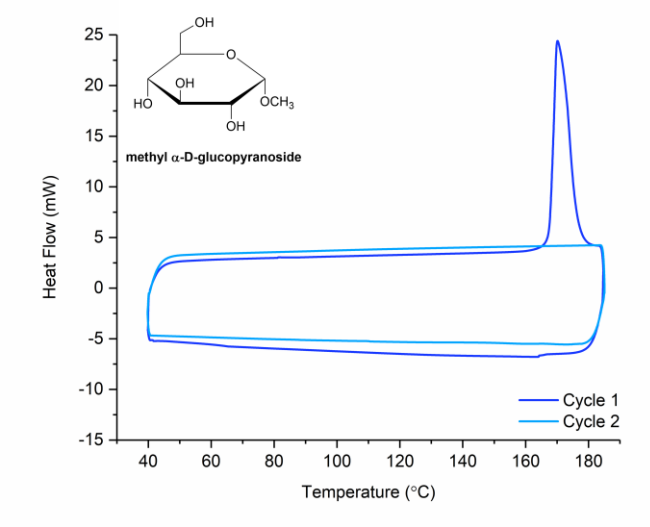

Figure 10. DSC curve of MG. Adapted from [202].

Conversely, the incorporation of distinct anions such as Br^-, $[NO_3]^-$, $[OMs]^-$ and $[BF_4]^-$, had a profound impact on the thermal properties on the resulting ionic

compounds. All of the salts from the [Glu][X] series were solid at rt. and revealed higher thermal stability (T_d) compared to nonmodified MG, with values spanning from 180 to 267 °C. The only exception was [Glu][BF_4], that decomposed at 180 °C. The examined salts displayed melting temperatures (T_m) within a range of 99 to 233 °C, accompanied by melting enthalpies (ΔH_f) varying from 39 to 109 J g^{-1}. Interestingly, unlike the unmodified sugar, two of the ionic compounds ([Glu][OMs] and [Glu][NO_3]) demonstrated the ability to undergo recrystallization during cooling cycles (**Figure 11**). Repetitive cooling and heating experiments conducted *via* DSC demonstrated a slight reduction in ΔH_f with each heating/cooling cycle for [Glu][OMs], possibly attributed to decomposition, incomplete crystallization, or a combination of both factors. Conversely, [Glu][NO_3] exhibited repetitive crystallization during 11 heating/cooling cycles.

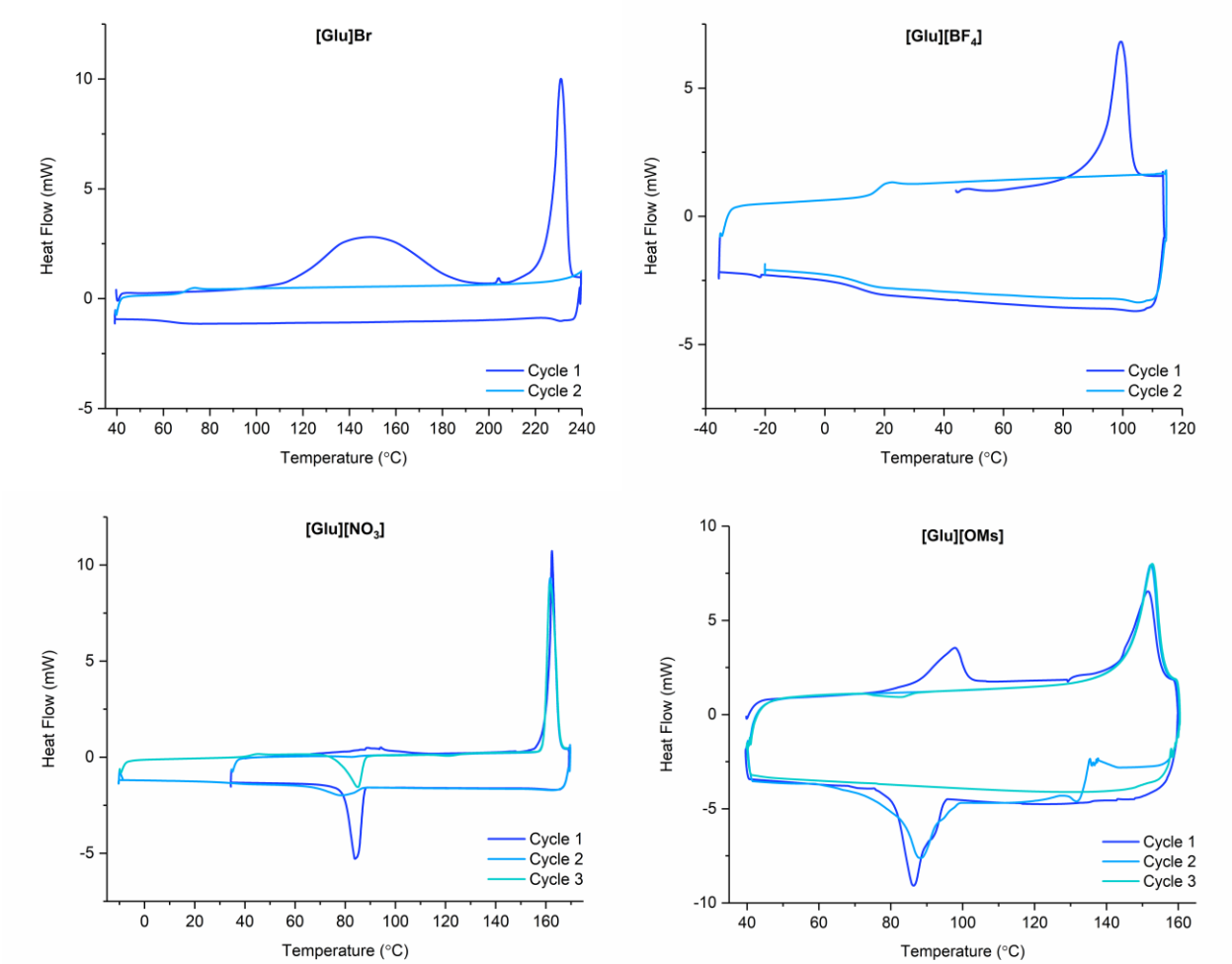

Figure 11. DSC curves of [Glu] series. Adapted from [202].

A parallel series featuring methylated hydroxyl groups ([TMGlu][X]) was synthesized to compare the thermal properties and validate the contribution of hydrogen bonding within the [Glu][X] series (**Table 3**). In this series, the salt [TMGlu][OMs] showed higher thermal stability (T_d = 250°C) compared to MG. Notably, in contrast to the unprotected series, all compounds in the [TMGlu][X] series (except for [TMGlu][NO_3]) were able to recrystallize. Nevetheless, for [TMGlu]Br, [TMGlu][OMs] and [TMGlu][NO_3], the values of ΔH_f were lower than for the corresponding compounds in the [Glu][X] series. These results encompass the two sides of hydrogen bonds: they are responsible for higher ΔH_f values, but simultaneously hinder recrystallization

due to the presence of the extensive hydrogen bonding network which is hard to recreate upon cooling.[147] Despite the salts were able to recrystallize, they suffered from significant decrease in ΔH_f after each heating/cooling cycle. The only exception from this trend was observed for the salt with the $[BF_4]^-$ anion which forms the least H-bonding with the cation among studied compounds, as revealed in the next section.

Crystallization in the methylated series occurred on the heating cycle (except for [TMGlu][BF_4]). This phenomenon is referred to as cold crystallization and is common in various glass-forming compounds.[203]

4.1.6. Crystallographic analysis of glucose-based ionic compounds

To gain deeper insights into the anions' impact on the thermal properties of the salts, the crystallography was employed to investigate the interplay between the ions in the solid state. The structures of [Glu][X] and [TMGlu][X] salts were determined using single crystal X-ray diffraction (XRD) and deposited in the Cambridge Crystallographic Data Centre ([Glu][BF_4] – 2232223, [Glu][OMs] – 2232222, [Glu][NO_3] – 2232221, [TMGlu][BF_4] – 2232220, [TMGlu][NO_3] – 2232219, [TMGlu]Br – 2232218). The [Glu]Br salt crystallized only as its monohydrate, despite extensive drying and recrystallization from anhydrous solvents, which excluded it from direct comparison with the other structures.

For the remaining salts in [Glu][X] series, ΔH_f values increased in the following order: [Glu][BF_4] < [Glu][OMs] < [Glu][NO_3] (with ΔH_f of 48, 56 and 88 J g^{-1}, respectively), aligning exactly with their crystallization capabilities. While analyzing the crystal structures of these salts, the primary focus was directed towards the hydrogen bonds present in their solid-state, as the disruption of H-bonds in the solid state during melting,

contributes to the overall ΔH_f value (**Figure 12**). In [Glu][BF_4] each cation forms 3 distinct hydrogen bonds, with one located between the cation and the anion (O–H···F) and the other 2 bonds are O–H···O interactions between adjacent cations. Interestingly, the H atom on O4 is a donor participating in asymmetric bifurcated H-bond, one toward F in $[BF_4]^-$ anion (D···A 2.98 Å, D-H···A 121°), and one toward O2 in the neighboring cation (D···A 3.10 Å, D-H···A 134°). The third hydrogen bond (D···A 2.76 Å, D-H···A 166°) is a canonical interaction between –OH groups located on two different cations, with H on O2 serving as a donor and O3 in the neighboring cation as an acceptor. Importantly, bifurcated hydrogen bonds are recognized to be relatively weaker compared to canonical hydrogen bonds.[204] Similarly, to unmodified carbohydrates, where hydrogen bonds between –OH groups are the only possibility, in [Glu][BF_4] the interactions between –OH groups remain dominant. Moreover, a significant deviation from the 180° angle in the H-bond involving the fluorine atom (121°), would suggest that this O–H···F interaction is relatively weak compared to the other hydrogen bonds observed in the series. Presumably, these observations collectively contribute to the lower heat of fusion of [Glu][BF_4] (48 J g^{-1}) and its inability to undergo recrystallization.

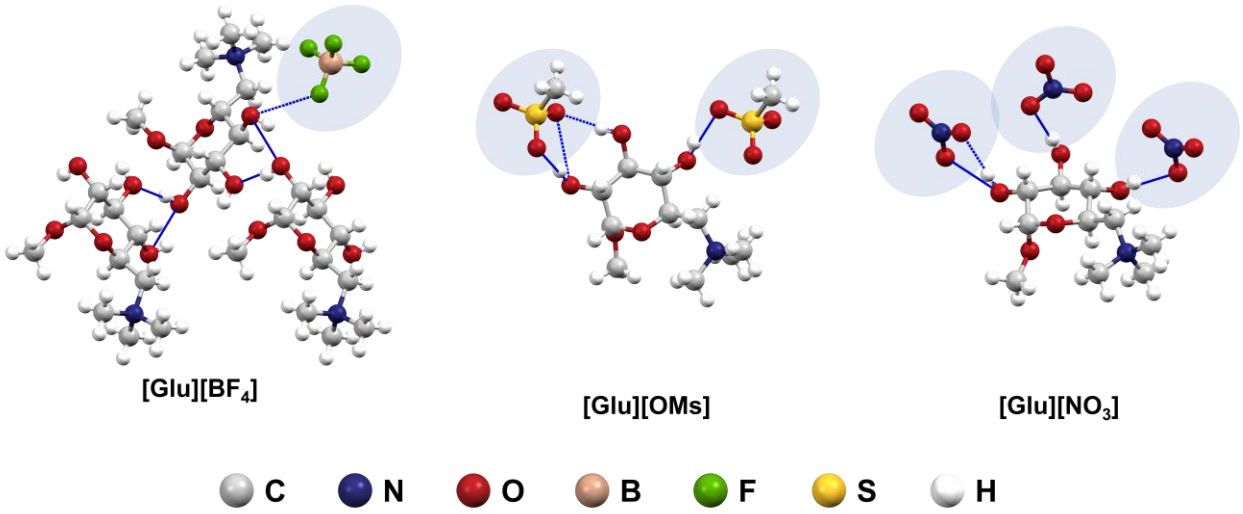

Figure 12. Hydrogen bonds in [Glu][BF4], [Glu][OMs] and [Glu][NO3]. Adapted from [202].

On the other hand, [Glu][OMs] as well as [Glu][NO_3], form 4 unique hydrogen bonds per cation, exclusively involving –OH groups in cations as donors and O atoms in surrounding anions as acceptors (**Figure 12**). Interestingly, both these salts have asymmetric bifurcated hydrogen bonds formed by –OH group at C2, with one bond shorter and more linear than the other. In [Glu][OMs], one cation is bonded to two different anions *via* H-bonds. One of the $[OMs]^-$ anions is bonded by a single H-bond involving the –OH group at C4, while the other $[OMs]^-$ anion is bonded by three H-bonds towards two different O atoms, donated by –OH group at C2 and C3 (including bifurcated bond from –OH group at C2). In [Glu][NO_3] –OH groups at C3 and C4 form a single H-bond with two different $[NO_3]^-$ anions, while the –OH group at C2 serves as a donor in the bifurcated bond to two different O atoms in the third neighboring $[NO_3]^-$ anion. Hydrogen bonds in [Glu][OMs] and [Glu][NO_3] have on average the same length (2.88 Å). This extended hydrogen bonding network provides additional rigidity to the structures in the solid state, resulting in increased values of ΔH_f of 56 and 88 J g^{-1} for $[OMs]^-$ and $[NO_3]^-$ salts respectively (**Table 3**). Both [Glu][OMs] and [Glu][NO_3] can crystallize readily upon cooling, in contrast to MG and [Glu][BF_4]. Based on this

observation, it is speculated that the compounds' ability to crystallize is assisted by the formation H-bonding between cations and anions. Synergy of hydrogen bonds and Coulombic interactions between oppositely charged ions may help to reorganize ions back into the crystal lattice, facilitating the crystallization process.

While comparing lattice structure of the [Glu][NO_3] to unmodified MG (**Figure 13**), the hydrogen bond network is more developed in the latter one. MG forms H-bonds using all 4 –OH groups present in the molecule.[205] In contrast, the salts in [Glu][X] series possess only 3 hydroxyl groups, as the –OH group at C6 was substituted for functionalization purposes. Every molecule in the crystalline MG, interacts *via* 8 hydrogen bonds with 8 adjacent molecules, wherein 4 bonds are unique. Intermolecular H-bonding interactions vary in length from 2.69 to 2.93 Å (avg = 2.76 Å) and angle from 123 to 165° (avg = 153°). The longest bond (2.93 Å), is donated to the neighboring molecule by the –OH group at C4 and at the same time it is the most deviated from 180° (123°), which likely makes it the weakest among all H-bonds in MG.[206] The remaining hydrogen bonds exhibit more favorable geometries, making them considerably stronger and thus contributing significantly to the high ΔH_f value (178 J g^{-1}). The complex H-bonding network along with the poor thermal stability of MG (T_m = 168 °C, T_d = 185 °C) appears to be the main factors behind its inability to undergo recrystallization. Severe supercooling in hydroxyl group-rich molecules, arises due to the numerous hydrogen bonding configurations in the liquid state, and difficulties in their propper rearrangement to form the crystalline state. The interactions between cations and anions presented herein underscore the profound influence of extended hydrogen bonding between these entities on the crystallization process. This phenomenon can be attributed to the additional Coulombic interactions that possess sufficient strength to enable the molecule to stabilize in a fixed position for crystallization. H-bonds in MG result in a 3-D supramolecular network in the crystal state, while the [Glu] salts form 2-D

ribbons, which are not hydrogen-bonded with each other (**Figure 13**). Clearly, the difference in hydrogen bonding interactions is an important contributor to the variance in ΔH_f between MG and the [Glu] salts. The extra dimensionality of the MG structure most likely plays a significant role in its resistance to recrystallization.

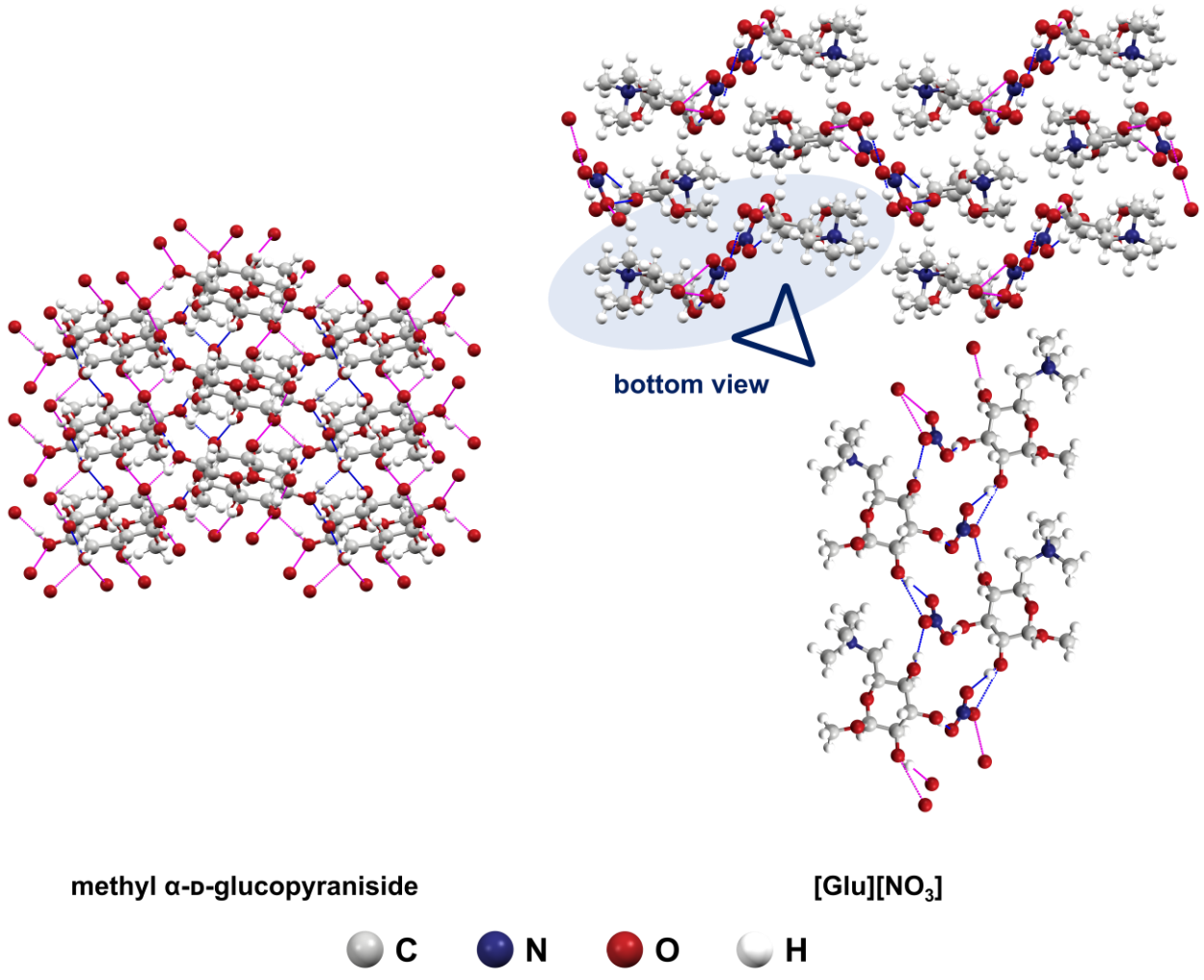

Figure 13. Lattice structure of MG and [Glu][NO_3]; view down the a axis and b axis respectively. Expanded hydrogen bonds are in blue and hanging hydrogen bonds are in magenta. Adapted from [202].

For the analogue series with methylated –OH groups the crystal structures for [TMGlu]Br, [TMGlu][NO_3] and [TMGlu][BF_4] were obtained, while [TMGlu][OMs]

was found to be too hygroscopic to form a single crystal for XRD analysis. Interestingly, the trend in ΔH_f values for the [TMGlu][X] series was opposite to that observed in the [Glu][X] series. For [TMGlu][NO_3], [TMGlu][OMs] and [TMGlu][BF_4], ΔH_f values were as follows: 30, 49 and 66 J g^{-1}. The [Glu][X] series, was expected to have higher values of ΔH_f due to the presence of hydrogen bond network, yet for $[BF_4]^-$ salts it was the opposite. Surprisingly, [TMGlu][BF_4] exhibited a slightly higher ΔH_f value than its [Glu][BF_4] counterpart (66 J g^{-1} and 48 J g^{-1} respectively). As there is no significant contribution of H-bonding to crystal packing in [Glu][BF_4], disruptions to Coulombic interactions may ultimately dictate ΔH_f. The higher ΔH_f for [TMGlu][BF_4] may be explained by the closer distances between the cation and the anion in the crystal lattice, compared to [Glu][BF_4].

Contrary to expectations, the [TMGlu][X] series with methylated –OH groups was observed to be more hygroscopic than the [Glu][X] series with free –OH groups, as showed in the straightforward hygroscopicity test (**Figure 14**). [Glu][NO_3] and [TMGlu][NO_3] salts were extensively dried and left at ambient conditions for 72 h, after which the [TMGlu][NO_3] salt was prone to absorb moisture, in contrary to the sample with free –OH groups. As it was previously demonstrated, the anions used in this study ($[NO_3]^-$, $[OMs]^-$, $[BF_4]^-$) tend to form hydrogen bonds. In the series with free hydroxyl groups ([Glu][X]), H-bonds can be formed between anions and cations, while in the series with methylated hydroxyl groups ([TMGlu][X]) such interactions are not possible. Therefore, it is speculated that the latter series is more susceptible to moisture absorption and forms hydrogen bonds between anions and absorbed water molecules.

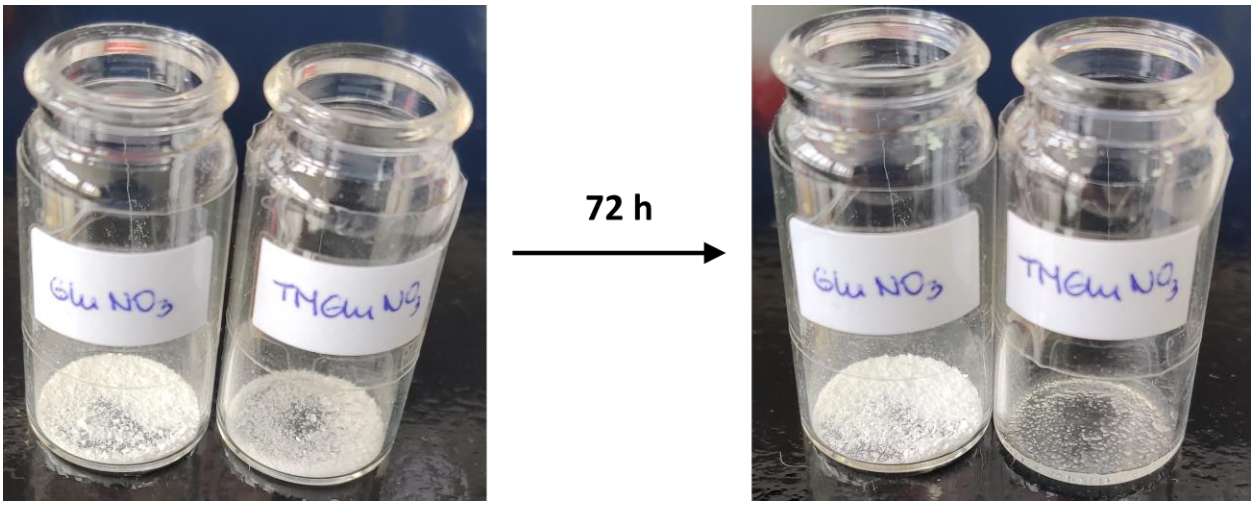

Figure 14. Hygroscopicity test for [Glu][NO₃] and [TMGlu][NO₃]. Adapted from [202].

4.1.7. Hirshfeld surface analysis of glucose-based ionic compounds

The molecular interactions in the investigated glucose-derived salts were further evaluated using Hirshfeld surface analysis. This analytical tool helps to visualize and quantify these interactions by generating a fingerprint plot using CrystalExplorer software, developed by Spackman and co-workers[207,208]. Generated 3-dimentional surface depicts distances from nuclei internal to the surface to the nearest nuclei external to the surface. Close contact interactions are marked in red, while the longer interactions are shown in blue. The disruption of the close contact interactions during melting likely contributes significantly to ΔH_f.[147]

When comparing the Hirshfield surfaces created for [Glu][BF_4], [Glu][OMs], [Glu][NO_3] and MG, it becomes evident that the $[BF_4]^-$ anion itself does make a substantial contribution to ΔH_f, evidenced by only very small red spots observed on its surface (**Figure 15**). In [Glu][BF_4], large red spots are present exclusively next to the C2 and C3 –OH groups, similarly, to MG, which also has large red spots next to the C2, C3 and C6 –OH groups, confirming that H-bonding interactions between sugar moieties (cations)

in [Glu][BF_4] are predominant. Conversely, in [Glu][OMs] and [Glu][NO_3] large red spots are located next to anions and –OH groups, which are engaged in H-bonds formation. The [TMGlu]Br salt, which cannot form any H-bonds, has only tiny red spots distributed across the surface.

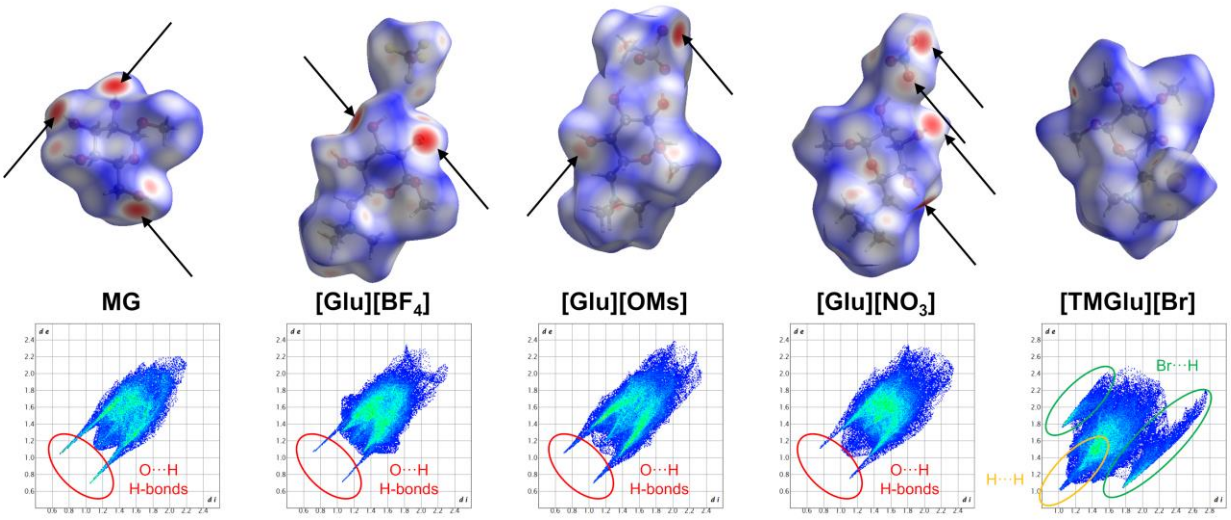

Figure 15. Hirshfeld surface area and fingerprint plots of MG, [Glu][BF_4], [Glu][OMs], [Glu][NO_3] and [TMGlu]Br. Black arrows point out the parts of the Hirshfeld surface, where intermolecular interactions are the closest. Adapted from [202].

Hirshfeld surface area can also be translated into a unique 2-dimensional histogram, which can be considered as a fingerprint of a compound. The axes in the histogram represent the distance between the internal nuclei (di) and the external nuclei (de) to the surface (**Figure 15**). The frequency of interactions occurrence between two nuclei at certain distance is shown in different colors spanning from blue (low frequency) to red (high frequency). Moreover, some characteristic patterns can be distinguished depending on the interaction of various atoms. For example, compounds with free –OH groups have two distinct spikes (marked with red ellipses) in each plot, denoting the presence of H-bonds. Notably, in the MG histogram, these

spikes appear lighter blue in color compared to the ionic compounds, signifying a higher occurrence of O–H···O interactions in the unmodified carbohydrate crystal structure. For [TMGlu]Br, instead of two spikes, a single spike is observed, which represents H···H interactions. This result is consistent with the structure of [TMGlu]Br, in which all the –OH groups were transformed into $–OCH_3$, resulting in the occurrence of H···H interactions at shorter distances. In addition, there are two characteristic areas marked with green ellipses in **Figure 15**, which correspond to Br···H interactions.

It is possible to break down the Hirshfeld surface area into a percentage contribution of the specific interactions between different atom nuclei. In the [Glu][X] series, $[Glu][NO_3]$ exhibits a higher overall contribution of O···H interactions (total of $O_{in}···H_{out}$ plus $H_{in}···O_{out}$) than [Glu][OMs] (54 and 44% respectively) (**Figure 16**). In contrast, $[Glu][BF_4]$ reaches only 18% for this interaction type, with F···H interactions more prevalent (43%). A comparison between $[TMGlu][BF_4]$ and $[Glu][BF_4]$ as well as $[TMGlu][NO_3]$ and $[Glu][NO_3]$, clearly reveals a lower percentage of H···H interactions in the compounds featuring free –OH groups. For $[TMGlu][NO_3]$ and $[TMGlu][BF_4]$ crystal structures were obtained, where one in two anions were refined with disorder. Therefore, for generation of their Hirshfeld surface areas, two ion pairs were used to obtain an approximation of the interactions in the overall structure.

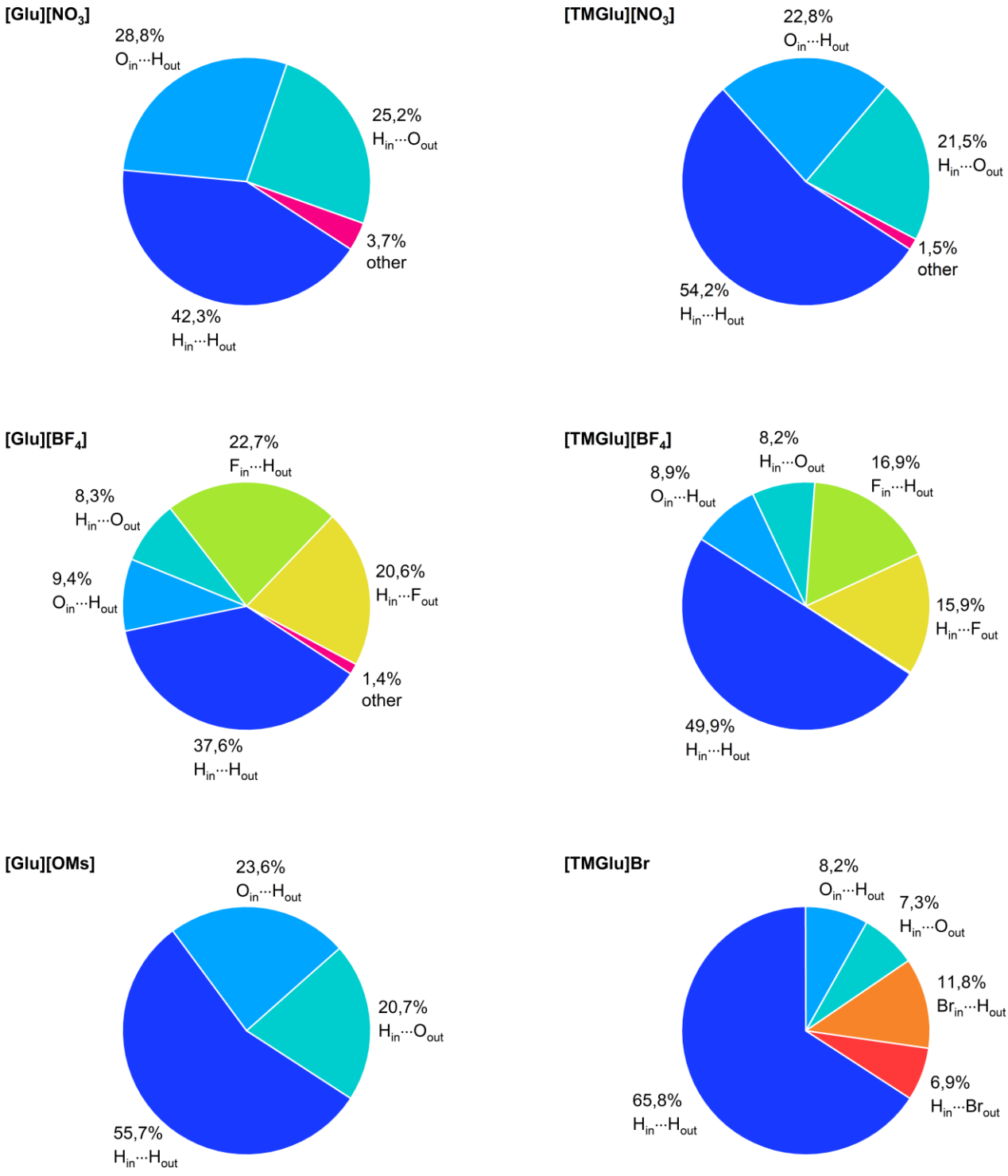

Figure 16. Percentage contribution of interactions between nuclei inside the Hirshfeld surface and nuclei outside the surface in [Glu][NO3], [Glu][BF4], [Glu][OMs], [TMGlu][NO3], [TMGlu][BF4] and [TMGlu]Br. Adapted from [202].

4.1.8. Hydrates (Confidential part)

4.1.9. Mannitol-derived organic salts as phase change materials

D-Mannitol consisting of six carbon atoms, is widely distributed in nature among others in olive trees, plane trees, and various fruits and vegetables. Additionally, numerous fungi and bacteria have the capability to synthesize this polyol from glucose, fructose, or sucrose.[252] Industrial production of mannitol typically involves fructose, fructose syrups, or sucrose as a feedstock. Catalytic hydrogenation is carried under high pressure in the presence of Raney nickel catalysts. Furthermore, D-glucose can be epimerized to D-mannose, which is subsequently hydrogenated directly to D-mannitol. It is commonly utilized in food industry as a sweetener and texturizer.

Encouraged by the results obtained for methyl *α*-D-glucopyranoside, the novel strategy to facilitate the crystallization of sugars by introducing additional Coulombic interactions was further investigated for linear sugar alcohol - D-mannitol. D-Mannitol reveals higher ΔH_f value (277 J g^{-1})[147] than glucopyranoside (178 J g^{-1})[202], due to its linear structure and the ability to form strong H-bonding interactions in the solid state.

4.1.10. Synthesis of mannitol-based phase change materials

A series of ionic compounds bearing D-mannitol-based cation and four anions i.e. Br^-, $[NO_3]^-$, $[OMs]^-$ and $[BF_4]^-$ was prepared. Transformation of sugar alcohol into ionic derivatives proved to be considerably more complicated, primarily due to its lower reactivity and poor solubility in organic solvents in comparison to methyl *α*-D-glucopyranoside. So far only the transformation of D-mannitol into organic salts having tosylate anions has been reported. Nevertheless, this method could not be applied

for the synthesis of salts with Br^-, $[NO_3]^-$, $[OMs]^-$ and $[BF_4]^-$ anions. According to the procedure reported by Thomas *et al.*[54] D-mannitol was tosylated to yield a 1,6 -*O,O'*-ditosyl derivative followed by quaternization with various amines, to give polycationic salts containing solely tosylate anions or mixtures of tosylate and halide anions. Further metathesis of tosylate anions is not feasible. To tackle this challenge and obtain ionic compounds based on sugar alcohol with the desired anions, bromination of D-mannitol was performed as the primary step instead of tosylation. The bromide anion can be further exchanged to different anions such as $[NO_3]^-$, $[OMs]^-$ and $[BF_4]^-$, as presented for methyl *α*-D-glucopyranoside derivatives. The synthesis of 1,6-dibromo-derivatives of D-mannitol and sorbitol (glucitol) using acetyl bromide was previously reported by Crombez-Robert *et al*.[253]

To prepare [Man][X] series (**Figure 17**) according to this method, the 2,3,4,5-tetra-*O*-acetyl-1,6-dibromo-1,6-dideoxy-D-mannitol (**16**) was obtained *via* bromination of D-mannitol in position 1 and 6 using acetyl bromide as a halogenating agent, followed by subsequent acetylation (**Figure 18**). Reaction was carried out in dry dioxane for 72 h at rt. The acetylation step was conducted *in situ*, without purification of intermediate 1,6-dibromo-1,6-dideoxy-D-mannitol to facilitate the purification process, according to previously described procedure.[253]

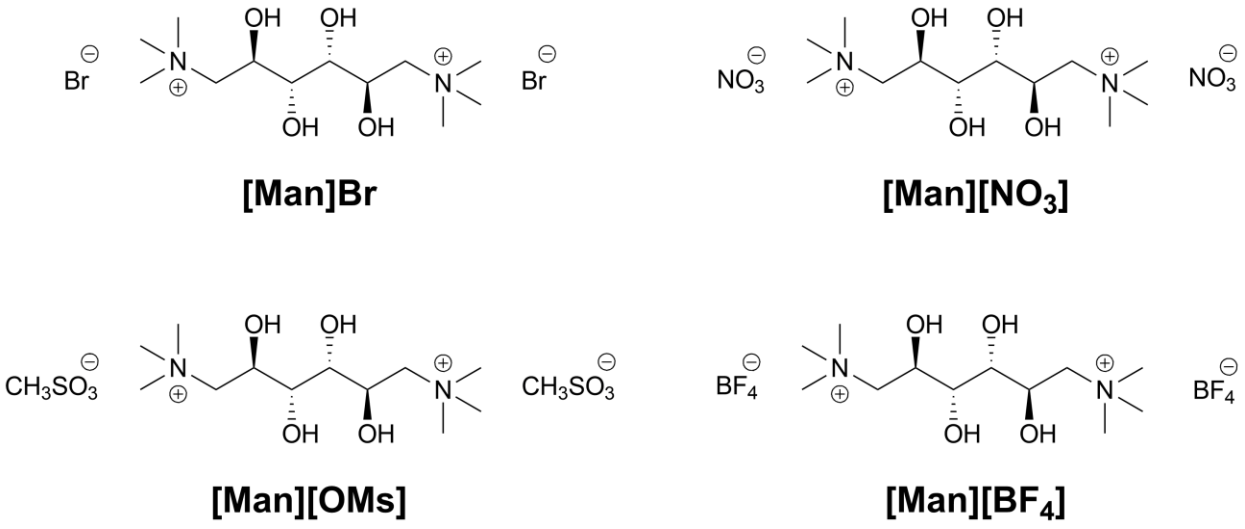

Figure 17. Sugar-based ionic compounds derived from D-mannitol (Man).

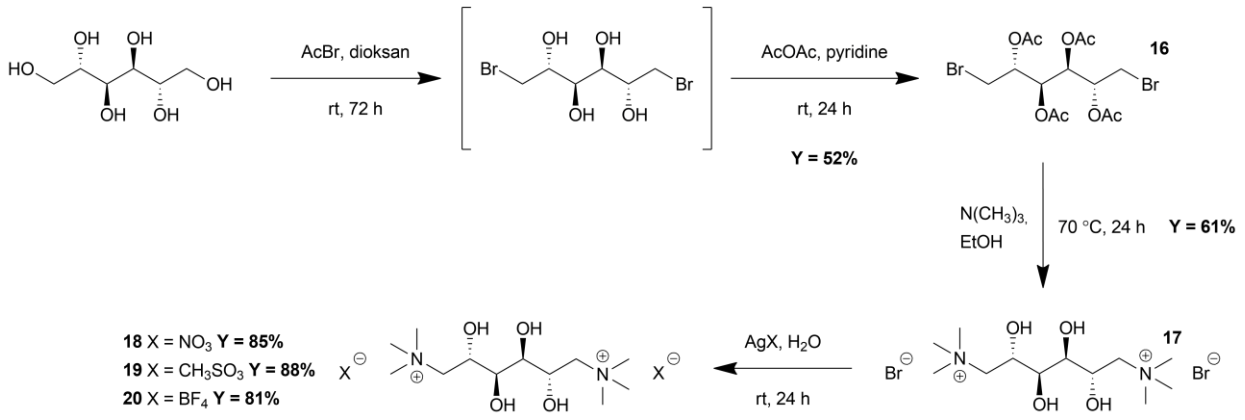

Figure 18. Synthetic procedure for [Man][X] series preparation.

As the result of the bromination reaction dibromo- and tribromo- derivatives were formed. Purification by column chromatography using hexane:EA 3:1 mixture as eluent was applied to isolate desired 1,6-dibromo-derivative with 52% yield. 2,3,4,5-tetra-*O*-acetyl-1,6-dibromo-1,6-dideoxy-D-mannitol (**16**) was then quaternized with trimethylamine (33% wt. ethanolic solution) in an autoclave for 24 h at 70 °C, yielding [Man]Br (**17**) (Y = 62%). Under the reaction conditions, the acyl groups were removed resulting in the ionic product with free hydroxyl groups. [Man]Br

was then subjected to anion metathesis, according to a previously described procedures, applied in the synthesis of glucose-based ionic salts. Dicationic D-mannitol-based salts [Man][NO_3] (**18**), [Man][OMs] (**19**) and [Man][BF_4] (**20**) were obtained with the yields of 86%, 88% and 81%, respectively.

4.1.11. Thermal properties of mannitol-based ionic compounds

The thermal properties of non-ionic precursor (D-mannitol (Man)) and [Man][X] series were investigated using differential scanning calorimetry (DSC). Melting temperature (T_m), enthalpy of fusion (ΔH_f), crystallization temperature (T_c) and enthalpy of crystallization (ΔH_c) were estimated based on DSC results. The decomposition onset was determined by thermogravimetric analysis (TGA). All of the data have been collected in **Table 4**.

Table 4. Physical properties of D-mannitol (Man), D-mannitol-based ionic compounds. (cc) – cold crystallization

Compound	T_m [°C]±2°C	ΔH_f [J g^{-1}]±5%	T_c [°C]±2°C	ΔH_c [J g^{-1}]±5%	T_d [°C]
Man	169	289	111	227	254
[Man]Br	280	154	-	-	222
[Man][NO_3]	221	80	149	53	214
[Man][OMs]	262	140	107 (cc)	61 (cc)	278
[Man][BF_4]	186	70	111 (cc)	42 (cc)	245

ΔH_f, T_m, ΔH_c and T_c values obtained for D-mannitol (289 J g^{-1}, 169 °C, 227 J g^{-1} and 111°C, respectively) are consistent with the data previously reported in the literature[154] (277 J g^{-1}, 166 °C, 228 J g^{-1} and 114°C). In other work by Solé *et al.*[254] initial values of ΔH_f and T_m for D-mannitol are slightly lower (235 J g^{-1} and 151 °C, respectively), but still comparable.

In the [Man] series, all salts except for [Man][OMs] revealed lower T_d values compared to unmodified D-mannitol (254 °C) (222, 214, 278 and 245 °C for [Man][Br], [Man][NO_3], [Man][OMs] and [Man][BF_4], respectively), what makes it comparable to the [TMGlu] series. Conversely, in the [Glu] series, the increase in T_d with respect to the starting material was valid for all of the salts except for [Glu][BF_4]. Obtained D-mannitol-based salts containing Br^-, $[NO_3]^-$, $[OMs]^-$ and $[BF_4]^-$ anions, had ΔH_f values spanning from 70 to 154 J g^{-1} and displayed T_m values within a range of 189 – 280 °C which is much higher than for the [Glu] series. D-Mannitol has a higher ΔH_f value than methyl α-D-glucopyranoside (289 and 178 J g^{-1}, respectively), so it is not surprising that D-mannitol-based salts containing Br^-, $[OMs]^-$ and $[BF_4]^-$ anions, also have higher melting enthalpies (154, 140, 70 J g^{-1}, respectively) than their counterparts from the [Glu][X] series (109, 59, 48 J g^{-1}, respectively). The only exception was nitrate salt, which shows ΔH_f value of 80 J g^{-1} , which is lower than that reported for [Glu][NO_3] (88 J g^{-1}). The possible reason behind it will be explained, based on the crystallography analysis.

[Man]Br did not show any crystallization, similarly to [Glu]Br, and no endothermic transition was observed prior to decomposition (T_d = 222 °C) (**Table 4**). In fact, the endothermic peak observed at 280 °C, could be a result of melting and decomposition overlap, or exclusively decomposition. For [Man][NO_3] endothermic peak is observed at 221 °C, which also exceeds T_d (214 °C) determined *via* TGA, but the difference here is less profound, than in case of [Man]Br. Nevertheless, the ΔH_f values for all three salts were significantly decreasing with each heating/cooling cycle and none of the obtained salts in the [Man] series was stable enough to endure thermal cycling. For [Man][OMs] and [Man][BF_4] crystallization occurred only during heating cycle (cold crystallization). Even though, the strategy applied that involved use of linear sugar alcohol instead of cyclic methyl α-D-glucopyranoside seems to have a positive

influence on ΔH_f values as expected, the salts obtained turned out to be unstable during cycling. The reason for this instability can be most probably ascribed to very high T_m values (186 – 280 °C) of the mannitol derivatives which is close to their T_d values (214 – 278 °C). To better understand the structure-property relationship, obtained salts were further investigated using single crystal X-ray diffraction (XRD).

4.1.12. Crystallographic analysis of mannitol-based ionic compounds

Crystallographic structures were successfully obtained for [Man]Br, [Man][NO_3] and [Man][OMs] (**Figure 19**). [Man][BF_4] crystallized only with ethanol molecules, trapped within its crystal lattice (anhydrous ethanol was used as a solvent to prepare single crystals of [Man][BF_4], used in the XRD experiment), therefore it was excluded from direct structure comparison with the remaining salts. [Man]Br was the only salt in the [Man] series, which does not form any H-bonds in the solid state (even between cations), despite the presence of free –OH groups. The cations in the crystal lattice are effectively separated by bulky –$N^+(CH_3)_3$ groups and large Br^- anions, resulting in large distances between the –OH groups (**Figure 19**). In [Man][NO_3] every cation forms 4 unique hydrogen bonds. Three of these bonds are formed between the cation and two adjacent $[NO_3]^-$ anions. One of these anions is an acceptor of H-bonds from the –OH groups attached to C2 and C4 (2.71 Å, 165° and 2.79 Å, 165° respectively), while the other is held by the –OH group at C5 (2.73 Å, 175°). Moreover the –OH group at C3 forms a H-bond to the neighboring cation (2.80 Å, 160°) and the –OH group at C5 is an acceptor of the H-bond from the other cation. On the other hand, in [Man][OMs], all of the –OH groups donate H-bonds to surrounding $[OMs]^-$ anions, each –OH group to one of four anions, forming four unique hydrogen bonds. In both [Man][OMs] and [Man][NO_3] average D-H···A length and angles are comparable (2.74 Å, 169° and 2.76 Å, 166°

respectively). In the [Man][X] series, ΔH_f increase as follows: [Man][BF_4] < [Man][NO_3] < [Man][OMs] < [Man]Br (with ΔH_f of 70, 80, 140 and 154 J g^{-1} respectively). In line with the results obtained for the cyclic derivatives, in the series of D-mannitol-based salts, the best crystallization behavior was observed for [Man][OMs] which shows the highest number of H-bonds between the cation and the anion (**Figure 19**). Most probably, this result supports the thesis that the ability to recrystallize is assisted by the H-bond formation between cations and anions in the solid state. Interestingly, in the series of methyl α-D-glucopyranoside-based salts, the highest number of H-bonds between cations and anions was observed for [Glu][NO_3] while in case of D-mannitol derivatives for [Man][OMs]. This example shows that structure-property relationships are hard to predict and depending on the cation structure, different anions may promote recrystallization.

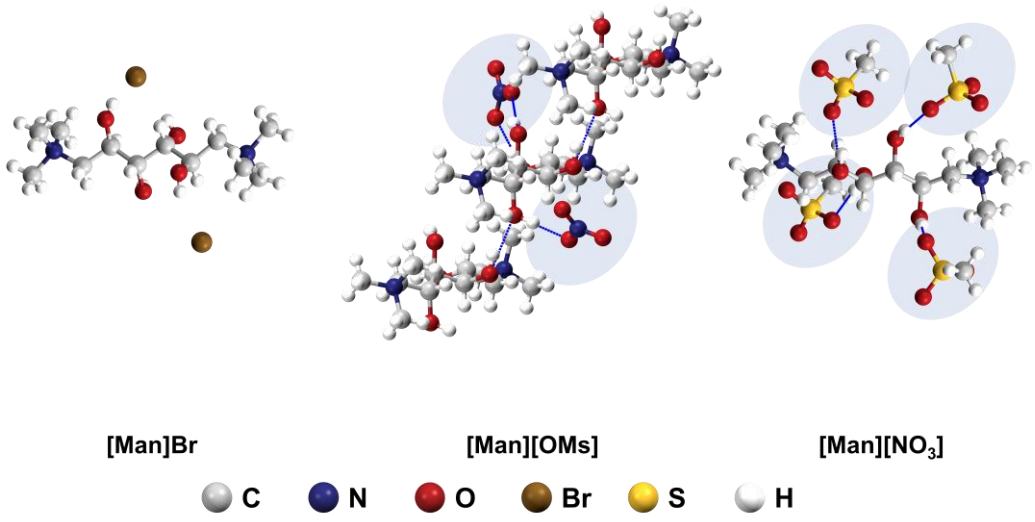

Figure 19. Hydrogen bonds in [Man]Br, [Man][OMs] and [Man][NO_3].

Similarly to MG, unmodified D-mannitol forms supramolecular hydrogen bond network, utilizing all of the –OH groups (**Figure 20**).[255] Each molecule participates in intermolecular hydrogen bonding interactions that span in length from 2.65 to 2.72 Å (avg = 2.69 Å) and angle from 166 to 175° (avg = 170°). In this network, all the –OH groups function as both donors and acceptors, and each molecule forms 6 unique H-bonds, interacting with 8 neighboring molecules. Those bonds on average are shorter and closer to 180° than in MG (avg = 2.76 Å, avg = 153°). Moreover, D-mannitol possess 6 –OH groups, while MG has only 4, hence facilitating the formation of the H-bonds, resulting in significantly higher ΔH_f value (289 and 178 J g^{-1}, respectively). On the other hand, [Man][OMs] and [Man][NO_3] form ribbons of ions hydrogen-bonded to each other as shown for [Man][OMs] in **Figure 20**. Alike in [Glu][X] series (**Figure 13**), those ribbons do not interact with one another *via* H-bonds.

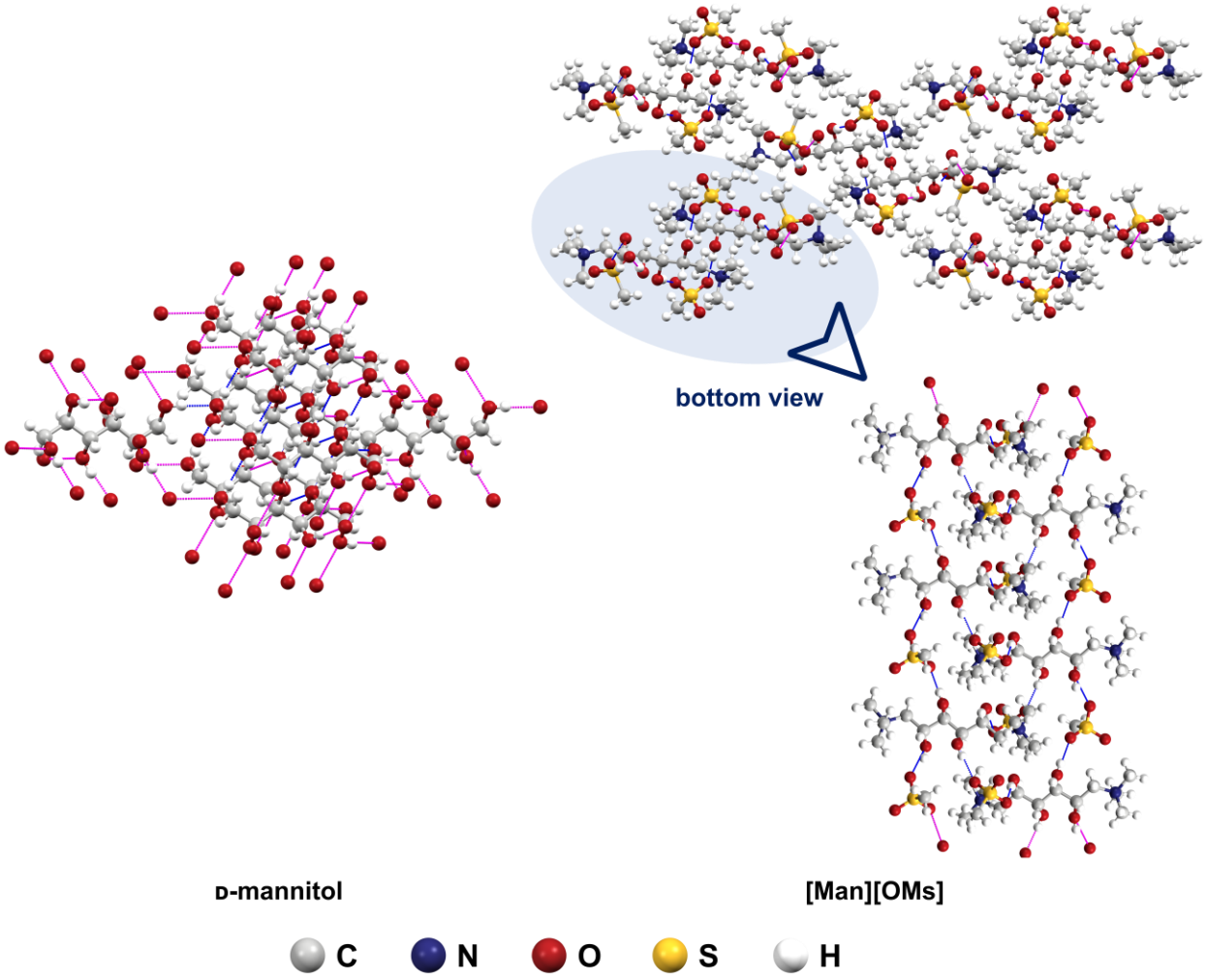

Figure 20. Lattice structure of Man and [Man][OMs]; view down the a axis and b axis respectively. Expanded hydrogen bonds are in blue and hanging hydrogen bonds are in magenta.

4.1.13. Hirshfeld surface analysis of mannitol-based ionic compounds

Comparing the Hirshfield surfaces created for D-mannitol, [Man][BF_4], [Man][OMs], [Man][NO_3] and [Man]Br, it can be observed that the D-mannitol in the solid state has the most significant contribution of close-contact intermolecular interactions, which are responsible for its exceptionally high ΔH_f (289 J g^{-1}) (**Figure 21**). Large red dots are visible next to each –OH group present in mannitol, showing that H-bond interactions between molecules have the main contribution to ΔH_f. In case of [Man]Br, large red dots

are present only next to –OH groups located near Br^- anions, however, those interactions are quite long, with O–H···Br length >3.2 Å, therefore they cannot be clearly identified as H-bonds. In [Man][NO_3] large red dots are located next to –OH, which form H-bonds to nearby cations, indicating that cation-cation interactions are more dominant than cation-anion interactions. For [Man][OMs], which has the best crystallizability, large red dots are in the proximity of the –OH groups in the cation and next to the oxygen atoms in the $[OMs]^-$ anion, which confirms strong H-bond interactions between oppositely charged ions, facilitating crystallization. Nevertheless, as discussed above, the high T_m value of [Man][OMs] (262 °C) is most probably responsible for its decomposition during cycling (unmodified D-mannitol melts at 169 °C). These results are in line with the conclusion of the investigation of [Glu][X] series.

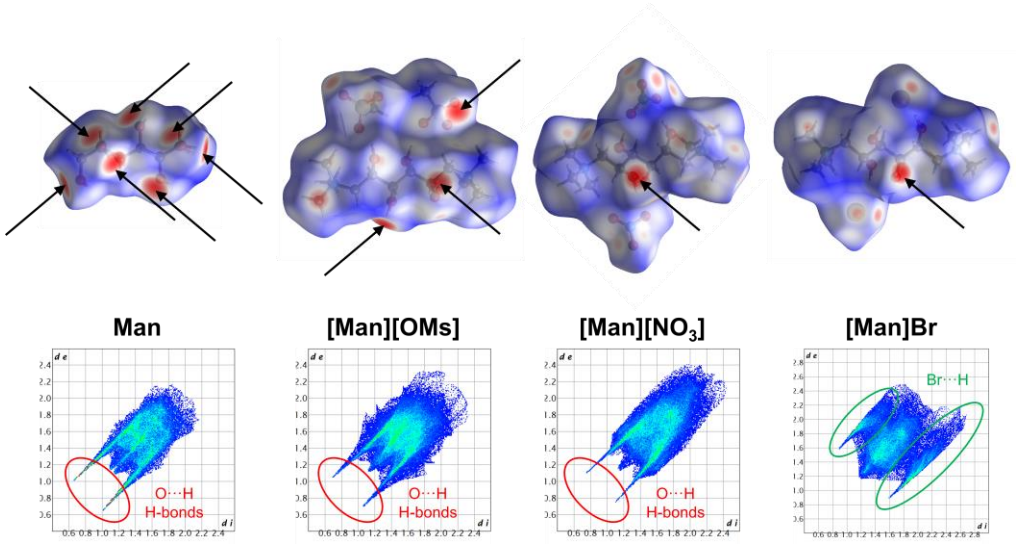

Figure 21. Hirshfeld surface area and fingerprint plots of Man, [Man][OMs], [Man][NO_3] and [Man]Br. Black arrows point out the parts of the Hirshfeld surface, where intermolecular interactions are the closest.

Comparing 2-dimensional histograms for the [Man] series, in case of [Man]Br, notably there are no characteristic spikes for H···O interactions (marked with red ellipses, indicating the presence of H-bonds) (**Figure 21**). [Man]Br has the lowest contribution

of O···H interactions (total of O_{in}···H_{out} plus H_{in}···O_{out}) in the series, totaling 12%, while for [Man][OMs], [Man][NO_3] or D-mannitol they account to >45%. In [Man]Br, the additional Br···H interactions are present and are highlighted with green ellipses (**Figure 21**).

4.1.14. Conclusions

This chapter was divided into public and confidential parts, therefore confidential parts were removed from this version of the doctoral thesis.

Taking into consideration the urgent need for the development of efficient and economical energy storage solutions and the large potential of sugar derivatives (e.g. sugar alcohols) in this application, novel carbohydrate-derived organic salts have been investigated as PCMs. Applying the strategy of transforming the model sugar derivatives (methyl-α-D-glucopyranoside and D-mannitol) into ionic compounds enhanced crystallization. Taking insight into the molecular interactions of the investigated organic salts in the solid state, it was found that the interplay between the anion and the cation *via* hydrogen bonding plays a key role in the crystallization process. The developed H-bonding network between the ionic species, facilitated the crystallization, through assisting the arrangement of ions back into the crystal lattice. Additional Coulombic interactions are likely the reason why hydrogen bonding between anions and cations is superior in terms of crystallizability over O–H···O bonds present between neutral molecules of carbohydrates and their non-ionic natural derivatives. In the [Glu] series, the introduction of the $[NO_3]^-$ anion formed the highest number of H-bonds with the cation while in the Man series, it was the $[OMs]^-$ anion. Nevertheless, the transformation of the model compounds into ionic species decreased ΔH_f resulting from the decreased number of H-bonds compared to unmodified sugar derivatives.

(Confidential part)

The results discussed demonstrate the significant, yet underexplored, potential of carbohydrate-derived organic salts as phase change materials (PCMs). Nevertheless, to fully harness the potential of the renewable and cost-effective sugars for development of sustainable PCMs, future research should focus on two key areas: 1) optimizing molecular design to promote ΔH_f and stability of the salts; 2) creating sustainable synthesis methods that align with Green Chemistry principles that preferably avoid purification steps like column chromatography and minimize the use of hazardous reagents and solvents. Such sustainable procedures for the development of sugar-derived organic salts have already been reported.[48] Moreover, future work should explore the development of low-cost protic salts, where anion incorporation does not involve silver salts, thus avoiding silver waste. Alternatively, sodium salts can be used for anion exchange, presenting another sustainable route.

Despite significant advancements in bio-derived[49,256] and sugar-based ILs and organic salts[48,76,78] over the past decade, the strongest emphasis has been focused on the understanding the structure–property relationships regarding their ability to form a liquid phase. Given the vast possibilities in sugar chemistry, there is still room for innovation, including experimenting with different sugar precursors and functionalization techniques to generate salts that form specific hydrogen-bonding networks. By correlating thermal properties with molecular structure (molecular interactions in specific), new efficient bio-derived systems for sustainable PCMs could be designed. Such advancements would support large-scale renewable energy storage applications, such as Carnot batteries, significantly reducing reliance on fossil fuels for electricity generation.[257]

The results on [Glu] and [TMGlu] series have been described in the research paper "*Transforming Sugars into Salts – A Novel Strategy to Reduce Supercooling in Polyol Phase-*

Change Materials", published in *ACS Sustainable Chemistry and Engineering*.[202] The data were collected at Monash University, thanks to the courtesy of Prof Douglas R. MacFarlane and Dr Karolina Matuszek.

4.2. Carbohydrate-based ionic liquids as N-doped carbon materials precursors

4.2.1. Introduction

Carbon materials were employed in diverse fields that include wastewater treatment, gas capture and storage, catalysis, sensing, separation, as electrode materials or electrocatalysts for energy conversion and storage. This is mainly due to their versatile characteristics such as high surface areas, electrical conductivity, low cost and exceptional chemical, mechanical, and thermal stability.[258–260] These materials are produced through the carbonization process, which relies on the thermal treatment of suitable precursors such as organic matter and polymers. During the process, a number of reactions occur, such as: elimination (e.g. H_2, H_2O, N_2, CO_2), polycondensation, polymerization and aromatization. The obtained product has a high carbon content, but may also contain heteroatoms that affect the properties of the obtained material.[138,261] Doping carbon materials with heteroatoms (such as N, B, P, F, or S) that either donate or withdraw electrons offers fine-tuning and controlling their physicochemical properties. This includes enhancing their electrical conductivity, basicity, oxidation resistance, and catalytic activity (both electrochemical and chemical).[137] The chemical composition of the precursor often leaves a distinct imprint on the resulting carbon structure, exerting substantial influence on characteristics such as carbon yield, porosity, surface area, graphitization, conductivity, and heteroatom doping. It should be noted that many organic compounds are entirely volatilized or decomposed into gaseous byproducts

during high-temperature treatment. At the beginning of the 21st century, the range of available precursors remained relatively restricted, primarily encompassing low-vapor-pressure natural or synthetic polymers.[262] Recently, considerable attention is being directed toward the carbonization of biomass, because of the economic, plentiful, and sustainable nature of this carbon source. Various feedstocks, including saccharides, cellulose, and lignin are used to yield carbon residues during biological, chemical, or thermochemical processes.[263] However, carbon materials derived from natural precursors, usually suffer from underdeveloped surface area and insufficient doping level. One of the approaches to tailor the properties of carbon materials derived from biomass is by employing ionic liquids (ILs).

Ionic liquids (ILs) have gained significant interest in the field of carbon materials synthesis because of their distinctive properties. ILs exhibit several unique features, such as: ability to remain in a liquid state across a wide temperature range, capacity to dissolve many substances, low vapor pressure along with high thermal stability. Moreover, ILs offer small-molecular carbon-rich structures, with N functionalities and tunability originating from countless cation/anion combinations, which paved their way in the synthesis of advanced and functional carbon materials. ILs can function as solvents for biomass during thermal treatment, sources of heteroatoms, stabilizing agents, pore-generating agents, or even serve as precursors of carbon materials themselves.[79,264,265]

Recently, there has been significant interest in the exploration of bio-derived ionic liquids (ILs) as sustainable alternatives to traditional ILs, often derived from fossil fuels. These bio-derived ILs combine the characteristics of biomass, such as its high carbon content, with the properties of ILs, which include excellent thermal stability, low vapor pressure, and nitrogen-rich molecular structures. During thermal treatment, nitrogen atoms can be equally distributed in the carbon structure through an *in situ* self-assembly

process.[266] Various biomass sources, ranging from amino acids[267–269], carbohydrates[79], glucamine[266], alginic acid[270], cellulose[271], and furfurylamine[272], have been successfully transformed into ILs and employed as precursors for *N*-doped carbon materials. By designing the precursor structures at the molecular level, the resulting carbonaceous materials properties, such as the *N*-doping level, carbonization yield and the surface properties, can be precisely controlled.[79,273]

4.2.2. Goal of the research

The purpose of this study was to transform methyl *α*-D-glucopyranoside into a quaternary ammonium cation and combine it with various cross-linkable cyano group-containing anions ($[SCN]^-$, $[DCA]^-$, $[TCM]^-$ and $[TCB]^-$). Moreover, the properties of the precursors themselves, as well as the influence of the structure of the precursors on the properties of the final carbon materials, such as carbon yield and heteroatom doping were investigated. The resulting carbon materials were also evaluated as electrocatalysts for the oxygen reduction reaction (ORR).

4.2.3. Synthesis of the *N*-doped carbon materials' precursors

N-(methyl-6-deoxy-*α*-D-glucopyranoside-6-yl)-*N*,*N*,*N*-trimethylammonium bromide ([Glu]Br) (**10**) was used for the synthesis of carbohydrate-based ionic compounds, which were used as precursors of *N*-doped carbon materials. The synthesis of [Glu]Br was described in Chapter 4.1.3. [Glu]Br was subjected to anion metathesis to incorporate bis(trifluoromethanesulfonyl)imide anion ($[NTf_2]^-$) or cross-linkable

cyano-based anions such as thiocyanate ([SCN]⁻), dicyanamide ([DCA]⁻), tricyanomethanide ([TCM]⁻) and tetracyanoborate ([TCB]⁻) (**Figure 22**).

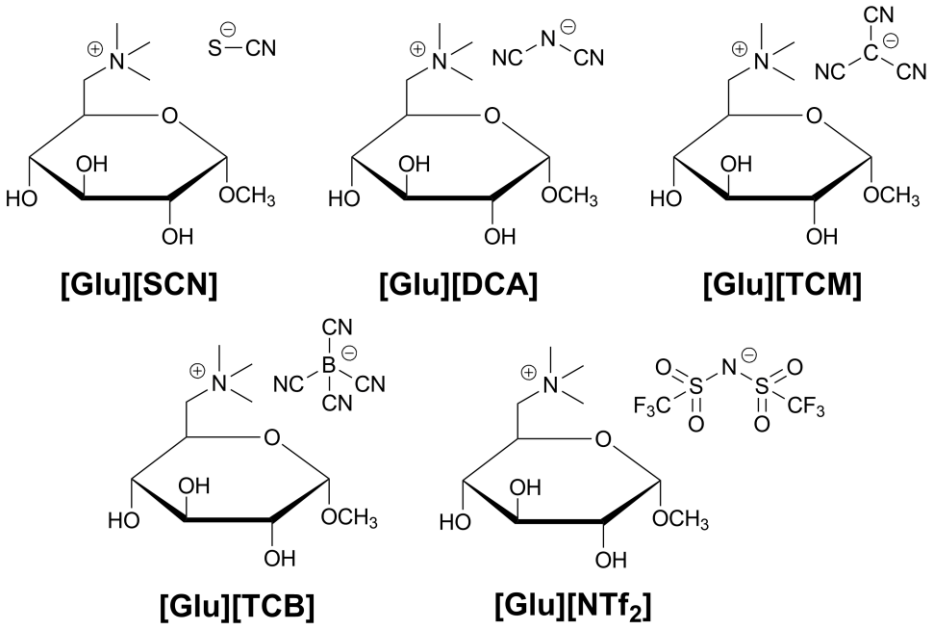

Figure 22. Structures of carbohydrate-based N-doped carbon materials' precursors.

These cyano group-containing anions are known to act as both a carbon source and a *N*-doping agent. Anion metathesis was carried out with silver salts containing [SCN]⁻, [DCA]⁻, [TCM]⁻ and [TCB]⁻ anions (**Figure 23**).[274] The salts were prepared from the corresponding potassium or sodium salts (KSCN, $NaN(CN)_2$, $KC(CN)_3$, $K(CN)_4$) and $AgNO_3$, yielding [Glu][SCN] (**21**), [Glu][DCA] (**22**), [Glu][TCM] (**23**) and [Glu][TCB] (**24**), respectively.

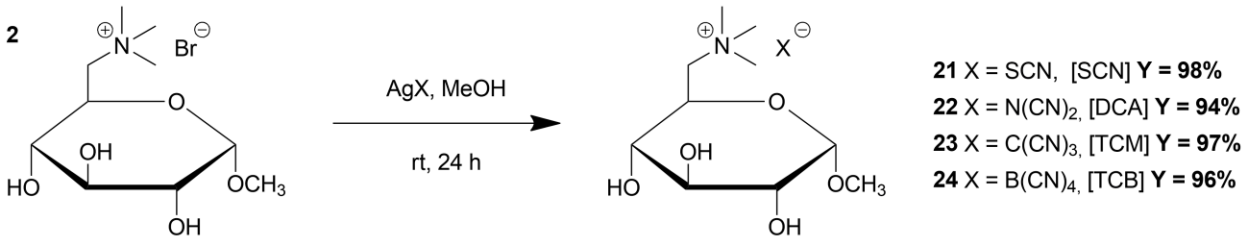

Figure 23. Synthesis of carbohydrate-based ionic compounds containing cyano-based anions.

For comparison, salt, containing the $[NTf_2]^-$ anion ([Glu][NTf_2]) (**25**) that is known as pore generating agents was prepared according to the procedure described previously by our group (**Figure 24**).[79]

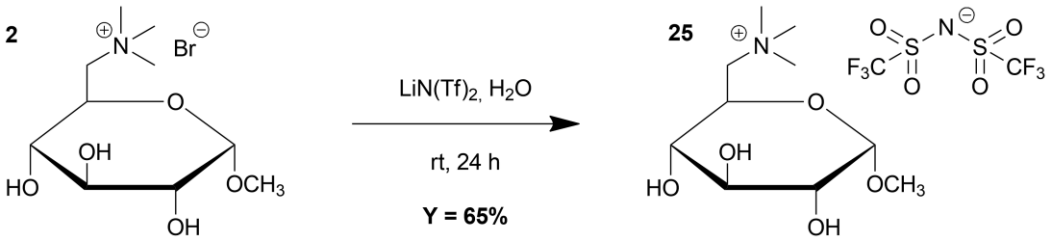

Figure 24. Synthesis of [Glu][NTf_2].

4.2.4. Thermal properties of the precursors

The carbohydrate-based ionic compounds containing various anions such as thiocyanate ($[SCN]^-$), dicyanamide ($[DCA]^-$), tricyanomethanide ($[TCM]^-$), tetracyanoborate ($[TCB]^-$) and bis(trifluoromethanesulfonyl)imide ($[NTf_2]^-$) anions were subjected to thermogravimetric analysis (TGA). Thermal stability is a crucial factor in the carbonization process's efficiency and TGA analysis helps to assess it. The thermal properties were further investigated using differential scanning calorimetry (DSC). The analysis was carried out in the range of 25 – 1000 °C. Based on the melting

temperatures, the precursors obtained were categorized into two groups: ionic liquids (ILs) with melting temperatures below 100 °C ([Glu][TCB], [Glu][TCM], [Glu][NTf_2]) and salts with melting temperatures exceeding 100 °C ([Glu][DCA], [Glu][SCN]). TGA and DSC results have been summarized in **Table 5** and **Figure 25**.

Table 5. Thermal properties of carbohydrate-based ILs and salts. Adapted from [274].

Compound	T_g [°C]±2°C	T_m [°C]±2°C	T_d [°C]	Appearance
[Glu][SCN]	23	173	229	solid
[Glu][DCA]	10	123	232	solid
[Glu][TCM]	-10	-	255	liquid, hygroscopic
[Glu][TCB]	-5	76	308	solid, hydroscopic
[Glu][NTf_2]	-	-	306	liquid

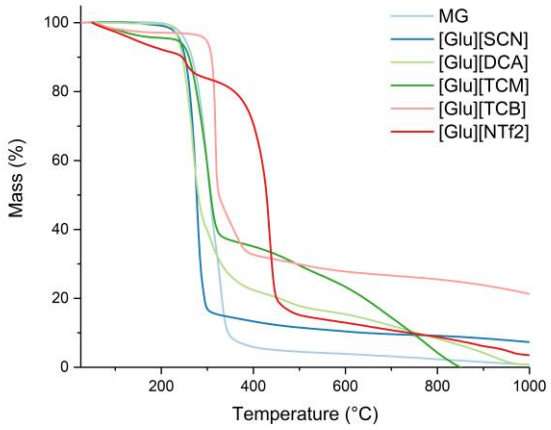

Figure 25. TGA of carbohydrate-based ILs and salts. Adapted from [274].

The decomposition temperature of methyl-α-D-glucopyranoside (MG) was 185°C, while for obtained ionic compounds [Glu][SCN], [Glu][DCA], [Glu][TCM], [Glu][TCB] and [Glu][NTf_2] T_d values were 229 °C, 232 °C, 255 °C, 308 °C and 306 °C, respectively (**Table 5**). Combining glucopyranoside-based cation with cross-linkable, cyano-based

anions, allowed to increase the thermal stability of the resulting salts. Nevertheless, the improvement of the T_d values was the most profound for the salts with $[TCB]^-$ and $[NTf_2]^-$ anions (by 65 °C and 63 °C, respectively). TGA also revealed that the increase in number of cyano group in the anion resulted in increasing thermal stability of the ionic compounds. Comparing the remaining mass percentage at high temperatures (500 °C, 600 °C and 800 °C), all ionic precursors yielded higher amounts of the residues than unmodified MG (**Figure 25**). At 600 °C, the ionic liquids retained 13-28% of their initial mass, while MG retained just about 4% of its initial mass. At 800°C, the ionic compounds still retained 4-26% of their masses, whereas MG retained only around 2% of its initial mass. Among all investigated compounds [Glu][TCB] showed the highest thermal stability and gave the highest amount of carbon chars among all investigated precursors above 500 °C (up to 26 % at 800 °C).

4.2.5. Synthesis of *N*-doped carbon materials

In 2009 Dai *et al*.[275] first used IL as a precursor in the carbonization process. Ionic liquids that had nitrile groups in imidazolium-based cations were carbonized at 800°C, obtaining carbonaceous materials with high yields of up to 44.2%. Nitrile groups undergo trimerization at higher temperatures, forming polytriazine networks, which are incorporated into the carbon structure and ultimately ensure regular doping of the material with nitrogen. A year later, Antonietti *et al*.[276] examined carbon materials obtained by direct carbonization of ionic liquids containing the dicyanamide anion ($[DCA]^-$), yielding materials with 10.4% of nitrogen after carbonization at 1000°C. Even higher values of nitrogen content were obtained for ILs with both cross-linkable cations and anions investigated as *N*-doped carbon precursors.[277–281] In particular, the combination of conventional imidazolium-based cation combined

with tetracyanoborate anion ($[TCB]^-$) yielded carbon with a nitrogen content that reaches up to 17.5% at 1000 °C.[280] Carbon residues with remarkable nitrogen doping of 26% were synthesized at 800 °C, with the $[DCA]^-$ anion playing a crucial role in this advancement.

The first *N*-doped carbon materials derived from carbohydrate-based ionic compounds such as [Glu][DCA] and [Glu][NTf_2] were obtained in the Chrobok group in 2019.[79] The precursors were pyrolyzed at 800 °C in Ar atmosphere, giving carbon material with specific properties. [Glu][DCA] gave a material with a high nitrogen content (9.6%) but at the same time poorly with a developed surface area (146 $m^2\ g^{-1}$), while [Glu][NTf_2] gave the material with a high specific surface area (946 $m^2\ g^{-1}$), but simultaneously with lower *N*-doping (4.8%) (**Table 6**).

Table 6. Characteristics of [DCA]-800 and [NTf_2]-800. T – carbonization temperature, Y – yield, S_{BET} – specific surface area.

Carbon material	T [°C]	Y [°C]	S_{BET} [$m^2\ g^{-1}$]	Pore size [nm]	Pore volume [$cm^3\ g^{-1}$]	N [%]	C [%]	H [%]
[DCA]-800	800	17	146	2	0.07	9.6	48.3	3.0
[NTf_2]-800	800	18	946	20	1.56	4.8	47.9	1.0

Investigating the possibility of obtaining carbon materials with higher *N-doping*, different ionic precursors were further developed under my Master's thesis and the work was continued under the doctoral thesis. To provide porosity to the materials obtained from ionic precursors with cross-linkable anions, the solution of colloidal silica (SiO_2) in water (Ludox® HS-40) was mixed with the precursors ([Glu][SCN], [Glu][DCA], [Glu][TCM] and [Glu][TCB]), which was further subjected to carbonization at 500 °C, 600 °C and 800 °C for 2 h. Colloidal silica is a common pore generating agent, functioning as a hard template. After carbonization, silica particles were leached from carbon materials with ammonium hydrogen difluoride (NH_4HF_2), washed with water and dried

in the oven. The methodology applied for the synthesis of doped carbon materials is presented in **Figure 26**.

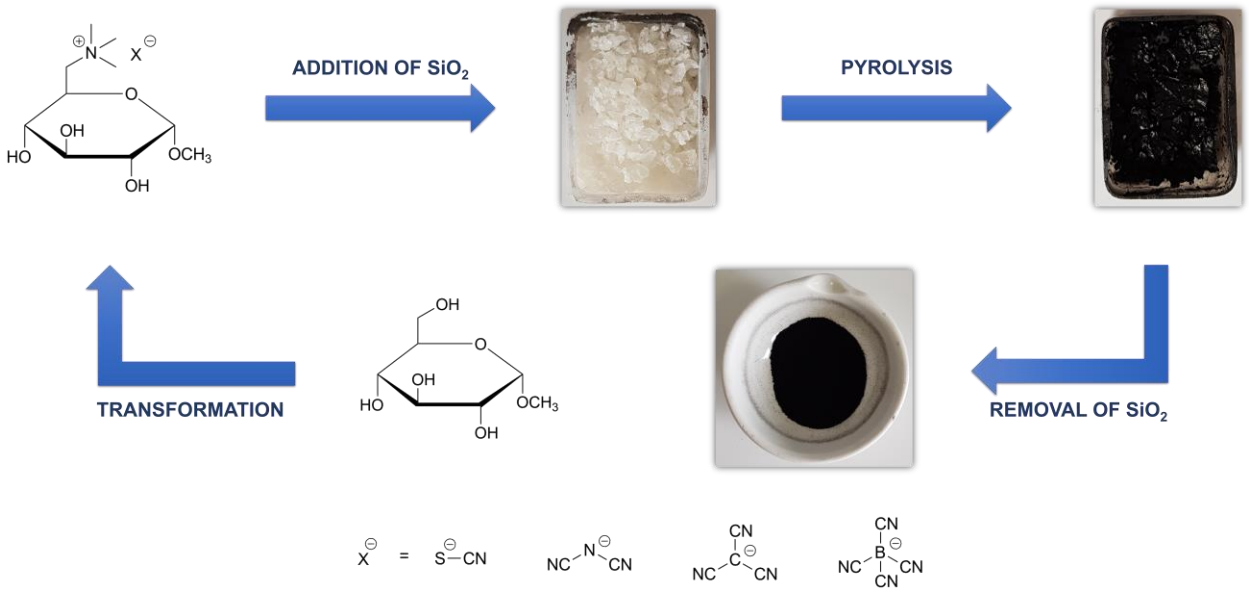

Figure 26. Preparation of N-doped and N,S dual-doped carbon materials in the presence of hard template.

4.2.6. Properties of *N*-doped carbon materials

All the precursors ([Glu][SCN], [Glu][DCA], [Glu][TCM] and [Glu][TCB]) afforded mesoporous carbon materials in the presence of the hard template with specific surface areas of S_{BET}~700 $m^2\ g^{-1}$ and an average pore size of 8–11 nm. Their elemental composition was investigated using elemental analysis (EA) and the results are collected in (**Table 7**). Samples synthesized at 600 °C from precursors containing $[DCA]^-$ and $[TCM]^-$ anions exhibited a maximum nitrogen doping of 11.1%. The lowest *N*-doping level was obtained from salts with $[SCN]^-$ and $[TCB]^-$ anions pyrolyzed at 800 °C (5.9 and 6.1%, respectively). The lower *N*-doping level is expected, when carbonization is carried out at higher temperatures, due to the intensification of NO_x and NH_3 emission, which is exemplified by all the materials obtained from [Glu][SCN], [Glu][DCA],

[Glu][TCM] and [Glu][TBC]. A similar trend was observed for imidazolium-based ILs with $[TCB]^-$ anion.[273] Comparing the materials synthesized at 800 °C from the precursor containing the $[DCA]^-$ anion, carbonization in the presence of SiO_2 nanoparticles resulted in a lower *N*-doping (8.7 %) than in the case of the carbonization of IL alone (9.6%)[79]. The same observations were reported by Paraknowitsch *et al*.[278] The addition of the SiO_2 nanoparticles to the thiazolium salts prior to carbonization at 1000 °C, resulted in lower doping in the carbon materials, up to 3% and 5% for nitrogen and sulfur, respectively. Carbonization of the ionic precursor at the same temperature, yet without the silica template, yielded material with N and S content equal 9% and 7%, respectively. The presence of the hard template induces alterations in the reaction mechanisms, leading to lower doping values compared to materials obtained solely from ionic liquids or salts. In this work, carbon materials with additional sulfur doping, spanning from 4.7% (carbonized at 500 °C) to 2.6% (carbonized at 800 °C), were produced from [Glu][SCN], depending on the carbonization temperature. Therefore, the elemental composition of the resulting samples was influenced by the carbonization temperature, the presence of a template and the structure of the precursor.

Table 7. Characteristics of doped carbon materials derived from [Glu][SCN], [Glu][DCA], [Glu][TCM] and [Glu][TCB]. T – carbonization temperature, Y – yield. Adapted from [274].

Carbon material	T [°C]	Y [%]	N [%]	C [%]	H [%]	S [%]
[SCN]-500	500	25.9	8.5	65.7	3.4	4.7
[SCN]-600	600	25.7	7.9	69.1	2.0	3.0
[SCN]-800	800	19.4	5.9	71.6	1.7	2.6
[DCA]-600	600	32.8	11.1	73.6	2.6	-
[DCA]-800	800	17.9	8.7	79.4	2.0	-
[TCM]-600	600	29.9	11.1	74.7	2.5	-
[TCM]-800	800	24.8	7.1	76.7	1.6	-
[TCB]-600	600	21.4	8.2	78.3	2.5	-
[TCB]-800	800	28.1	6.1	69.1	1.7	-

When comparing the doping levels achieved for materials derived from sugar-based salts with their pyridinium or imidazolium analogs ([C_2MIm][DCA] and [C_2MIm][TCB]), the latter yielded carbon residues with notably higher *N*-doping levels, reaching as high as 23–24% nitrogen content at 800 °C.[280,281] Nevertheless, those materials were obtained without silica template. Comparing the carbonization yield of sugar-based cations combined with $[DCA]^-$, $[TCM]^-$, and $[TCB]^-$ anions with traditional pyridinium and imidazolium analogs, the latter yielded more carbon residues, despite the high carbon content in the carbohydrate-derived precursors.[277,280] The final carbon yields predominantly result from the presence of the cross-linkable anions, but for the pyridinium and imidazolium analogs, the higher yield can also be attributed to the aromatic cation structure. Although cations lacking cross-linkable functional groups typically decompose during thermal treatments, the aromatic moieties in their structure contribute to higher carbon yields. These aromatic structures are confined within the three-dimensional carbonaceous frameworks formed during the cyclotrimerization reaction of the anions.[273]

Direct comparison of the mass loss from thermogravimetric analysis shows that [C_2MIm][SCN] already yielded only 2.5% of ash at 450 °C, and no further decrease in yield was observed up to 850 °C.[282] In contrast, [Glu][SCN] yielded 12% of carbon residues at 450 °C and 8.7% at 850 °C, exceeding the yields obtained for derivatives with $[DCA]^-$ and $[TCM]^-$ anions at 850 °C. On the other hand, [C_2MIm][DCA] left 33% of the carbon residues at 450°C and 13.3% at 850 °C, while the carbohydrate-derived analog gave 20% and 6.3% respectively. The differences were even more pronounced for the [Glu][TCM] derivative, which, at 450 °C, yielded 33% carbon residues, but, at 850 °C, it underwent complete decomposition into volatiles, whereas its imidazolium analog still produced 26% carbon residues.

4.2.7. Conclusions

Methyl α-D-glucopyranoside was transformed into a quaternary ammonium cation and combined with various cross-linkable cyano group-containing anions ($[SCN]^-$, $[DCA]^-$, $[TCM]^-$ and $[TCB]^-$). The resulting ionic precursors served as a multifunctional source of nitrogen-doped carbon materials, offering an alternative to traditional imidazolium-based ILs. The electrochemical activity of these carbon materials in the oxygen reduction reaction (ORR) was further evaluated by cyclic voltammetry (CV), linear sweep voltammetry (LSV) and rotating ring-disc electrode (RRDE) experiments performed in the Chrobok group.[274] Among the investigated materials, the carbon materials derived at 800 °C ([SCN]-800, [DCA]-800, [TCM]-800 and [TCB]-800) showed the best performance. The onset potential was between −0.12 and −0.14 V, while the electron transfer numbers for these materials was ranging from 3.56 to 3.74. These results indicate that carbonization at higher temperatures enhances formation of graphitic structures with higher aromaticity, directly contributing to improved electrocatalytic activity. The [SCN]-800 material exhibited the most promising performance, with the highest onset potential (−0.12 V). Notably, S and N dual-doped carbons led to a higher electron transfer number compared to single *N*-doped carbons carbonized at the same temperature. This observation underscores the remarkable impact of N and S dual-doping.[283] Dual-doping not only positively shifted the onset potential, but also resulted in a high electron transfer number (3.74), making it comparable to the commercial Pt/C catalyst. In addition, the specific surface area of the carbon materials had a substantial impact on their activity. The use of a silica hard template during the carbonization process greatly increased the surface area. For comparison, the material carbonized in the presence of the silica template ([DCA]-800) gave an S_{BET}~700 $m^2\ g^{-1}$, while when carbonized without a template gave only 146 $m^2\ g^{-1}$. This

demonstrates the importance of both surface area and doping strategy in achieving high electrocatalytic performance. The results on doped carbon materials synthesized ILs and salts containing cyano anions have been described in the research paper "Bioderived ionic liquids and salts with various cyano anions as precursors for doped carbon materials", published in *International Journal of Molecular Sciences*.[274]

4.3. Carbohydrate-based ionic liquids as surface active agents

4.3.1. Introduction

Surface active agents, or surfactants, are compounds that reduce the surface of aqueous media (e.g. air-water), and the interfacial tension of liquid-liquid (e.g. oil-water or water-oil) or liquid–solid systems (e.g. wetting phenomena).[284] They consist of two parts: a hydrophilic (polar, water-soluble) and a hydrophobic (non-polar, water-insoluble), which allows them to interact with both water and non-polar substances like oils or organic solvents. Surfactants aggregate at the interface of these substances, altering surface properties and facilitating interaction between phases. Surfactants are widely employed in the petroleum[285], food[286], agricultural[287], cosmetics[288] and pharmaceutical[289] industry, hence eventually most of these chemicals enter the environment through household and industrial wastewater. Therefore, there is a growing shift towards green products that meet consumer demands while minimizing environmental harm.[290]

Surfactants are classified according to the charge of their head group: anionic if the head group carries a negative charge, cationic if it carries a positive charge, zwitterionic if the polar head contains both positive and negative charges, and non-ionic if the head group is neutral.[291] Surfactants can be classified not only by their head group

charge but also by their origin – natural or synthetic. Natural surfactants (obtained by separation, extraction, precipitation or distillation), including biosurfactants of microbial origin, are highly desirable for their environmental benefits.[292] However, due to challenges such as low yield, high cost, and slow production rates, their large-scale commercialization remains difficult. As a result, synthetic surfactants, which are more easily and inexpensively manufactured, dominated the market. The growing demand for sustainable solutions has focused interest on renewable-source synthetic surfactants, offering an eco-friendlier alternative while maintaining cost-effectiveness and scalability.

4.3.2. Goal of the research

The production of sugar-based surfactants has increased in the last years due to their properties such as high biodegradability, low toxicity and high biocompatibility. The most common precursors of such surfactants are glucose, sucrose and sorbitol.[293] There are many reports of sugar-based surfactants of various types including non-ionic[284,294] (such as: alkylglucosides, alkylglucamides and sugar esters), anionic[295,296] (containing sulfate group) and cationic[297] (containing quaternary ammonium group). Nevertheless, in all of them sugar moiety is a part of the ion possessing surface active properties.

The goal of the research was to develop novel sugar-based surfactants with carbohydrate moiety separated from the counter ion with surface active properties. For this purpose, β-D-glucose pentaacetate was transformed into a cation by modification at the anomeric position and combined with dodecyl sulfate ($[DS]^-$), cholate ($[C]^-$) and deoxycholate ($[DOC]^-$) anions, known to have surface active properties. Those anions are constituents of commercially available surfactants in a form of sodium salts and are routinely used to suspend single-walled carbon nanotubes (SWCNTs) mixtures

and promote their partitioning.[298–300] Four carbohydrate-based surfactants were further characterized in terms of determining their surface active properties. Furthermore, the influence of sugar-based cations on SWCNTs partitioning using aqueous two-phase extraction (ATPE) method was investigated. To my best knowledge, salts presented herein are the first examples of carbohydrate-based surfactants, in which sugar moiety (in the form of a cation) is separated from the anions with surface active properties.

4.3.3. Synthesis of carbohydrate-based ionic surface active agents

Four organic salts containing a sugar moiety in the cation (*N*-[2-(β-D-glucopyranosyloxy)ethyl]-*N*,*N*,*N*-trimethylammonium cation ($[AGlu]^+$) and *N*-[2-(2,3,4,6-tetra-*O*-acetyl-β-D-glucopyranosyloxy)ethyl]-*N*,*N*,*N*-trimethylammonium cation ($[ATAGlu]^+$)) and anions with surface-active properties (dodecyl sulfate $[DS]^-$, cholate $[C]^-$ and deoxycholate $[DOC]^-$ were synthesized (**Figure 27**).[301]

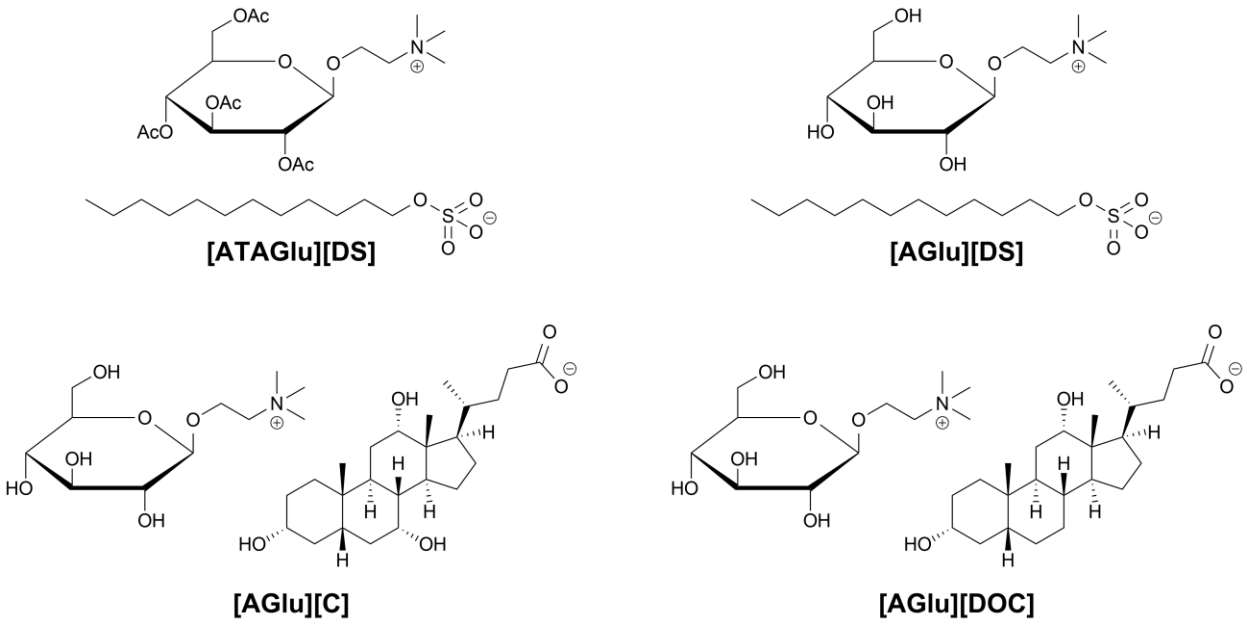

Figure 27. Structures of carbohydrate-based surface active agents.

As a cation precursor, commercially available β-D-glucose pentaacetate was used and transformed into ionic moiety ([ATAGlu]Br, **27**) *via* glycosylation and quaternization reactions (**Figure 28**), based on previously reported procedure[56,79]. The desired $[DS]^-$ anion was incorporated through anion metathesis with sodium dodecyl sulfate (Na[DS]) to obtain [ATAGlu][DS] (**28**). The desired product was extracted from the remaining sodium bromide salt solution with an organic solvent (EA). Subsequent acyl group deprotection under basic conditions yielded an ionic derivative with hydroxyl-group-rich structure ([AGlu][DS] (**29**)).

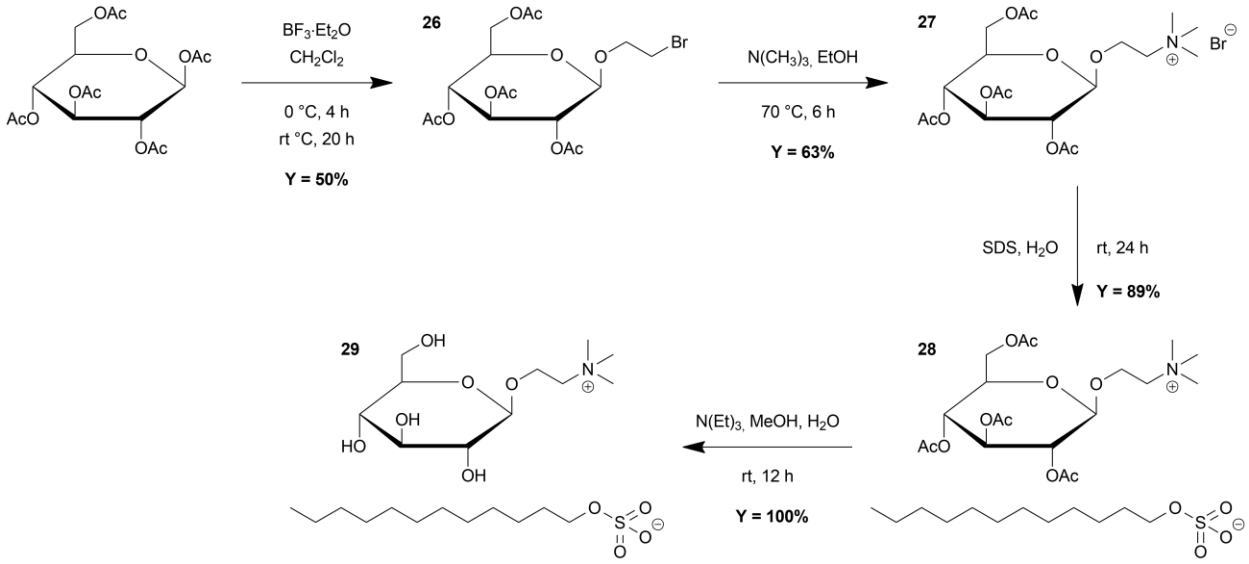

Figure 28. Synthesis of [ATAGlu][DS] and [AGlu][DS].

For the synthesis of [AGlu][C] (**32**) and [AGlu][DOC] (**33**) (**Figure 29**), another procedure was applied, as the extraction of the product after anion exchange between [ATAGlu]Br (**30**) and the corresponding sodium salts (Na[C] and Na[DOC]) failed. The alternative procedure (**Figure 29**) required acyl group deprotection in [ATAGlu]Br (**27**) under basic conditions (analogously to the synthesis of [AGlu][DS] (**29**) from [ATAGlu][DS] (**28**)), which yielded [AGlu]Br (**30**). In the next step, the hydroxide

([AGlu]OH (**31**)) was obtained with the use of ion exchange resin. [AGlu][C] (**32**) and [AGlu][DOC] (**33**) were finally obtained by neutralization of [AGlu]OH (**31**) with cholic and deoxycholic acid, respectively. The different synthetic routes for the latter compounds were dictated by the purification difficulties of the resulting salts from the sodium bromide salt. It was attributed to the higher polarity of [ATAGlu][C] and [ATAGlu][DOC] formed during anion metathesis, compared to [ATAGlu][DS]. The applied neutralization of [AGlu]OH eliminated the formation of sodium bromide and made the extraction step unnecessary.

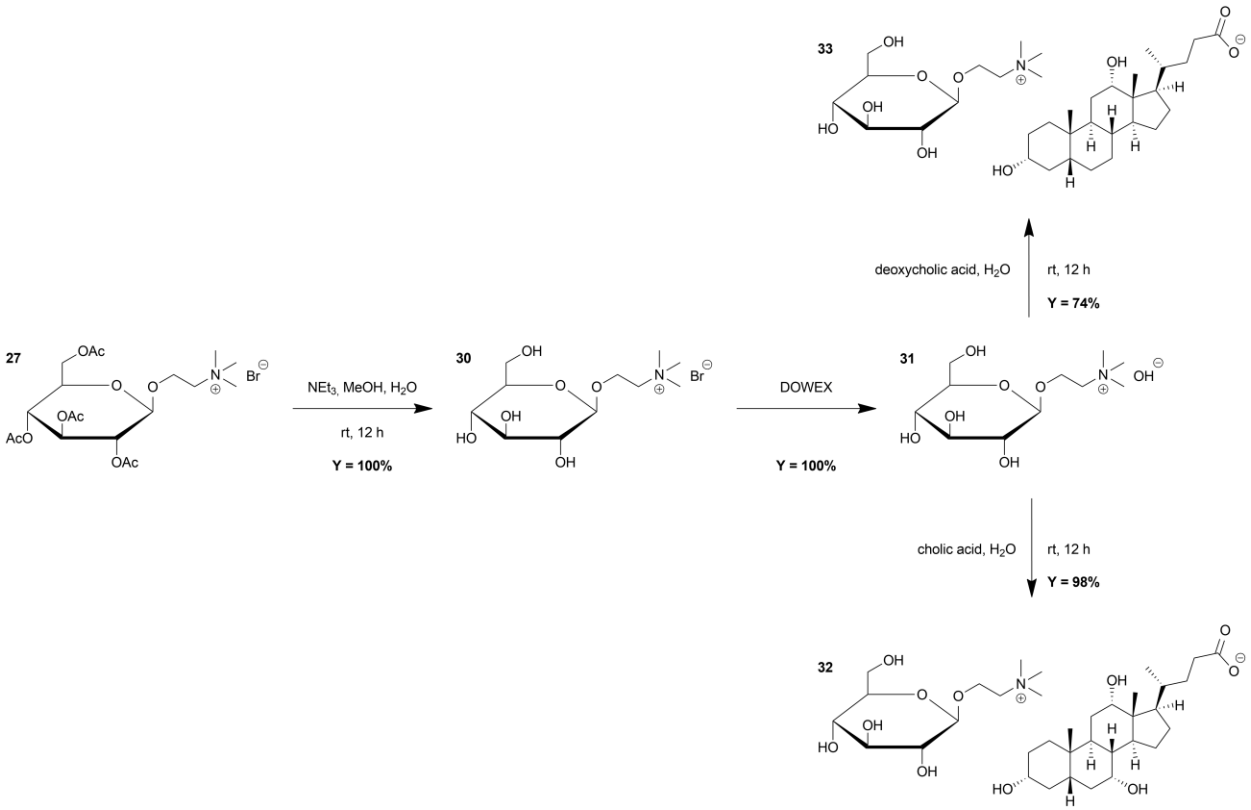

Figure 29. Synthesis of [AGlu][C] and [AGlu][DOC].

4.3.4. Determination of critical micelle concentration

The surface active agents are able to self-organize in spherical aggregates, called micelles, when a certain concentration is exceeded. The key parameter that determines that concentration above which micelles are formed is called critical micelle concentration (CMC) and can be measured by several experimental methods (**Figure 30**).[302] The most common method is based on surface tension measurements. Micelles can be formed in the aqueous phase and no lipophilic phase is necessary. Due to the absorption at the air-water interface, the surface tension decreases with increasing concentration until the surface is saturated and a stable value is obtained. The CMC is defined by the breakpoint, beyond which any additional surfactant will contribute to the formation of micelle-like aggregates. The CMC value reflects the efficiency of the surfactants, therefore the more efficient surfactants the lower is its CMC value.[284] In lipophilic, medium reverse micelles can also be formed and their formation is dictated by another parameter - water load (w_0), however it is beyond this discussion.

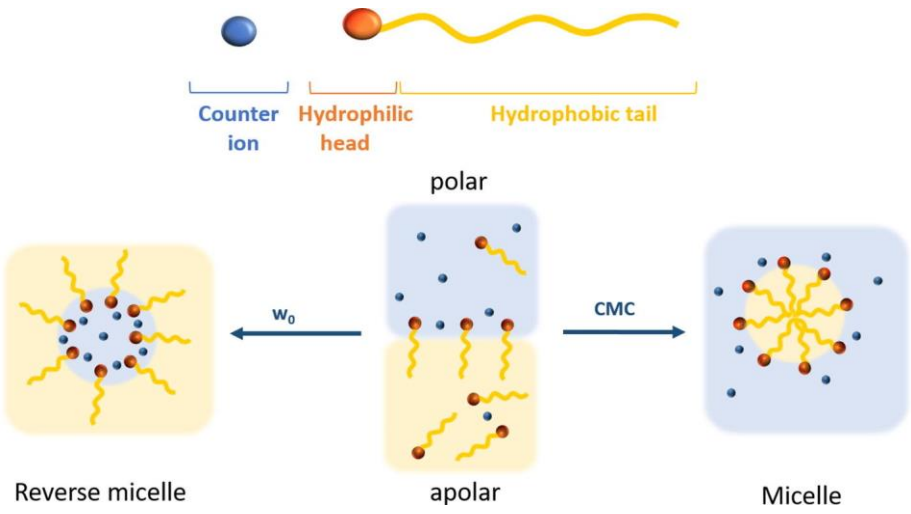

Figure 30. Amphiphile structure (top) forming (reverse) micelles (bottom). Reprinted from [302].

The surface tension was measured using a stalagmometer for four carbohydrate-based surface active agents ([ATAGlu][DS], [AGlu][DS], [AGlu][C] and [AGlu][DOC]). 10 aqueous solutions of each compound with concentrations in the range of 0.25 – 120 mmol L^{-1} were examined (**Figure 31-34**). For each solution, the number of drops formed upon the outflow was counted. Before each measurement, the stalagmometer was rinsed with the tested solution. The measurements were repeated three times for each compound and the average number of drops was calculated. An analogous measurement was performed for pure water. The volume of the droplet flowing out of the stalagmometer depends on the surface tension (σ) of the solution. Knowing the value of the surface tension of water, the surface tension of tested compounds solutions was calculated using the formula:

$$\sigma = \frac{n_w}{n_x} \cdot \sigma_x$$

Where:

σ – surface tension of the solution,

σ_x – surface tension of water, σ_x = 72.6 [mN/m],

n_w – the number of water drops,

n_x – the number of drops of the tested solution

Based on the results, the critical micelle concentration (CMC) of [ATAGlu][DS] (**Figure 31**), [AGlu][DS] (**Figure 32**), [AGlu][C] (**Figure 33**) and [AGlu][DOC] (**Figure 34**) was determined as the concentration below which surface tension increased rapidly. The CMC value for [ATAGlu][DS] and [AGlu][DS] was 2.50 mmol L^{-1}, while for [AGlu][C] and [AGlu][DOC] it was 15.00 mmol L^{-1}. For comparison, the CMC values of analogous sodium salts, commonly used as surfactants, are as follows: Na[DS] (8.00 mmol L^{-1})[296], Na[C] (12.73 mmol L^{-1}), Na[DOC] (4.25 mmol L^{-1})[303]. When compared to other glucose-

based cationic surfactants, (obtained *via* derivatization of glucose and subsequent quaternization with tertiary amine containing long alkyl chain) their CMC values range from 0.01 – 16.00 mmol L^{-1}.[297] In general, the longer the alkyl chain in the final product (C_8, C_{10}, C_{12}, C_{14} or C_{16}) the lower CMC. The CMC values reported for glucose-based cationic surfactants containing C_{12} alkyl chains (as in $[DS]^-$) were in the range of 0.10 – 4.89. Alternatively, anionic surfactants derived from glucose, galactose and xylose with C_{12} alkyl chains had CMC values from 2.00 to 4.10 mmol L^{-1}.[296]

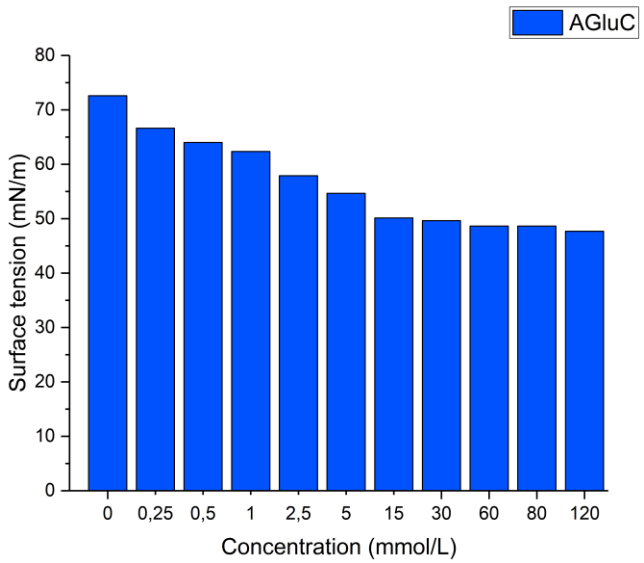

Figure 31. Determination of the surface tension of aqueous solutions of [ATAGlu][DS].

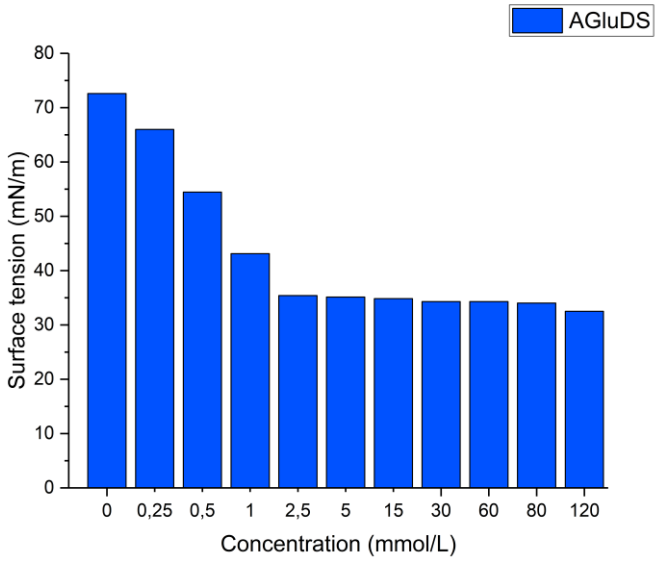

Figure 32. Determination of the surface tension of aqueous solutions of [AGlu][DS].

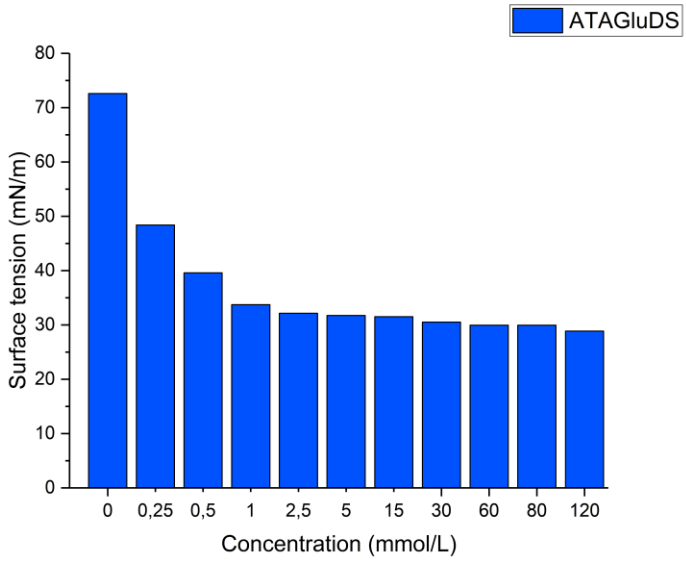

Figure 33. Determination of the surface tension of aqueous solutions of [AGlu][C].

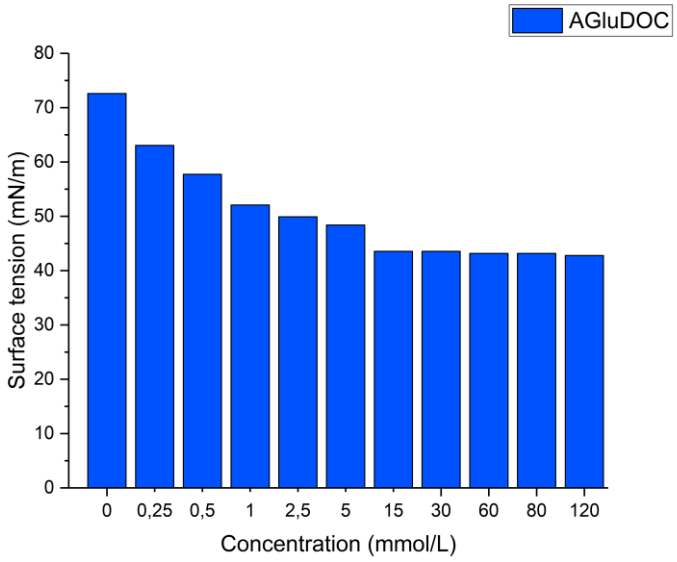

Figure 34. Determination of the surface tension of aqueous solutions of [AGlu][DOC].

4.3.5. Conclusions

Four carbohydrate-based surface active agents ([ATAGlu][DS], [AGlu][DS], [AGlu][C] and [AGlu][DOC]) were synthesized. Their CMC values were evaluated based on surface tension measurements and compared to commercially available surfactants, such as sodium dodecyl sulfate, sodium cholate and sodium deoxycholate, and to synthetic sugar-based ionic surfactants described in the literature. New synthetic approach was presented in this work, leading to surfactants in which the cationic sugar moiety is separated from the anions with surface active properties (dodecyl sulfate $[DS]^-$, cholate $[C]^-$ and deoxycholate $[DOC]^-$). Thus far, Janas *et al*.[301] evaluated the performance of presented herein sugar-based surfactants, including [ATAGlu][DS], [AGlu][DS], [AGlu][C], and [AGlu][DOC], in the aqueous two-phase extraction (ATPE) method for purifying single-walled carbon nanotubes (SWCNTs). SWCNTs possess unique properties based on the spatial arrangement of their carbon atoms and these fine-tuned properties for specific applications can be obtained by isolating monochiral fractions

of SWCNTs. Hence, the ATPE method is a promising approach in the context of cost-effective and scalable SWCNTs separation. The performance of sugar-based surfactants was evaluated in two-phase systems composed of poly(ethylene glycol) (top phase) and dextran (bottom phase), in which the addition of modulators and surfactants resulted in the migration of specific SWCNTs from the bottom phase to the top phase. In the study, the sugar-based surfactants were used as alternatives and in cooperation with their commercially available analogues like sodium dodecyl sulfate (Na[DS]), sodium cholate (Na[C]) and sodium deoxycholate (Na[DOC]). Despite the ATPE mechanism remains unsolved, introduction of sugar-based cations into the system, enabled altering the course of biphasic extraction.

Moreover, recently the Chrobok group showed effectiveness of carbohydrate-based surfactants in phase transfer catalysis (PTCs)[88] and as part of the catalytic system[89], therefore the studies on the abovementioned compounds, their biodegradability and catalytic applications will be continued.

5. Summary

Although sugar chemistry is well understood, transformations involving carbohydrates often require multiple synthetic steps. These processes typically involve harmful reagents and large volumes of organic solvents for product purification. However, recent advances in synthetic methodologies aligned with the principles of green chemistry have led to more sustainable approaches. These developments are particularly relevant in light of the recently published Biomass Strategy[304,305], which emphasizes transforming waste biomass into useful chemicals and materials as part of the circular economy. Given the amount of waste biomass, which consists mainly of lignocellulose, sugars are a promising raw material. Hence, this work lifts the potential of renewable raw materials by exploring novel sugar derived organic salts as sustainable functional materials for use in different emerging areas, such as energy-related applications.

The results presented herein covering practical applications of carbohydrate-based ILs as phase change materials (PCMs) for thermal energy storage, multifunctional precursors of heteroatom-doped carbon materials used in electrocatalysis, or as surfactants for single-walled carbon nanotubes (SWCNTs) purification, provide a solid foundation for developing the applications discussed. Given the nearly infinite design potential of ionic liquids through variations in cation and anion combinations, this research highlights the significant possibilities for further development. While much attention has historically focused on the ability of ILs to form a liquid phase, crucial for applications like electrolytes and solvents, this study demonstrates the broader potential of underexplored organic salts. Understanding the relationship between molecular structure and properties is essential for designing task-specific, sustainable materials with improved functionality.

In summary, this work expands the emerging field of sugar-based ILs, offering a generalizable approach to design ILs based on monosaccharide units, for specific functions. This opens the door to environmentally friendly processes, providing a foundation for future research on creating diverse and sustainable ILs from renewable resources like carbohydrates.

6. Experimental part

6.1. Synthetic procedures

Methyl 6-bromo-6-deoxy-α-D-glucopyranoside

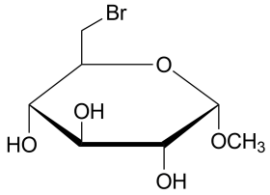

To a solution of methyl α-D-glucopyranoside (38.84 g, 200 mmol) in anhydrous pyridine (600 mL), triphenylphosphine (104.92 g, 400 mmol) and carbon tetrabromide (99.50 g, 300 mmol) were added and the resulting solution was stirred at 0 °C for 15 min, followed by raising the temperature to 65 °C and stirring for the next 4 h. The reaction was carried under inert gas atmosphere. Reaction progress was monitored by TLC (CH_2Cl_2:MeOH 9:1). After completion of the reaction, methanol (100 mL) was added to quench the reaction. The solvent was evaporated by co-distillation with toluene and the residue was purified by column chromatography (CH_2Cl_2 to CH_2Cl_2:MeOH 9:1 and subsequent flash column chromatography: EA:MeOH 9:1). Methyl 6-bromo-6-deoxy-α-D-glucopyranoside was afforded as a white crystalline solid (37.60 g, 73%).

^{1}H NMR (400 MHz, DMSO-d_6) δ 5.20 (d, J = 5.8 Hz, 1H, –OH), 4.88 (d, J = 5.0 Hz, 1H, –OH), 4.80 (d, J = 6.4 Hz, 1H, –OH), 4.56 (d, J = 3.7 Hz, 1H, H-1), 3.74 (dd, J = 10.3, 1.7 Hz, 1H), 3.59 – 3.45 (m, 2H), 3.38 (td, J = 9.1, 4.8 Hz, 1H), 3.29 (s, 3H, –OCH_3), 3.20 (ddd, J = 9.8, 6.4, 3.7 Hz, 1H), 3.03 (td, J = 8.9, 5.8 Hz, 1H).

^{13}C NMR (101 MHz, DMSO-d_6) δ 99.80 (C-1), 72.99, 72.37, 71.82 (C-2, C-3, C4), 70.97 (C-5), 54.51 (–OCH_3), 35.18 (C-6).

_N_-(methyl-6-deoxy-α-D-glucopyranoside-6-yl)-_N,N,N_-trimethylammonium bromide ([Glu]Br)

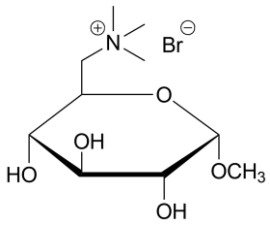

Methyl 6-bromo-6-deoxy-α-D-glucopyranoside (6.06 g, 23.6 mmol) and trimethylamine (13.93 g, 236.0 mmol, 56.3 mL 33% ethanolic solution) were placed in an autoclave and the reaction mixture was left for 24 h at 70 °C. The resulting solid was filtered off and washed with ethanol and hexane. N-(methyl-6-deoxy-α-D-glucopyranoside-6-yl)-N,N,N-trimethylammonium bromide was afforded as a white crystalline solid (7.00 g, 94%).

^{1}H NMR (400 MHz, DMSO-d_6) δ 5.43 (d, J = 5.9 Hz, 1H, –OH), 5.01 (d, J = 5.0 Hz, 1H, –OH), 4.91 (d, J = 6.3 Hz, 1H, –OH), 4.59 (d, J = 3.7 Hz, 1H, H-1), 3.88 (t, J = 9.5 Hz, 1H, H-6b), 3.66 (dd, J = 13.9, 1.3 Hz, 1H, H-6a), 3.56 – 3.39 (m, 2H, H-4, H-5), 3.37 (s, 3H, –OCH_3), 3.21 (ddd, J = 9.9, 6.3, 3.7 Hz, 1H, H-3), 3.15 (s, 9H, –$N^+(CH_3)_3$), 2.92 (ddd, J = 9.8, 8.6, 5.9 Hz, 1H, H-2).

^{13}C NMR (101 MHz, DMSO-d_6) δ 100.70 (C-1), 72.38, 71.67, 71.17 (C-2, C-3, C4), 67.05, 66.91 (C-5, C-6), 56.50 (–OCH_3), 53.39 (–$N^+(CH_3)_3$).

Methyl 6-iodo-6-deoxy-α-D-glucopyranoside

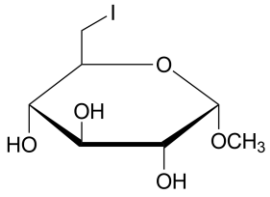

To a solution of methyl α-D-glucopyranoside (20.00 g, 0.103 mol) in anhydrous THF imidazole (13.61 g, 0.206 mol), triphenylphosphine (51.24 g, 0.154 mol) and iodine (39.21 g, 0.154 mol) were added to the solution and stirred for 15 min at rt. Subsequently the mixture was stirred under reflux at 70 °C for 4 h. The resulting solid was filtered off and the and the filtrate was condensed using rotary evaporator. The product was purified by column chromatography ($CHCl_3$ to $CHCl_3$:MeOH 12:1).

Methyl 6-iodo-6-deoxy-α-D-glucopyranoside was afforded as a white crystalline solid (29.13 g, 93%).

^{1}H NMR (400 MHz, DMSO-d_6) δ 5.18 (d, J = 5.8 Hz, 1H, –OH), 4.87 (d, J = 5.0 Hz, 1H, –OH), 4.79 (d, J = 6.4 Hz, 1H, –OH), 4.55 (d, J = 3.6 Hz, 1H, H-1), 3.57 – 3.53 (m, 1H), 3.39 (td, J = 9.3, 4.3 Hz, 1H), 3.32 (s, 3H, –OCH_3), 3.28 – 3.17 (m, 3H), 2.92 (td, J = 8.8, 5.7 Hz, 1H).

^{13}C NMR (101 MHz, DMSO-d_6) δ 99.76 (C-1), 73.99, 72.60, 71.78 (C-2, C-3, C-4), 70.81 (C-5), 54.47 (–OCH_3), 9.43 (C-6).

_N_-(methyl-6-deoxy-α-D-glucopyranoside-6-yl)-_N,N,N_-trimethylammonium iodide ([Glu]I)

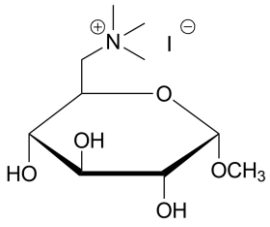

Methyl 6-iodo-6-deoxy-α-D-glucopyranoside (9.00 g, 29.6 mmol) and trimethylamine (17.50 g, 296.0 mmol, 70.7 mL 33% ethanolic solution) were placed in an autoclave and the reaction mixture was left for 24 h at 70 °C. The resulting solid was filtered off and washed with ethanol and hexane. N-(methyl-6-deoxy-α-D-glucopyranoside-6-yl)-N,N,N-trimethylammonium iodide was afforded as a white crystalline solid (9.30 g, 87%).

^{1}H NMR (400 MHz, DMSO-d_6) δ 5.43 (d, J = 5.9 Hz, 1H, –OH), 5.02 (d, J = 5.1 Hz, 1H, –OH), 4.91 (d, J = 6.4 Hz, 1H, –OH), 4.60 (d, J = 3.6 Hz, 1H, H-1), 3.89 (t, J = 9.1 Hz, 1H, H-6b), 3.67 – 3.59 (dd, J = 13.9, 1.3 Hz, 1H, H-6a), 3.54 – 3.41 (m, 2H, H-4, H-5), 3.39 (s, 3H, –OCH_3), 3.22 (ddd, J = 9.9, 6.4, 3.7 Hz, 1H, H-3), 3.14 (s, 9H, –$N^+(CH_3)_3$), 2.92 (ddd, J = 9.8, 8.6, 6.0 Hz, 1H, H-2).

^{13}C NMR (101 MHz, DMSO-d_6) δ 100.72 (C-1), 72.43, 71.64, 71.19 (C-2, C-3, C4), 67.03, 66.88 (C-5, C-6), 56.51 (–OCH_3), 53.42 (–$N^+(CH_3)_3$).

_N_-(methyl-6-deoxy-α-D-glucopyranoside-6-yl)-_N,N,N_-trimethylammonium nitrate ([Glu][NO_3])

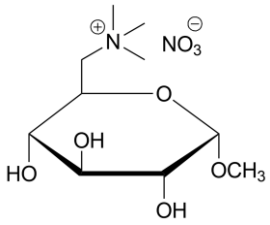

_N_-(methyl-6-deoxy-α-D-glucopyranoside-6-yl)-_N,N,N_-trimethylammonium bromide (3 g, 9.5 mmol) was dissolved in methanol (50 mL), and silver nitrate (1.61 g, 9.5 mmol) was added. The resulting suspension was covered from light and stirred for 24 h. The precipitate was filtered off, while the liquid phase was collected and the solvent was evaporated. _N_-(methyl-6-deoxy-α-D-glucopyranoside-6-yl)-_N,N,N_-trimethylammonium nitrate was obtained as a white solid (2.50 g, 95%, m.p. = 163 °C).

^{1}H NMR (400 MHz, DMSO-d_6) δ 5.46 (d, J = 5.9 Hz, 1H, –OH), 5.04 (d, J = 5.0 Hz, 1H, –OH), 4.93 (d, J = 6.3 Hz, 1H, –OH), 4.60 (d, J = 3.6 Hz, 1H, H-1), 3.89 (t, J = 9.1 Hz, 1H, H-6b), 3.63 (dd, J = 13.9, 1.4 Hz, 1H, H-6a), 3.55 – 3.40 (m, 2H, H-4, H-5), 3.39 (s, 3H, –OCH_3), 3.22 (ddd, J = 9.7, 6.0, 3.6 Hz, 1H, H-3), 3.13 (s, 9H, –$N^+(CH_3)_3$), 2.92 (ddd, J = 9.7, 8.6, 5.9 Hz, 1H, H-2).

^{13}C NMR (101 MHz, DMSO-d_6) δ 100.74 (C-1), 72.45, 71.67, 71.22 (C-2, C-3, C-4), 67.05, 66.92 (C-5, C-6), 56.50 (–OCH_3), 53.42 (–$N^+(CH_3)_3$).

_N_-(methyl-6-deoxy-α-D-glucopyranoside-6-yl)-_N,N,N_-trimethylammonium mesylate ([Glu][OMs])

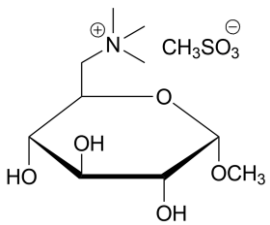

_N_-(methyl-6-deoxy-α-D-glucopyranoside-6-yl)-_N,N,N_-trimethylammonium bromide (2.85 g, 9.0 mmol) was dissolved in methanol (50 mL), and silver mesylate (1.83 g, 9.0 mmol) was added. The resulting suspension was covered from light and stirred for 24 h. The precipitate was filtered off, while the liquid phase was collected,

and the solvent was evaporated. *N*-(methyl-6-deoxy-*α*-D-glucopyranoside-6-yl)-*N,N,N*-trimethylammonium mesylate was obtained as a white solid (2.92 g, 88%, m.p. = 138 °C).

^{1}H NMR (400 MHz, DMSO-d_6) δ 5.47 (d, J = 6.0 Hz, 1H, –OH), 5.04 (d, J = 5.1 Hz, 1H, –OH), 4.93 (d, J = 6.3 Hz, 1H, –OH), 4.60 (d, J = 3.6 Hz, 1H, H-1), 3.89 (t, J = 9.3 Hz, 1H, H-6b), 3.65 (d, J = 13.8 Hz, 1H, H-6a), 3.55 – 3.39 (m, 2H, H-4, H-5), 3.39 (s, 3H, –OCH_3), 3.21 (td, J = 6.1, 3.0 Hz, 1H, H-3), 3.13 (s, 9H, –$N^+(CH_3)_3$), 2.92 (ddd, J = 9.8, 8.7, 6.0 Hz, 1H, H-2), 2.31 (s, 3H, $CH_3SO_3^-$).

^{13}C NMR (101 MHz, DMSO-d_6) δ 100.74 (C-1), 72.41, 71.68, 71.21 (C-2, C-3, C-4), 67.05, 66.95 (C-5, C-6), 56.48 (–OCH_3), 53.39 (–$N^+(CH_3)_3$), 39.75 ($CH_3SO_3^-$).

_N_-(methyl-6-deoxy-_α_-D-glucopyranoside-6-yl)-_N,N,N_-trimethylammonium tetrafluoroborate ([Glu][BF_4])

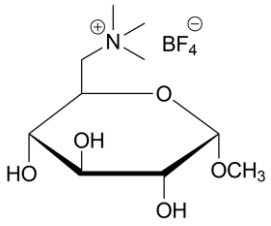

Silver oxide (1.1 g, 4.7 mmol) was stirred in methanol (50 mL) and tetrafluoroboric acid (48% solution in H_2O) was added dropwise (0.84 g, 0,6 mL, 9.5 mmol). The reaction mixture was stirred for 1 h at rt, until homogeneous colourless solution was obtained. It was followed by addition of *N*-(methyl-6-deoxy-*α*-D-glucopyranoside-6-yl)-*N,N,N*-trimethylammonium bromide (3 g, 9.5 mmol). The resulting suspension was covered from light and stirred for 24 h. The precipitate was filtered off, while the liquid phase was collected, and the solvent was evaporated. *N*-(methyl-6-deoxy-*α*-D-glucopyranoside-6-yl)-*N,N,N*-trimethylammonium tetrafluoroborate was obtained as a white solid (2.91 g, 98%, m.p. = 99 °C).

^{1}H NMR (400 MHz, DMSO-d_6) δ 4.60 (d, J = 3.7 Hz, 1H, H-1), 3.89 (t, J = 9.1 Hz, 1H, H-6b), 3.62 (d, J = 13.0 Hz, 1H, H-6a), 3.54 – 3.40 (m, 2H, H-4, H-5), 3.39 (s, 3H, –OCH_3), 3.21 (dd, J = 9.8, 3.7 Hz, 1H, H-3), 3.12 (s, 9H, –$N^+(CH_3)_3$), 2.94 – 2.88 (m, 1H, H-2).

13C NMR (101 MHz, DMSO-d_6) δ 100.74 (C-1), 72.45, 71.67, 71.21 (C-2, C-3, C-4), 67.04, 66.91 (C-5, C-6), 56.50 (–OCH_3), 53.42 (–$N^+(CH_3)_3$).

Methyl 6-*O*-trityl-*α*-D-glucopyranoside

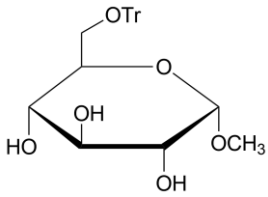

Methyl *α*-D-glucopyranoside (60.0 g, 309 mmol), trityl chloride (129.21 g, 463.5 mmol) and triethylamine (150.51 g, 207 mL, 1.49 mol) were dissolved in dichloromethane (770 mL) and stirred overnight at rt. Reaction mixture was condensed using rotary evaporator and the residue was purified by flash column chromatography (PE:EA 4:1 to EA) yielding methyl 6-*O*-trityl-*α*-D-glucopyranoside (6) as a white solid (86.24 g, 64%).

^{1}H NMR (400 MHz, DMSO-d_6) δ 7.48 – 7.18 (m, 15H, Ar-H), 4.82 (d, J = 5.9 Hz, 1H, –OH), 4.77 (d, J = 4.9 Hz, 1H, –OH), 4.74 (d, J = 6.4 Hz, 1H, –OH), 4.63 (d, J = 3.7 Hz, 1H, H-1), 3.62 (ddd, J = 9.5, 7.2, 1.7 Hz, 1H, H-5), 3.41 (s, 3H, –OCH_3), 3.40 – 3.35 (m, 1H, H-3), 3.29 – 3.19 (m, 2H, H-2, H-6a), 3.05 – 2.93 (m, 2H, H-4, H-6b).

^{13}C NMR (101 MHz, DMSO-d_6) δ 143.98 (C_{Ar}), 128.29, 127.82, 126.91 (CH_{Ar}), 99.64 (C-1), 85.61 (–CPh_3), 73.59, 71.90, 70.96, 70.76 (C-2, C-3, C-4, C-5), 63.80 (C-6), 54.17 (–OCH_3).

Methyl 6-*O*-trityl-2,3,4-*O*-methyl-*α*-D-glucopyranoside

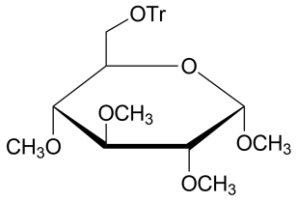

Methyl 6-*O*-trityl-*α*-D-glucopyranoside (86.24, 197.6 mmol) was dissolved in dry DMF (1500 mL) and cooled to 0 °C. Sodium hydride 60% dispersion in mineral oil (1.3 eq per OH group) was added in portions and the resulting mixture was stirred for 30 min. Subsequently methyl iodide was added (2.0 eq per OH group) and the reaction

was stirred overnight at rt. The solvent was evaporated, dichloromethane (3500 mL) was added, and the mixture was washed with water (3x 1000 mL). Organic phase was condensed using rotary evaporator and the residue was purified by column chromatography (PE:EA 3:1) yielding methyl 6-*O*-trityl-2,3,4-*O*-methyl-*α*-D-glucopyranoside as a white solid (78.50 g, 83%).

^{1}H NMR (400 MHz, DMSO-d_6) δ 7.52 – 7.18 (m, 15H, Ar-H), 4.94 (d, *J* = 3.4 Hz, 1H, H-1), 3.54 – 3.46 (m, 1H), 3.43 (s, 3H, –OCH_3), 3.37 (s, 3H, –OCH_3), 3.35 (s, 3H, –OCH_3), 3.27 – 3.10 (m, 4H), 3.16 (s, 3H, –OCH_3), 3.00 (dd, *J* = 10.0, 5.1 Hz, 1H).

^{13}C NMR (101 MHz, DMSO-d_6) δ 143.98 (C_{Ar}), 128.29, 127.82, 126.91 (CH_{Ar}), 99.64 (C-1), 85.61 (–CPh_3), 73.59, 71.90, 70.96, 70.76 (C-2, C-3, C-4, C-5), 63.80 (C-6), 54.17 (–OCH_3).

Methyl 2,3,4-*O*-methyl-*α*-D-glucopyranoside

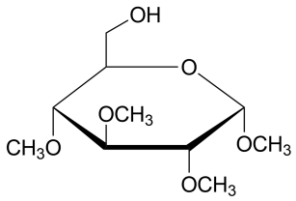

Methyl 6-*O*-trityl-2,3,4-*O*-methyl-*α*-D-glucopyranoside (11.20 g, 23.4 mmol) was dissolved in 70% acetic acid solution (120 mL), heated to 70 °C and stirred for 1 h. The solvent was removed using toluene. The residue was purified by column chromatography (PE:EA 3:1 to PE:EA 1:2) yielding methyl 2,3,4-*O*-methyl-*α*-D-glucopyranoside as a white solid (4.95 g, 90%).

^{1}H NMR (400 MHz, chloroform-*d*) δ 4.76 (d, *J* = 3.6 Hz, 1H, H-1), 3.78 (dd, *J* = 11.8, 2.9 Hz, 1H), 3.69 (dd, *J* = 11.8, 4.2 Hz, 1H), 3.58 (s, 3H, –OCH_3), 3.52 (s, 3H, –OCH_3), 3.52 – 3.49 (m, 2H), 3.48 (s, 3H, –OCH_3), 3.37 (s, 3H, –OCH_3), 3.15 – 3.09 (m, 2H).

^{13}C NMR (101 MHz, chloroform-d) δ 97.59 (C-1), 83.48, 81.92, 79.67 (C-2, C-3, C4), 70.71 (C-5), 61.92 (C-6), 60.91, 60.60, 59.09, 55.21 (4x –OCH_3).

Methyl 2,3,4-*O*-methyl-6-bromo-*α*-D-glucopyranoside

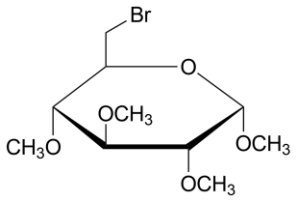

To a solution of methyl 2,3,4-*O*-methyl-*α*-D-glucopyranoside (4.93 g, 20.9 mmol) in anhydrous pyridine (60 mL), carbon tetrabromide (10.38 g, 31.3 mmol) and triphenylphosphine (10.95 g, 41.7 mmol) were added and the solution was stirred for 15 min at 0 °C. It was followed by heating the reaction to 65 °C and stirring for another 4 h. Reaction was carried under inert gas atmosphere. Reaction progress was monitored by TLC (EA). After completion of the reaction, methanol (10 mL) was added to quench the reaction. The solvent was evaporated by co-distillation with toluene and the residue was purified by column chromatography (PE:EA 3:1 to EA) yielding methyl 2,3,4-*O*-methyl-6-bromo-*α*-D-glucopyranoside as a cream-coloured solid (5.10 g, 82%).

^{1}H NMR (400 MHz, chloroform-*d*) δ 4.84 (d, *J* = 3.6 Hz, 1H, H-1), 3.70 – 3.64 (m, 2H), 3.62 (s, 3H, –OCH$_3$), 3.62 – 3.49 (m, 2H), 3.60 (s, 3H, –OCH$_3$), 3.52 (s, 3H, –OCH$_3$), 3.44 (s, 3H, –OCH$_3$), 3.21 (dd, *J* = 9.6, 3.6 Hz, 1H), 3.12 (t, *J* = 9.0 Hz, 1H).

^{13}C NMR (101 MHz, chloroform-*d*) δ 97.53 (C-1), 83.34, 81.75, 81.42 (C-2, C-3, C4), 69.43 (C-5), 60.90, 60.77, 59.06, 55.38 (–OCH$_3$), 33.54 (C-6).

***N*-(methyl 2,3,4-*O*-methyl-6-deoxy-*α*-D-glucopyranoside-6-yl)-*N*,*N*,*N*-trimethylammonium bromide ([TMGlu]Br)**

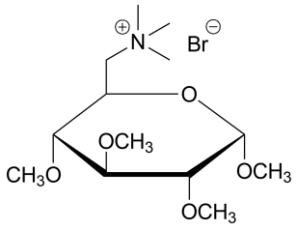

Methyl 2,3,4-*O*-methyl-6-bromo-*α*-D-glucopyranoside (6.09 g 20.4 mmol) and trimethylamine (12.03 g, 204.0 mmol, 48.6 mL 33% ethanolic solution) were placed in an autoclave and the reaction mixture was left for 48 h at 70 °C. The reaction mixture was condensed using rotary evaporator. The residue was stirred with EA (50 mL) at 70 °C

overnight. The slurry was filtered and obtained solid was further purified by column chromatography by elution with methanol, yielding *N*-(methyl 2,3,4-*O*-methyl-6-deoxy-*α*-D-glucopyranoside-6-yl)-*N,N,N*-trimethylammonium bromide as a white solid (4.90 g 65%)

^{1}H NMR (400 MHz, chloroform-*d*) δ 4.81 (d, *J* = 3.5 Hz, 1H, H-1), 3.97 (t, *J* = 8.6 Hz, 1H, H-6b), 3.80-3.85 (m, 1H), 3.71-3.75 (m, 1H), 3.62 (s, 3H, –OCH_3), 3.60 (s, 3H, –OCH_3), 3.59 (s, 9H, –$N^+(CH_3)_3$), 3.52 (s, 3H, –OCH_3), 3.50 (s, 3H, –OCH_3), 3.49-3.54 (m, 1H), 3.17 (dd, *J* = 9.8, 3.5 Hz, 1H), 2.90 (dd, *J* = 9.8, 8.6 Hz, 1H).

^{13}C NMR (101 MHz, chloroform-*d*) δ 98.55 (C-1), 82.92, 81.07, 80.35 (C-2, C-3, C4), 68.08, 66.28 (C-5, C-6), 61.33, 60.83, 59.32, 57.45 (–OCH_3), 54.72 (–$N^+(CH_3)_3$).

_N_-(methyl 2,3,4-_O_-methyl-6-deoxy-_α_-D-glucopyranoside-6-yl)-_N,N,N_-trimethylammonium nitrate ([TMGlu][NO_3])

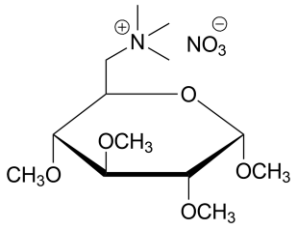

N-(methyl-6-deoxy-2,3,4-*O*-methyl-*α*-D-glucopyranoside-6-yl)-*N,N,N*-trimethylammonium bromide (1 g, 2.8 mmol) was dissolved in methanol (50 mL), and silver nitrate (0.47 g, 2.8 mmol) was added. The resulting suspension was covered from light and stirred for 24 h. The precipitate was filtered off, while the liquid phase was collected, and the solvent was evaporated. *N*-(methyl 2,3,4-*O*-methyl-6-deoxy-*α*-D-glucopyranoside-6-yl)-*N,N,N*-trimethylammonium nitrate was obtained as a white solid (0.92 g, 97%, m.p. = 105 °C).

^{1}H NMR (400 MHz, chloroform-*d*) δ 4.81 (d, *J* = 3.5 Hz, 1H, H-1), 3.96 (dt, *J* = 9.8, 4.8 Hz, 1H, H-6b), 3.70 (d, *J* = 5.1 Hz, 2H), 3.60 (s, 3H, –OCH_3), 3.59 (s, 3H, –OCH_3), 3.52 (s, 3H, –OCH_3), 3.51 (dd, *J* = 9.6, 8.7 Hz, 1H), 3.51 (s, 3H, –OCH_3), 3.41 (s, 9H, –$N^+(CH_3)_3$), 3.17 (dd, *J* = 9.8, 3.5 Hz, 1H), 2.89 (dd, *J* = 9.8, 8.6 Hz, 1H).

^{13}C NMR (101 MHz, chloroform-*d*) δ 98.56 (C-1), 82.90, 81.06, 80.39 (C-2, C-3, C4), 67.95, 66.37 (C-5, C-6), 61.07, 60.82, 59.30, 57.40 (–OCH_3), 54.58 (–$N^+(CH_3)_3$).

_N_-(methyl 2,3,4-_O_-methyl-6-deoxy-α-D-glucopyranoside-6-yl)-_N,N,N_-trimethylammonium mesylate ([TMGlu][OMs])

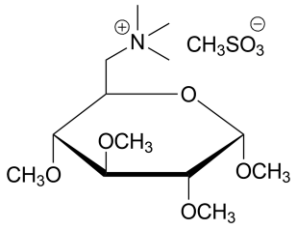

N-(methyl-6-deoxy-2,3,4-*O*-methyl-α-D-glucopyranoside-6-yl)-*N,N,N*-trimethylammonium bromide (1 g, 2.8 mmol) was dissolved in methanol (30 mL), and silver mesylate (0.57 g, 2.8 mmol) was added. The resulting suspension was covered from light and stirred for 24 h. The precipitate was filtered, while the liquid phase was collected, and the solvent was evaporated. *N*-(methyl 2,3,4-*O*-methyl-6-deoxy-α-D-glucopyranoside-6-yl)-*N,N,N*-trimethylammonium mesylate was obtained as a white solid (0.90 g, 87%, m.p. = 135 °C).

^{1}H NMR (400 MHz, chloroform-*d*) δ 4.79 (d, *J* = 3.5 Hz, 1H), 3.96 (ddd, *J* = 9.9, 7.5, 2.4 Hz, 1H), 3.73 – 3.64 (m, 2H), 3.60 (s, 3H, –OCH_3), 3.60 (s, 3H, –OCH_3), 3.52 (s, 3H, –OCH_3), 3.51 (dd, *J* = 9.7, 8.8 Hz, 1H), 3.49 (s, 3H, –OCH_3), 3.46 (s, 9H, –$N^+(CH_3)_3$), 3.16 (dd, *J* = 9.8, 3.5 Hz, 1H), 2.88 (dd, *J* = 9.8, 8.6 Hz, 1H), 2.77 (s, 3H, $CH_3SO_3^-$).

^{13}C NMR (101 MHz, chloroform-*d*) δ 98.52 (C-1), 82.92, 81.10, 80.49 (C-2, C-3, C4), 67.76, 66.36 (C-5, C-6), 61.09, 60.84, 59.30, 57.36 (–OCH_3), 54.42 (–$N^+(CH_3)_3$), 39.68 ($CH_3SO_3^-$).

_N_-(methyl 2,3,4-_O_-methyl-6-deoxy-α-D-glucopyranoside-6-yl)-_N,N,N_-trimethylammonium tetrafluoroborate ([TMGlu][BF4])

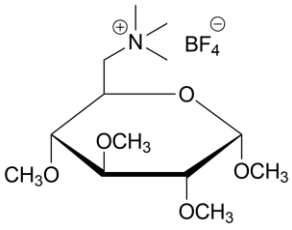

Silver oxide (0.32 g, 1.4 mmol) was stirred in methanol (30 mL) and tetrafluoroboric acid (48% solution in H_2O) was added dropwise (0.25 g, 0,37 mL, 2.8 mmol). Reaction was stirred for 1 h at rt, until homogeneous colourless solution was obtained. It was followed by addition of _N_-(methyl-6-deoxy-α-D-glucopyranoside-6-yl)-_N,N,N_-trimethylammonium bromide (1 g, 2.8 mmol). The resulting suspension was covered from light and stirred for 24 h. The slurry was filtered off, while the liquid phase was collected, and the solvent was evaporated. _N_-(methyl 2,3,4-_O_-methyl-6-deoxy-α-D-glucopyranoside-6-yl)-_N,N,N_-trimethylammonium tetrafluoroborate was obtained as a white solid (0.96 g, 94%, m.p. = 146 °C).

^{1}H NMR (400 MHz, chloroform-_d_) δ 4.81 (d, _J_ = 3.5 Hz, 1H, H-1), 3.95 (dd, _J_ = 9.6, 7.2 Hz, 1H, H-6b), 3.68 – 3.47 (m, 3H), 3.60 (s, 3H, –OCH_3), 3.59 (s, 3H, –OCH_3), 3.52 (s, 3H, –OCH_3), 3.51 (s, 3H, –OCH_3), 3.30 (s, 9H, –$N^+(CH_3)_3$), 3.17 (dd, _J_ = 9.8, 3.5 Hz, 1H), 2.88 (dd, _J_ = 9.8, 8.6 Hz, 1H).

^{13}C NMR (101 MHz, chloroform-_d_) δ 98.51 (C-1), 82.89, 81.05, 80.37 (C-2, C-3, C4), 67.95, 66.34 (C-5, C-6), 61.03, 60.80, 59.26, 57.38 (–OCH_3), 54.52 (–$N^+(CH_3)_3$).

2,3,4,5-tetra-_O_-acetyl-1,6-dibromo-1,6-dideoxy-D-mannitol

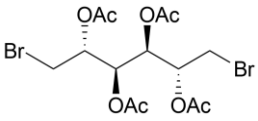

To a suspension of mannitol (6.89 g, 38 mmol) in dry 1,4-dioxane (110 mL), acetyl bromide (11.19 g, 91 mmol, 6,8 mL) was added dropwise and the solution was stirred for 72 h at rt under inert gas atmosphere. Resulting mixture was condensed using rotary evaporator and subsequently, pyridine (40 mL) and acetic anhydride (79.79 g, 782 mmol, 74 mL) were added to the condensate

and stirred overnight. Resulting mixture was condensed using rotary evaporator and the residue was purified by column chromatography (hexane:EA 6:1 to hexane:EA 3:1), yielding pale brown solid (9.37 g, 52%).

^{1}H NMR (400 MHz, chloroform-*d*) δ 5.43 – 5.40 (m, 2H, H-3, H-4), 5.13 – 5.08 (m, 2H, H-2, H-5), 3.55 (dd, *J* = 11.5, 3.7 Hz, 2H, H-1a, H-6a), 3.37 (dd, *J* = 11.5, 6.0 Hz, 2H, H-1b, H-6b), 2.12 (s, 6H), 2.11 (s, 6H) (4x C=O, –Ac).

^{13}C NMR (101 MHz, chloroform-*d*) δ 169.78, 169.67 (4x C=O, –Ac), 69.17 (C-3, C-4), 68.95 (C-2, C-5), 30.63 (C-1, C-6), 20.81, 20.72 (4x –CH_3, –Ac).

(2S,3S,4S,5S)-2,3,4,5-tetrahydroxy-*N*^{1},*N*^{1},*N*^{1},*N*^{6},*N*^{6},*N*^{6}-hexamethylhexane-1,6-diaminium bromide ([Man]Br)

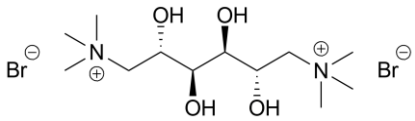

2,3,4,5-tetra-O-acetyl-1,6-dibromo-1,6-dideoxy-D-mannitol (2.25 g 4.7 mmol) and trimethylamine (5.59 g, 95 mmol, 22.5 mL 33% ethanolic solution) were placed in an autoclave and the reaction mixture was left for 24 h at 70 °C. The slurry filtered and resulting solid was washed with ethanol and hexane. (2S,3S,4S,5S)-2,3,4,5-tetrahydroxy-N1,N1,N1,N6,N6,N6-hexamethylhexane-1,6-diaminium bromide (2) was afforded as a white crystalline solid by recrystallization from anhydrous methanol using Monowave reactor (120 °C, 5 min) (1.24 g, 62%).

^{1}H NMR (400 MHz, DMSO-d_6) δ 5.43 (d, *J* = 7.2 Hz, 2H, 2x –OH), 4.72 (d, *J* = 8.0 Hz, 2H, 2x –OH), 4.07 (q, *J* = 8.6 Hz, 2H, H-3, H-4), 3.67 (dd, *J* = 13.5, 1.4 Hz, 2H, H-2, H-5), 3.53 (t, *J* = 8.4 Hz, 2H, H-1a, H-6a), 3.38 (dd, *J* = 13.4, 9.5 Hz, 2H, H-1b, H-6b), 3.17 (s, 18H, 2x –$N^{+}(CH_3)_3$).

^{13}C NMR (101 MHz, DMSO) δ 69.89 (C-3, C-4), 69.05 (C-2, C-5), 65.22 (C-1, C-6), 53.53 (2x –CH_3), 53.50 (2x –CH_3), 53.46 (2x –CH_3).

(2S,3S,4S,5S)-2,3,4,5-tetrahydroxy-*N*^{1},*N*^{1},*N*^{1},*N*^{6},*N*^{6},*N*^{6}-hexamethylhexane-1,6-diaminium nitrate ([Man][NO_3])

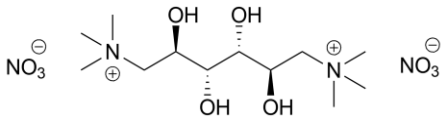

(2S,3S,4S,5S)-2,3,4,5-tetrahydroxy-*N*^{1},*N*^{1},*N*^{1},*N*^{6},*N*^{6},*N*^{6}-hexamethylhexane-1,6-diaminium bromide (0.5 g, 1.2 mmol) was dissolved in water (15 mL), and silver nitrate (0.4 g, 2.4 mmol) was added. The resulting suspension was covered from light and stirred for 24 h. The slurry was filtered, while the liquid phase was collected, and the solvent was evaporated. A white solid was obtained and recrystallized from anhydrous methanol using Monowave reactor (120 °C, 5 min) (0.39 g, 85%).

^{1}H NMR (400 MHz, DMSO-d_6) δ 5.48 (d, J = 6.4 Hz, 2H, 2x –OH), 4.79 (s, 2H, 2x –OH), 4.04 (s, 2H, H-3, H-4), 3.65 (dd, J = 13.4, 1.4 Hz, 2H, H-2, H-5), 3.52 (d, J = 8.6 Hz, 2H, H-1a, H-6a), 3.36 (dd, J = 13.7, 9.7 Hz, 2H, H-1b, H-6b), 3.15 (s, 18H, 2x –$N^+(CH_3)_3$).

^{13}C NMR (101 MHz, DMSO-d_6) δ 69.95 (C-3, C-4), 69.16 (C-2, C-5), 65.39 (C-1, C-6), 53.52 (2x –$N^+(CH_3)_3$).

(2S,3S,4S,5S)-2,3,4,5-tetrahydroxy-*N*^{1},*N*^{1},*N*^{1},*N*^{6},*N*^{6},*N*^{6}-hexamethylhexane-1,6-diaminium mesylate ([Man][OMs])

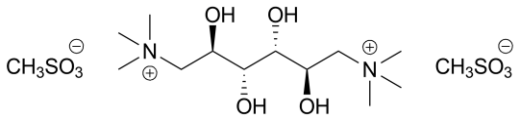

(2S,3S,4S,5S)-2,3,4,5-tetrahydroxy-*N*^{1},*N*^{1},*N*^{1},*N*^{6},*N*^{6},*N*^{6}-hexamethylhexane-1,6-diaminium bromide (0.5 g, 1.2 mmol) was dissolved was dissolved in water (15 mL), and silver mesylate (0.48 g, 2.4 mmol) was added. The resulting suspension was covered

from light and stirred for 24 h. The slurry was filtered, while the liquid phase was collected, and the solvent was evaporated. A white solid was obtained and recrystallized from anhydrous methanol using Monowave reactor (120 °C, 5 min) (0.47 g, 88%).

^{1}H NMR (400 MHz, DMSO-d_6) δ 5.53 (d, J = 7.2 Hz, 2H, 2x –OH), 4.84 (d, J = 8.0 Hz, 2H, 2x –OH), 4.03 (d, J = 8.4 Hz, 2H, H-3, H-4), 3.66 – 3.63 (m, 2H, H-2, H-5), 3.52 (t, J = 8.4 Hz, 2H, H-1a, H-6a), 3.36 (dd, J = 13.7, 9.6 Hz, 2H, H-1b, H-6b), 3.15 (s, 18H, 2x –$N^+(CH_3)_3$), 2.36 (s, 6H, 2x $CH_3SO_3^-$).

^{13}C NMR (101 MHz, DMSO-d_6) δ 69.87 (C-3, C-4), 69.21 (C-2, C-5), 65.35 (C-1, C-6), 53.48 (2x –$N^+(CH_3)_3$), 39.68 (s, 6H, 2x $CH_3SO_3^-$).

(2S,3S,4S,5S)-2,3,4,5-tetrahydroxy-*N*^{1},*N*^{1},*N*^{1},*N*^{6},*N*^{6},*N*^{6}-hexamethylhexane-1,6-diaminium tetrafluoroborate ([Man][BF_4])

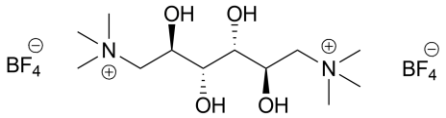

Silver oxide (0.27 g, 1.2 mmol) was stirred in water (15 mL) and tetrafluoroboric acid (48% solution in H_2O) was added dropwise (0.43 g, 0.31 mL, 2.4 mmol). Reaction was stirred for 1 h at rt, until homogeneous colourless solution was obtained. It was followed by addition of (2S,3S,4S,5S)-2,3,4,5-tetrahydroxy-*N*^{1},*N*^{1},*N*^{1},*N*^{6},*N*^{6},*N*^{6}-hexamethylhexane-1,6-diaminium bromide (0.5 g, 1.2 mmol). The resulting suspension was covered from light and stirred for 24 h. The slurry was filtered, while the liquid phase was collected, and the solvent was evaporated. A white solid was obtained and recrystallized from anhydrous methanol using Monowave reactor (120 °C, 5 min) (0.42 g, 81%).

^{1}H NMR (400 MHz, DMSO-d_6) δ 5.42 (s, 2H, 2x –OH), 4.75 (s, 2H, 2x –OH), 3.99 (t, J = 9.2 Hz, 2H, H-3, H-4), 3.62 (dd, J = 13.5, 1.5 Hz, 2H, H-2, H-5), 3.51 (d, J = 8.7 Hz, 2H, H-1a, H-6a), 3.33 (dd, J = 13.5, 9.5 Hz, 2H, H-1b, H-6b), 3.14 (s, 18H, 2x –$N^+(CH_3)_3$).

13C NMR (101 MHz, DMSO-d_6) δ 69.98 (C-3, C-4), 69.22 (C-2, C-5), 65.59 (C-1, C-6), 53.55 (2x $-N^+(CH_3)_3$).

Silver Thiocyanate (AgSCN)

Potassium thiocyanate (17.54 g, 180 mmol) and silver nitrate (33.67 g, 198 mmol) were each dissolved in 140 mL of water. The silver nitrate solution was added dropwise to the potassium thiocyanate solution, with a brownish precipitate being immediately formed. The reaction was covered from the light and stirred for 24 h. The precipitated product was filtered off, washed with water, and dried (29.42 g, 98%).

Silver Dicyanamide ($AgN(CN)_2$)

Sodium dicyanamide (25.00 g, 281 mmol) and silver nitrate (47.70 g, 281 mmol) were each dissolved in 150 mL of water. The silver nitrate solution was added dropwise to the sodium dicyanamide solution, with a violet precipitate being immediately formed. The reaction was covered from light and stirred for 24 h. The precipitated product was filtered off, washed with water, and dried (25.30 g, 95%).

Silver Tricyanomethanide ($AgC(CN)_3$)

Potassium tricyanomethanide (4.02 g, 31 mmol) and silver nitrate (5.82 g, 34 mmol) were each dissolved in 40 mL of water. The silver nitrate solution was added dropwise to the potassium tricyanomethanide solution, with a cream precipitate being immediately formed. The reaction was covered from light and stirred for 24 h. The precipitated product was filtered off, washed with water, and dried (6.00 g, 97%).

Silver Tetracyanoborate ($AgB(CN)_4$)

Potassium tetracyanoborate (4.92 g, 32 mmol) and silver nitrate (5.97 g, 35 mmol) were each dissolved in 40 mL of water. The silver nitrate solution was added dropwise to the potassium tetracyanoborate solution, with a light-gray precipitate being immediately formed. The reaction was covered from light and stirred for 24 h. The precipitated product was filtered off, washed with water, and dried (6.94 g, 98%).

***N*-(6-deoxy-1-*O*-methoxy-*α*-D-glucopyranoside)-*N*,*N*,*N*-trimethylammonium thiocyanate ([Glu][SCN])**

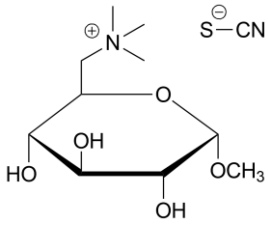

N-(6-deoxy-1-*O*-methoxy-*α*-D-glucopyranoside)-*N*,*N*,*N*-trimethylammonium bromide (17.59 g, 56 mmol) was dissolved in methanol (350 mL), and silver thiocyanate (9.49 g, 57 mmol) was added. The resulting suspension was covered from light and stirred for 24 h. The slurry was filtered, while the liquid phase was collected and the solvent was evaporated. *N*-(6-deoxy-1-*O*-methoxy-*α*-D-glucopyranoside)-*N*,*N*,*N*-trimethylammonium thiocyanate was obtained as a white solid (15.97 g, 98%, m.p. = 173 °C).

^{1}H NMR (400 MHz, DMSO-d_6) δ 5.45 (d, 1H, –OH; J = 6.0 Hz), 5.03 (d, 1H, –OH; J = 5.1 Hz), 4.92 (d, 1H, –OH; J = 6.4 Hz), 4.60 (d, 1H, H-1; J = 3.7 Hz), 3.89 (t, 1H, H-6b; J = 9.0 Hz), 3.63 (d, 1H, H-6a; J = 13.3 Hz), 3.41–3.53 (m, 2H, H-4, H-5) 3.39 (s, 3H, –OCH_3), 3.19–3.24 (m, 1H, H-3), 3.13 (s, 9H, –$N^+(CH_3)_3$), 2.88–2.95 (m, 1H, H-3).

^{13}C NMR (101 MHz, DMSO-d_6) δ 129.06 (–CN), 100.63 (C-1), 72.33, 71.54, 71.09 (C-2, C-3, C-4), 66.93, 66.79 (C-5, C-6), 56.40 (–OCH_3), 53.32 (–$N^+(CH_3)_3$).

ESI-MS: [M^+] calculated: 236.1498; found: 236.1504; [M^-] calculated: 57.9751; found: 57.9772.

_N_-(6-deoxy-1-_O_-methoxy-_α_-D-glucopyranoside)-_N_,_N_,_N_-trimethylammonium dicyanamide ([Glu][DCA])

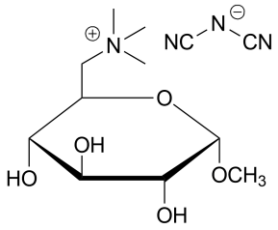

_N_-(6-deoxy-1-_O_-methoxy-_α_-D-glucopyranoside)-_N_,_N_,_N_-trimethylammonium bromide (14.35 g, 45 mmol) was dissolved in methanol (200 mL), and silver dicyanamide (7.89 g, 45 mmol) was added. The resulting suspension was covered from light and stirred for 24 h. The slurry was filtered, while the liquid phase was collected and the solvent was evaporated. _N_-(6-deoxy-1-_O_-methoxy-_α_-D-glucopyranoside)-_N_,_N_,_N_-trimethylammonium dicyanamide was obtained as a white solid (12.80 g, 94%, m.p. = 123 °C).

^{1}H NMR (400 MHz, DMSO-d_6) δ 5.45 (d, 1H, –OH; J = 6.0 Hz), 5.03 (d, 1H, –OH; J = 5.2 Hz), 4.92 (d, 1H, –OH; J = 6.4 Hz), 4.60 (d, 1H, H-1; J = 3.7 Hz), 3.89 (t, 1H, H-6b; J = 9.0 Hz), 3.63 (d, 1H, H-6a; J = 13.1 Hz), 3.41–3.52 (m, 2H, H-4, H-5), 3.39 (s, 3H, –OCH_3), 3.19–3.24 (m, 1H, H-3), 3.12 (s, 9H, –$N^+(CH_3)_3$), 2.90–2.94 (m, 1H, H-3).

^{13}C NMR (101 MHz, DMSO-d_6) δ 118.98 (–CN), 100.64 (C-1), 72.34, 71.55, 71.10 (C-2, C-3, C-4), 66.94, 66.80 (C-5, C-6), 56.40 (–OCH_3), 53.32 (–$N^+(CH_3)_3$).

ESI-MS: [M^+] calculated: 236.1498; found: 236.1498; [M^-] calculated: 66.0092; found: 66.0108.

_N_-(6-deoxy-1-_O_-methoxy-α-D-glucopyranoside)-_N,N,N_-trimethylammonium tricyanomethanide ([Glu][TCM])

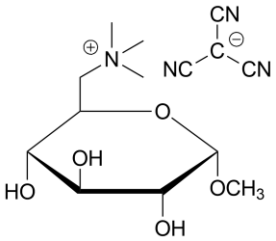

_N_-(6-deoxy-1-_O_-methoxy-α-D-glucopyranoside)-_N,N,N_-trimethylammonium bromide (9.58 g, 30 mmol) was dissolved in methanol (200 mL), and silver tricyanomethanide (6.00 g, 30 mmol) was added. The resulting suspension was covered from light and stirred for 24 h. The slurry was filtered, while the liquid phase was collected and the solvent was evaporated. N-(6-deoxy-1-O-methoxy-α-D-glucopyranoside)-N,N,N-trimethylammonium tricyanomethanide was obtained as a cream-colored viscous liquid (9.61 g, 97%).

^{1}H NMR (400 MHz, DMSO-d_6) δ 5.45 (d, 1H, –OH; J = 6.0 Hz), 5.04 (d, 1H, –OH; J = 5.2 Hz), 4.92 (d, 1H, –OH; J = 6.4 Hz), 4.60 (d, 1H, H-1; J = 3.7 Hz), 3.89 (t, 1H, H-6b; J = 9.0 Hz), 3.63 (d, 1H, H-6a; J = 13.2 Hz), 3.41–3.52 (m, 2H, H-4, H-5), 3.39 (s, 3H, –OCH_3), 3.19–3.24 (m, 1H, H-3), 3.12 (s, 9H, –$N^+(CH_3)_3$), 2.91–2.95 (m, 1H, H-2).

^{13}C NMR (101 MHz, DMSO-d_6) δ 120.38 (–CN), 100.66 (C-1), 72.36, 71.55, 71.10 (C-2, C-3, C-4), 66.94, 66.80 (C-5, C-6), 56.41 (–OCH_3), 53.33 (–$N^+(CH_3)_3$), 4.64 ($C(CN)_3^-$).

ESI-MS: [M^+] calculated: 236.1498; found: 236.1498; [M^-] calculated: 90.0092; found: 90.0127.

_N_-(6-deoxy-1-_O_-methoxy-α-D-glucopyranoside)-_N,N,N_-trimethylammonium tetracyanoborate ([Glu][TCB])

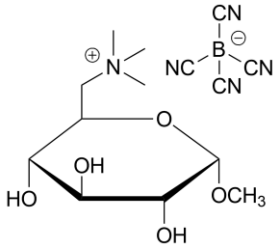

_N_-(6-deoxy-1-_O_-methoxy-α-D-glucopyranoside)-_N,N,N_-trimethylammonium bromide (9.85 g, 31 mmol) was dissolved in methanol (200 mL), and silver tetracyanoborate (6.94 g, 31 mmol) was added. The resulting suspension was covered from light and stirred for 24 h. The slurry was filtered, while the liquid phase was collected and the solvent was evaporated. _N_-(6-deoxy-1-_O_-methoxy-α-D-glucopyranoside)-_N,N,N_-trimethylammonium tetracyanoborate was obtained as a yellow solid (10.55 g, 96%, m.p. = 76 °C).

^{1}H NMR (400 MHz, DMSO-d_6) δ 5.45 (d, 1H, –OH; J = 6.0 Hz), 5.04 (d, 1H, –OH; J = 5.1 Hz), 4.92 (d, 1H, –OH; J = 6.4 Hz), 4.60 (d, 1H, H-1; J = 3.7 Hz), 3.89 (t, 1H, H-6b; J = 9.0 Hz), 3.63 (d, 1H, H-6a; J = 13.2 Hz), 3.43–3.52 (m, 2H, H-4, H-5), 3.39 (s, 3H, –OCH_3), 3.20–3.25 (m, 1H, H-3), 3.12 (s, 9H, –$N^+(CH_3)_3$), 2.91–2.95 (m, 1H, H-2).

^{13}C NMR (101 MHz, DMSO-d_6) δ 122.68, 121.98, 121.27, 120.57 (–CN), 100.63 (C-1), 72.34, 71.53, 71.09 (C-2, C-3, C-4), 66.92, 66.79 (C-5, C-6), 56.38 (–OCH_3), 53.31 (–$N^+(CH_3)_3$).

ESI-MS: [M^+] calculated: 236.1498; found: 236.1498; [M^-] calculated: 115.0216; found: 115.0238.

_N_-(6-deoxy-1-_O_-methoxy-α-D-glucopyranoside)-_N,N,N_-trimethylammonium bis(trifluoromethanesulfonyl)imide ([Glu][NTf_2])

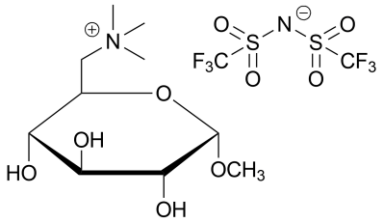

_N_-(6-deoxy-1-_O_-methoxy-α-D-glucopyranoside)-_N,N,N_-trimethylammonium bromide (3.01 g, 10 mmol) was dissolved in water (20 mL), followed by addition of lithium bis(trifluoromethanesulfonyl)imide (3.01 g, 11 mmol). Solution was stirred for 24 h. Product was extracted from the reaction mixture using EA (5 x 25 ml). Organic phase was condensed and washed with water (20 mL), followed by addition of drying agent and filtration. Product was dried in vacuum overnight. _N_-(6-deoxy-1-_O_-methoxy-α-D-glucopyranoside)-_N,N,N_-trimethylammonium bis(trifluoromethanesulfonyl)imide was obtained as yellow viscous liquid (3.20 g, 65%).

^{1}H NMR (400 MHz, DMSO-d_6) δ 5.45 (d, 1H, –OH; J = 6.0 Hz), 5.04 (d, 1H, –OH; J = 5.1 Hz), 4.93 (d, 1H, –OH; J = 6.4 Hz), 4.60 (d, 1H, H-1; J = 3.7 Hz), 3.89 (t, 1H, H-6b; J = 9.1 Hz), 3.63 (d, 1H, H-6a; J = 13.2 Hz), 3.44-3.48 (m, 2H, H-4, H-5), 3.38 (s, 3H, –OCH_3), 3.20-3.24 (m, 1H, H-3), 3.12 (s, 9H, –$N^+(CH_3)_3$), 2.89-2.93 (m, 1H, H-2).

^{13}C NMR (101 MHz, DMSO-d_6) δ 123.95, 120.63, 117.43, 114.18 (–CF_3), 100.30 (C-1), 72.01, 71.21, 70.76 (C-2, C-3, C-4), 66.62, 66.47 (C-5, C-6), 56.03 (–OCH_3), 53.00 (–$N^+(CH_3)_3$).

ESI-MS: [M^+] calcd.: 236,1498; found: 236,1500; [M^-] calcd.: 279,9173; found: 279,9176.

2-bromoethyl-2,3,4,6-tetra-_O_-acetyl-β-D-glucopyranoside

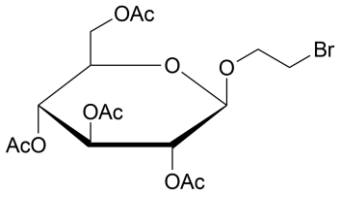

β-D-glucose pentaacetate (64.00 g, 0.16 mol) was placed in a flask equipped with a dropping funnel and dissolved in dichloromethane (250 mL). The resulting mixture was stirred

at 0 °C, while being protected from ambient light. Subsequently, 2-bromoethanol (24.6 g, 0.20 mol, 13.95 mL) was added. Boron trifluoride diethyl etherate ($BF_3 \cdot Et_2O$) was added dropwise (116.4 g, 0.82 mol, 101.18 mL) over 70 min. The reaction was stirred for 3 h at 0°C and then 20 h at rt. It was then diluted with dichloromethane (100 mL) and cold water (250 ml) and stirred vigorously. The organic layer was separated, washed with saturated $NaHCO_3$ aqueous solution, dried with anhydrous $MgSO_4$, filtered, and the solvent evaporated. The product was purified using column chromatography with 2% MeOH in dichloromethane as an eluent. 2-bromoethyl-2,3,4,6-tetra-*O*-acetyl-β-D-glucopyranoside was obtained as a white solid (37.30 g, 50%).

^{1}H NMR (600 MHz, chloroform-*d*) δ 5.22 (t, J = 9.5 Hz, 1H, H-1), 5.09 (dd, J = 10.0, 9.4 Hz, 1H), 5.02 (dd, J = 9.7, 8.0 Hz, 1H), 4.58 (d, J = 8.0 Hz, 1H), 4.26 (dd, J = 12.3, 4.8 Hz, 1H), 4.19 – 4.12 (m, 2H), 3.82 (ddd, J = 11.3, 7.5, 6.1 Hz, 1H), 3.72 (ddd, J = 10.0, 4.8, 2.4 Hz, 1H), 3.47 (ddd, J = 7.6, 5.8, 5.1 Hz, 2H), 2.09 (s, 3H), 2.07 (s, 3H), 2.03 (s, 3H), 2.01 (s, 3H) (4x –CH_3, –Ac).

^{13}C NMR (151 MHz, chloroform-*d*) δ 173.23, 172.84, 172.25, 172.00 (4x C=O, –Ac), 103.64 (C-1), 75.24, 74.58, 73.67, 72.39, 70.98 (C-2, C-3, C-4, C-5, C-6), 64.49 (–O–CH_2–), 32.47 (–CH_2–Br), 23.48, 23.35, 23.31, 23.21 (4x –CH_3, –Ac).

ESI-MS: $[M+Na]^+$ calculated: 477.0372, found: 477.0375.

_N_-[2-(2,3,4,6-tetra-_O_-acetyl-β-D-glucopyranosyloxy)ethyl]-_N_,_N_,_N_-trimethylammonium bromide ([ATAGlu]Br)

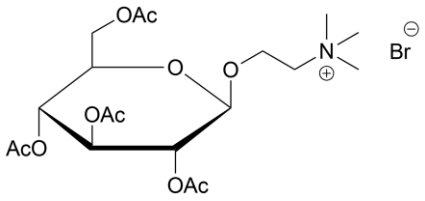

2-bromoethyl-2,3,4,6-tetra-*O*-acetyl-β-D-glucopyranoside (37.3 g 0.08 mol) and trimethyl ammine 33% ethanolic solution (48.4 g, 0.82 mol, 200 mL) were stirred at 70 °C under reflux for 6 h. Resulting precipitate

was filtered off and washed with cold ethanol and hexane. *N*-[2-(2,3,4,6-tetra-*O*-acetyl-β-D-glucopyranosyloxy)ethyl]-*N*,*N*,*N*-trimethylammonium bromide was obtained as a white solid (26.6 g, 63%).

^{1}H NMR (400 MHz, DMSO-d_6) δ 5.28 (t, J = 9.6 Hz, 1H, H-1), 4.99 – 4.89 (m, 2H), 4.82 (dd, J = 9.8, 8.0 Hz, 1H), 4.19 (dd, J = 12.3, 5.0 Hz, 1H), 4.14 – 3.99 (m, 4H), 3.58 (t, J = 4.8 Hz, 2H), 3.09 (s, 9H, –N^{+}(CH$_3$)$_3$), 2.03 (s, 3H, –CH$_3$, –Ac), 2.02 (s, 3H, –CH$_3$, –Ac), 2.00 (s, 3H, –CH$_3$, –Ac), 1.95 (s, 3H, –CH$_3$, –Ac).

^{13}C NMR (101 MHz, DMSO-d_6) δ 170.50, 169.98, 169.72, 169.57 (4x C=O, –Ac), 99.23 (C-1), 72.31, 71.22, 71.11 (C-2, C-3, C-4), 68.47, 64.78 (C-5, C-6), 62.99, 61.99 (–O–CH$_2$–, –N^{+}–CH$_2$–), 53.48 (–N^{+}(CH$_3$)$_3$), 20.97, 20.82, 20.81, 20.69 (4x –CH$_3$, –Ac).

ESI-MS: [M^{+}] calculated: 434.2026; found: 434.2054; [M^{-}] calculated: 78.9183; found: 78.9226.

_N_-[2-(2,3,4,6-tetra-_O_-acetyl-β-D-glucopyranosyloxy)ethyl]-_N_,_N_,_N_-trimethylammonium dodecyl sulfate ([ATAGlu][DS])

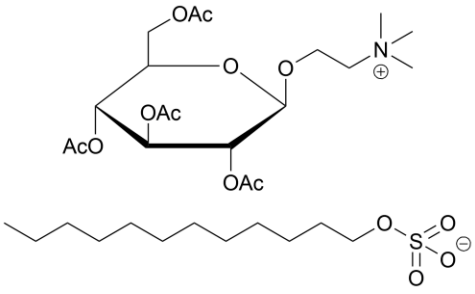

N-[2-(2,3,4,6-tetra-*O*-acetyl-β-D-glucopyranosyloxy)ethyl]-*N*,*N*,*N*-trimethylammonium bromide (15.00 g, 0.029 mol) was dissolved in water (45 mL). Subsequently sodium dodecyl sulfate (8.41 g 0.029 mol) was added and left overnight. Resulting mixture was washed with EA (8x20 mL). Organic phase was dried with MgSO$_4$ and the solvent was evaporated. *N*-[2-(2,3,4,6-tetra-*O*-acetyl-β-D-glucopyranosyloxy)ethyl]-*N*,*N*,*N*-trimethylammonium dodecyl sulfate was obtained as a white solid (18.41 g, 89%).

^{1}H NMR (400 MHz, chloroform-*d*) δ 5.21 (t, J = 9.5 Hz, 1H, H-1), 5.06 (dd, J = 10.1, 9.3 Hz, 1H), 4.95 (dd, J = 9.7, 8.1 Hz, 1H), 4.63 (d, J = 8.0 Hz, 1H), 4.36 – 4.07 (m, 4H), 3.99 (t, J = 6.9 Hz, 2H), 3.95 – 3.74 (m, 3H), 3.30 (s, 9H, –$N^{+}(CH_3)_3$), 2.10 (s, 3H), 2.06 (s, 3H), 2.03 (s, 3H), 2.00 (s, 3H) (4x –CH_3, –Ac), 1.69 – 1.62 (m, 2H, –CH_2–, DS), 1.38 – 1.25 (m, 18H, 10x –CH_2–, DS), 0.88 (t, J = 6.5 Hz, 3H, –CH_3, DS).

^{13}C NMR (101 MHz, chloroform-*d*) δ 170.66, 169.97, 169.59, 169.46 (4x C=O, –Ac), 100.47 (C-1), 72.45, 72.24, 71.01 (C-2, C-3, C-4), 68.12, 67.95 (C-5, C-6), 65.50 (–CH_2–OSO_3^{-}), 63.90, 61.43 (–O–CH_2–, –N^{+}–CH_2–), 54.53 (–$N^{+}(CH_3)_3$), 31.93, 29.72, 29.70, 29.66, 29.65, 29.55, 29.45, 29.37, 25.91, 22.69 (10x –CH_2–, DS), 20.83, 20.71, 20.58, 20.55 (4x –CH_3, –Ac), 14.12 (–CH_3, DS).

ESI-MS: [M^{+}] calculated: 434.2026; found: 434.2034; [M^{-}] calculated: 265.1474; found: 265.2902.

_N_-[2-(β-D-glucopyranosyloxy)ethyl]-_N,N,N_-trimethylammonium dodecyl sulfate ([AGlu][DS])

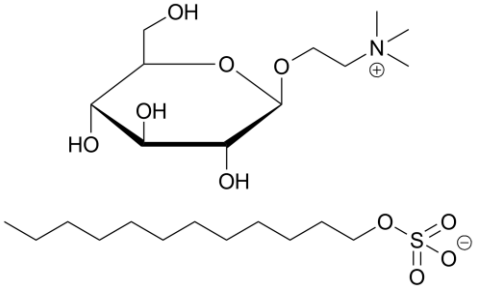

N-[2-(2,3,4,6-tetra-*O*-acetyl-β-D-glucopyranosyloxy)ethyl]-*N,N,N*-trimethylammonium dodecyl sulfate (10.00 g, 0.014 mol) was introduced to a mixture of water (100 mL), MeOH (100 mL) and NEt_3 (10 mL) and stirred overnight. The resulting mixture was then condensed on rotary evaporator and extensively dried using a Schlenk line. *N*-[2-(β-D-glucopyranosyloxy)ethyl]-*N,N,N*-trimethylammonium dodecyl sulfate was obtained as a white solid (7.6 g, 100%).

^{1}H NMR (400 MHz, DMSO-d_6) δ 5.14 – 4.92 (m, 3H, –OH), 4.51 (t, J = 5.9 Hz, 1H, –OH), 4.26 (d, J = 7.8 Hz, 1H, H-1), 4.18 – 4.09 (m, 1H), 4.01 – 3.92 (m, 1H), 3.73 – 3.62 (m,

3H) (H-2, H-3, H-4, –CH_2–OSO_3^-), 3.57 (t, J = 4.9 Hz, 2H), 3.44 (dt, J = 11.3, 5.3 Hz, 1H), 3.20 – 3.07 (m, 2H), 3.12 (s, 9H, –$N^+(CH_3)_3$), 3.08 – 2.93 (m, 2H), 1.47 (t, J = 6.8 Hz, 2H, –CH_2–, DS), 1.33 – 1.14 (m, 18H, 9x –CH_2–, DS), 0.86 (t, J = 6.9 Hz, 3H, –CH_3, DS).

^{13}C NMR (101 MHz, DMSO-d_6) δ 102.35 (C-1), 76.99, 76.59, 73.13 (C-2, C-3, C-4), 69.98 (C-6), 65.38 (–CH_2–OSO_3^-), 64.39 (C-5), 62.32, 61.03 (–O–CH_2–, –N^+–CH_2–), 53.22, 53.18, 53.15 (–$N^+(CH_3)_3$), 31.20, 29.00, 28.97, 28.95, 28.93, 28.70, 28.62, 28.61, 25.44, 22.00 (10x –CH_2–, DS), 13.86 (–CH_3, DS).

ESI-MS: [M^+] calculated: 266.1604; found: 266.1201; [M^-] calculated: 265.1474; found: 265.2902.

_N_-[2-(β-D-glucopyranosyloxy)ethyl]-_N,N,N_-trimethylammonium bromide ([AGlu]Br)

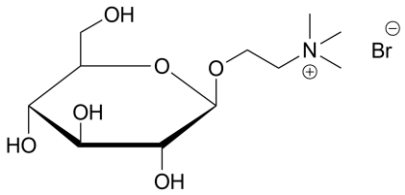

N-[2-(2,3,4,6-tetra-*O*-acetyl-β-D-glucopyranosyloxy)ethyl]-*N,N,N*-trimethylammonium bromide (3.00 g, 0.006 mol) was introduced to a mixture of water (30 mL), MeOH (30 mL) and NEt_3 (3 mL) and stirred overnight. The resulting mixture was then condensed on rotary evaporator and extensively dried using a Schlenk line. *N*-[2-(β-D-glucopyranosyloxy)ethyl]-*N,N,N*-trimethylammonium bromide was obtained as a white solid (2.0 g, 100%).

^{1}H NMR (400 MHz, DMSO-d_6) δ 5.11 (d, J = 5.2 Hz, 1H, –OH), 5.01 (d, J = 4.6 Hz, 1H, –OH), 4.96 (d, J = 5.3 Hz, 1H, –OH), 4.52 (t, J = 5.9 Hz, 1H, –OH), 4.27 (d, J = 7.8 Hz, 1H, H-1), 4.18 – 4.10 (m, 1H), 4.01 – 3.93 (m, 1H), 3.69 (ddd, J = 11.7, 6.1, 2.1 Hz, 1H) (H-2, H-3, H-4), 3.59 (t, J = 4.9 Hz, 2H), 3.44 (dt, J = 11.8, 5.9 Hz, 1H), 3.21 – 3.09 (m, 2H), 3.14 (s, 9H, –$N^+(CH_3)_3$) 3.08 – 2.93 (m, 2H).

^{13}C NMR (101 MHz, DMSO-d_6) δ 102.40 (C-1), 77.06, 76.67, 73.22 (C-2, C-3, C-4), 70.06 (C-6), 64.46 (C-5), 62.41, 61.09 (–O–CH_2–, –N^+–CH_2–), 53.27 (–$N^+(CH_3)_3$).

ESI-MS: [M^+] calculated: 266.1604; found: 266.0671; [M^-] calculated: 78.9183; found: 78.9198.

_N_-[2-(β-D-glucopyranosyloxy)ethyl]-_N,N,N_-trimethylammonium hydroxide ([AGlu]OH)

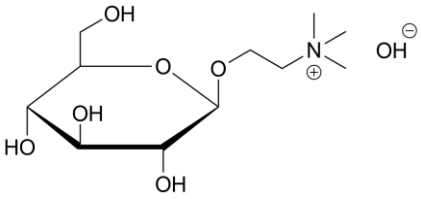

DOWEX® resin (40 g) was introduced into a 5% NaOH solution (200 mL) and transferred to a glass column. It was rinsed with 5% NaOH solution (1 L) and then with water (ca. 200 mL) until a 5% $AgNO_3$ solution did not cause the formation of a brown precipitate (indicating the presence of OH^- ions). _N_-[2-(β-D-glucopyranosyloxy)ethyl]-_N,N,N_-trimethylammonium bromide (1.97 g, 0.006 mol) was dissolved in water (98 mL) and filtrated through the column to give _N_-[2-(β-D-glucopyranosyloxy)ethyl]-_N,N,N_-trimethylammonium hydroxide as an aqueous solution, used in situ in the next synthetic step.

Cholic acid

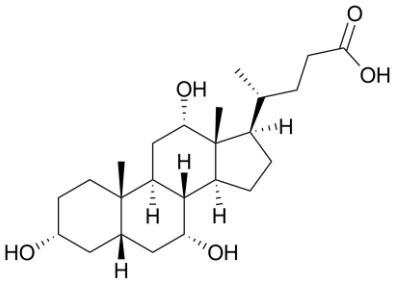

Sodium cholate (1g, 2.3 mmol) was dissolved in water (50 mL). 36% HCl was added dropwise (0.24 g, 2.3 mmol, 0.21 mL), and a white precipitate appeared. It was filtered off, washed with water, and dried. Cholic acid was obtained as a white solid (0.91 g, 96%).

Deoxycholic acid

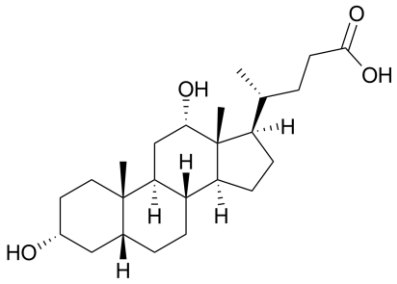

Sodium deoxycholate (1g, 2.4 mmol) was dissolved in water (50 mL). 36% HCl was added dropwise (0.25 g, 2.4 mmol, 0.21 mL), and, as a result, a white precipitate appeared. The obtained precipitate was filtered off, washed with water, and dried. Deoxycholic acid was obtained as a white solid (0.71 g, 75%).

***N*-[2-(β-D-glucopyranosyloxy)ethyl]-*N*,*N*,*N*-trimethylammonium cholate ([AGlu][C])**

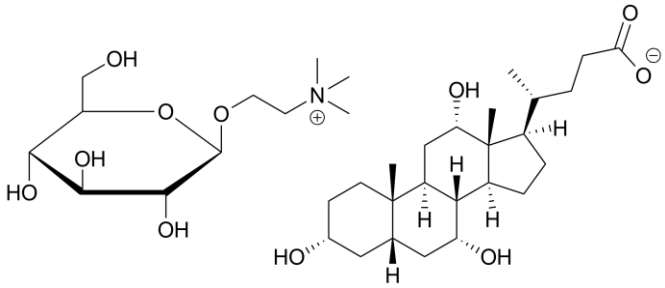

Cholic acid (1.27 g, 3.11 mmol) was added to an aqueous solution of *N*-[2-(β-D-glucopyranosyloxy)ethyl]-*N*,*N*,*N*-trimethylammonium hydroxide (0.80 g, 2.82 mmol) and stirred overnight at rt. The resulting mixture was filtered from the excess cholic acid. The filtrate was concentrated under reduced pressure and extensively dried using a Schlenk line. *N*-[2-(β-D-glucopyranosyloxy)ethyl]-*N*,*N*,*N*-trimethylammonium cholate was obtained as a white solid (1.86 g, 98%).

^{1}H NMR (400 MHz, deuterium oxide) δ 4.53 (dd, J = 8.0, 1.1 Hz, 1H, H-1), 4.47 – 4.32 (m, 1H), 4.18 – 4.02 (m, 2H), 3.99 – 3.86 (m, 2H), 3.75 (ddd, J = 12.3, 5.9, 1.2 Hz, 1H), 3.71 – 3.66 (m, 2H), 3.56 – 3.45 (m, 3H), 3.44 – 3.29 (m, 2H), 3.23 (s, 9H, $-N^+(CH_3)_3$), 2.34 – 0.98 (m, 27H), 0.93 (s, 3H), 0.74 (s, 3H).

13C NMR (101 MHz, deuterium oxide) δ 184.28 ($-COO^-$), 102.14 (C-1), 75.95, 75.61, 73.07, 73.01, 72.86, 71.50, 69.51, 68.21, 68.15, 65.49, 63.26, 60.58, 53.93, 53.89, 53.85, 46.45,

46.04, 41.42, 41.07, 39.24, 38.28, 35.48, 34.85, 34.39, 34.32, 33.81, 32.22, 29.15, 27.67, 27.20, 26.28, 22.90, 22.09, 16.68, 12.09.

ESI-MS: [M^+] calculated: 266.1604; found: 266.0651; [M^-] calculated: 407.2797; found: 407.2877.

_N_-[2-(β-D-glucopyranosyloxy)ethyl]-_N,N,N_-trimethylammonium deoxycholate ([AGlu][DOC])

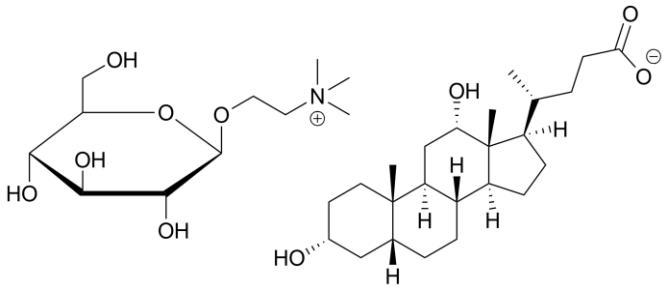

Deoxycholic acid (1.22 g, 3.11 mmol) was added to the aqueous solution of _N_-[2-(β-D-glucopyranosyloxy)ethyl]-_N,N,N_-trimethylammonium hydroxide (0.80 g, 2.82 mmol) and stirred overnight at rt. The resulting mixture was filtrated from the excess deoxycholic acid. The filtrate was concentrated under reduced pressure and extensively dried using a Schlenk line. _N_-[2-(β-D-glucopyranosyloxy)ethyl]-_N,N,N_-trimethylammonium cholate was obtained as a white solid (1.37 g, 74%).

^{1}H NMR (400 MHz, deuterium oxide) δ 4.57 – 4.50 (m, 1H, H-1), 4.46 – 4.32 (m, 1H), 4.23 – 4.04 (m, 2H), 3.96 (dq, J = 12.3, 1.8 Hz, 1H), 3.76 (ddt, J = 12.3, 5.9, 1.5 Hz, 1H), 3.73 – 3.59 (m, 3H), 3.56 – 3.46 (m, 2H), 3.46 – 3.29 (m, 2H), 3.23 (s, 9H, $-N^+(CH_3)_3$), 2.31 – 0.99 (m, 29H), 0.96 (s, 3H), 0.74 (s, 3H).

^{13}C NMR (101 MHz, deuterium oxide) δ 183.93 ($-COO^-$), 102.15 (C-1), 75.96, 75.62, 73.14, 72.86, 71.36, 69.51, 65.52, 65.49, 65.46, 63.25, 60.59, 53.94, 53.90, 53.86, 47.74, 46.47, 46.12, 41.99, 35.92, 35.71, 35.19, 35.05, 34.27, 33.84, 33.33, 32.18, 29.11, 28.20, 27.49, 27.04, 26.03, 23.67, 22.89, 16.65, 12.50.

ESI-MS: [M^+] calculated: 266.1604; found: 266.1109; [M^-] calculated: 391.2848; found: 391.3659.

6.2. Methods

NMR characterization

^1H NMR and ^{13}C NMR spectra were recorded with a 400 MHz Agilent spectrometer. Chemical shifts (ppm) are reported relative to tetramethylsilane as an internal standard. DMSO-d_6, $CDCl_3$ and deuterium oxide were used as solvents.

MS characterization

High-resolution mass spectrometry analyses were carried out on a Waters Xevo G2 Q-TOF mass spectrometer equipped with an ESI source operating in the positive and negative ion modes. The accurate mass and composition of the molecular ions were calculated using MassLynx software.

Thermogravimetric Analysis (TGA)

Thermal stability was determined by thermogravimetric analysis using a PerkinElmer Pyris 1 TGA with Pyris Software over a range of 30–550 °C under N_2 (30 mL min^{-1}) at a heating rate of 10 °C min^{-1}.

Differential Scanning Calorimetry (DSC)

Phase transition temperatures (melting and freezing) and heat of fusion (ΔH_f) were determined by DSC using a TA Q200 calorimeter (TA Instruments). The equipment was calibrated by using standards of indium (TA Instruments, T_m = 156 °C, ΔHf = 28.45 J g^{-1}) and cyclohexane (Sigma-Aldrich, T_m = 8 °C). Measurements were performed under a nitrogen atmosphere in triplicate with sample sizes of 3–8 mg and a heating rate of 10 °C min^{-1}. Presented values were taken from the second run of the DSC cycle. Melting point (T_m) and crystallization temperature (T_c) were considered as the peak maximum, and ΔH_f was determined from the area of the melting peak. While T_m determined as peak maximum represents the upper bound of the true melting point, due to the thermal lag of the sample and instrument, it is the most direct and objective way to compare a family of materials. The onset of the melting peak is subjective and can vary depending on the researcher's approach to examining the baseline and the leading-edge tangent of the peak. Additionally, the onset is disrupted by impurities. Therefore, in this work, T_m as the peak maximum was chosen.

Crystallography

Data for [TMGlu][BF_4] and [TMGlu][NO_3] were collected on the Micro Crystallography–MX2 beamline at the Australian Synchrotron[306], at 100 K. The data collection and integration were performed within the Blu-Ice[307] and XDS software programs.[308] Data for [TMGlu][Br], [Glu][OMs], and [Glu][NO_3] was collected on a Rigaku Xtalab Synergy Dualflex using Cu-Kα (λ = 1.5418 Å) radiation, at 123 K. Data were processed using proprietary software CrysAlisPro.[309] All structures were solved and refined using the SHELX[310,311] software suite, and refined against F2 using Olex2[312] as a graphical interface. Non-hydrogen atoms were refined with anisotropic

displacement parameters, and hydrogen atoms attached to carbon were included in calculated positions (riding model); for the [Glu] salts, the positions of the hydrogen atoms attached to oxygen were located in the difference Fourier map and refined.

Carbonization of Ionic Precursors

Carbohydrate-derived precursors were carbonized with Ludox® HS-40. The carbonization conditions were as follows: 0–750 °C (10° min^{-1}), 750–800 °C (1.7° min^{-1}), 800 °C (2 h), Ar 100 mL min^{-1} or 0–160 °C (4° min^{-1}), 160–600 °C (10° min^{-1}), 600 °C (2 h), Ar 100 mL/min. After carbonization, the silica was removed by washing with 4 M ammonium hydrogen difluoride (NH_4HF_2). For each 1 g of silica present in the obtained carbon materials, 45 mL of the NH_4HF_2 solution was used. The samples were denoted indicating the precursor used and carbonization temperature, e.g., [SCN]-800 for the material derived from [Carb][SCN] at 800 °C.

6.3.Materials

2-bromoethanol (CH_3CH_2Br, 95%) – Sigma-Aldrich

4-(dimethylamino)pyridine (ReagentPlus®, ⩾99%) – Sigma-Aldrich

Acetic acid (CH_3COOH, glacial, ReagentPlus®, ⩾99%) – Sigma-Aldrich

Anhydrous pyridine (99.8%) – Sigma-Aldrich

Boron trifluoride diethyl etherate ($BF_3{\cdot}Et_2O$, for synthesis) – Sigma-Aldrich

Chloroform ($CHCl_3$, 98%)– Chempur

Dichloromethane (CH_2Cl_2, 99.8%) – Chempur

DOWEX® resin – Sigma-Aldrich

Ethyl acetate (EtOAc, 99.8%) – Chempur

Hexane (C_6H_{14}, 95%)– Chempur

Hydrochloric acid (HCl, 35-38%) – Chempur

Iodomethane (CH_3I, ReagentPlus®, 99%) – Sigma-Aldrich

Ludox® HS-40 colloidal silica (SiO_2, 40 wt.% suspension in H_2O) – Sigma-Aldrich

Magnesium sulfate ($MgSO_4$, 98%) – Chempur

Methanesulfonic acid (MsOH, ≥99%) – Sigma-Aldrich

Methanol (MeOH, 99.5%) – Chempur

Methyl α-D-glucopyranoside (≥99%) – Sigma-Aldrich

Petroleum ether (boiling range 40-60 °C) – Chempur

Potassium tetracyanoborate ($KB(CN)_4$, 97%) – SelectLab Chemicals

Potassium tricyanomethanide ($KC(CN)_3$, 98%) – Strem

Silver nitrate ($AgNO_3$, 99.9%) – POCH

Silver(I) oxide (Ag_2O, ≥99.99% trace metals basis) – Sigma-Aldrich

Sodium bicarbonate ($NaHCO_3$, 98%) – Chempur

Sodium dicyanamide ($NaN(CN)_2$, 96%) – Sigma-Aldrich

Sodium hydride (NaH, 60 % dispersion in mineral oil) – Sigma-Aldrich

Sodium hydroxide (NaOH, 98%) – Chempur

Tetrabromomethane (CBr_4, 99%) – Sigma-Aldrich

Tetrafluoroboric acid solution (HBF_4, 48 wt. % in H_2O) – Sigma-Aldrich

Triethylamine (NEt_3, ⩾99%) – Sigma-Aldrich

Trimethylamine ($N(CH_3)_3$) 31–35 wt.% in ethanol solution – Sigma-Aldrich

Triphenylphosphine (PPh_3, 99%) – Sigma-Aldrich

Trityl chloride (CPh_3Cl, 97%) – Sigma-Aldrich

β-D-glucose pentaacetate (98%) – Sigma-Aldrich

7. Literature

1 M. Kar, K. Matuszek and D. R. MacFarlane, *Kirk-Othmer Encycl. Chem. Technol.*, 2019, 1–29.

2 S. Gabriel, *Berichte der Dtsch. Chem. Gesellschaft*, 1891, **24**, 1110–1121.

3 P. Walden, *Bull. Acad. Imper. Sci. (St. Petersburg)*, 1914, **8**, 405–422.

4 C. A. Angell, *J. Phys. Chem.*, 1966, **70**, 2793–2803.

5 C. A. Angell, *J. Chem. Phys.*, 1967, **46**, 4673–4679.

6 C. T. Moynihan, *J. Phys. Chem. J. Phys. Chem.*, 1966, **70**, 3399–3403.

7 H. L. Chum, V. R. Koch, L. L. Miller and R. A. Osteryoung, *J. Am. Chem. Soc.*, 1975, **97**, 3264–3265.

8 J. S. Wilkes, J. A. Levisky, R. A. Wilson and C. L. Hussey, *Inorg. Chem.*, 1982, **21**, 1263–1264.

9 J. S. Wilkes and M. J. Zaworotko, *J. Chem. Soc. Chem. Commun.*, 1992, 965–967.

10 E. I. Cooper and E. J. M. O'Sullivan, *Proc. Electrochem. Soc.*, 1992, **1992–16**, 386–396.

11 M. Galiński, A. Lewandowski and I. Stepniak, *Electrochim. Acta*, 2006, **51**, 5567–5580.

12 N. V. Plechkova and K. R. Seddon, *Chem. Soc. Rev.*, 2008, **37**, 123–150.

13 J. P. Hallett and T. Welton, *Chem. Rev.*, 2011, 111, 3508–3576.

14 R. L. Vekariya, *J. Mol. Liq.*, 2017, **227**, 44.

15 W. L. Hough, M. Smiglak, H. Rodríguez, R. P. Swatloski, S. K. Spear, D. T. Daly, J. Pernak, J. E. Grisel, R. D. Carliss, M. D. Soutullo, J. H. Davis and R. D. Rogers, *New J. Chem.*, 2007, **31**, 1429–1436.

16 K. S. Egorova, E. G. Gordeev and V. P. Ananikov, *Chem. Rev.*, 2017, **117**, 7132–7189.

17 K. Matuszek, S. L. Piper, A. Brzęczek-Szafran, B. Roy, S. Saher, J. M. Pringle and D. R. MacFarlane, *Adv. Mater.*, 2024, **2313023**, 1–26.

18 D. R. MacFarlane, A. L. Chong, M. Forsyth, M. Kar, R. Vijayaraghavan, A. Somers and J. M. Pringle, *Faraday Discuss.*, 2018, **206**, 9–28.

19 C. Florindo, F. Lima, B. D. Ribeiro and I. M. Marrucho, *Curr. Opin. Green Sustain. Chem.*, 2019, **18**, 31–36.

20 B. B. Hansen, S. Spittle, B. Chen, D. Poe, Y. Zhang, J. M. Klein, A. Horton, L. Adhikari, T. Zelovich, B. W. Doherty, B. Gurkan, E. J. Maginn, A. Ragauskas, M. Dadmun, T. A. Zawodzinski, G. A. Baker, M. E. Tuckerman, R. F. Savinell and J. R. Sangoro, *Chem. Rev.*, 2021, **121**, 1232–1285.

21 F. Coleman, G. Srinivasan and M. Swadźba-Kwaśny, *Angew. Chemie - Int. Ed.*, 2013, **52**, 12582–12586.

22 J. M. Hogg, F. Coleman, A. Ferrer-Ugalde, M. P. Atkins and M. Swadźba-Kwaśny, *Green Chem.*, 2015, **17**, 1831–1841.

23 K. Matuszek, A. Chrobok, J. M. Hogg, F. Coleman and M. Swadźba-Kwaśny, *Green Chem.*, 2015, **17**, 4255–4262.

24 J. M. Hogg, L. C. Brown, K. Matuszek, P. Latos, A. Chrobok and M. Swadźba-Kwaśny, *Dalt. Trans.*, 2017, **46**, 11561–11574.

25 D. J. Eyckens and L. C. Henderson, *Front. Chem.*, 2019, **7**, 1–15.

26 T. Mandai, K. Yoshida, K. Ueno, K. Dokko and M. Watanabe, *Phys. Chem. Chem. Phys.*, 2014, **16**, 8761–8772.

27 K. Ueno, R. Tatara, S. Tsuzuki, S. Saito, H. Doi, K. Yoshida, T. Mandai, M.

Matsugami, Y. Umebayashi, K. Dokko and M. Watanabe, *Phys. Chem. Chem. Phys.*, 2015, **17**, 8248–8257.

28 M. Watanabe, K. Dokko, K. Ueno and M. L. Thomas, *Bull. Chem. Soc. Jpn.*, 2018, **91**, 1660–1682.

29 V. A. Azov, K. S. Egorova, M. M. Seitkalieva, A. S. Kashina and V. P. Ananikov, *Chem. Soc. Rev.*, 2018, **47**, 1250–1284.

30 W. M. Haynes, *CRC Handbook of Chemistry and Physics*, CRC Press, Boca Raton, 2011.

31 R. D. Rogers and K. R. Seddon, *Science (80-.).*, 2003, **302**, 792–793.

32 A. Stark and K. R. Seddon, *Kirk-Othmer Encyclopaedia of Chemical Technology*, John Wiley & Sons, New Jersey, 2007.

33 M. Freemantle, *An Introduction to Ionic Liquids*, RSC Publishing, Cambridge, 2009.

34 J. Pernak and J. Feder-Kubis, *Chem. Eur. J.*, 2005, **11**, 4441–4449.

35 G. H. Tao, L. He, W. S. Liu, L. Xu, W. Xiong, T. Wang and Y. Kou, *Green Chem.*, 2006, **8**, 639–646.

36 Suresh and J. S. Sandhu, *Green Chem. Lett. Rev.*, 2011, **4**, 289–310.

37 V. M. Egorov, D. I. Djigailo, D. S. Momotenko, D. V. Chernyshov, I. I. Torocheshnikova, S. V. Smirnova and I. V. Pletnev, *Talanta*, 2010, **80**, 1177–1182.

38 L. Xiao, D. Su, C. Yue and W. Wu, *J. CO2 Util.*, 2014, **6**, 1–6.

39 K. Materna, T. Rzemieniecki and J. Pernak, *Chemik*, 2016, **70**, 471–480.

40 T. L. Greaves and C. J. Drummond, *Chem. Rev.*, 2008, **108**, 206–237.

41 R. A. Patil, M. Talebi, C. Xu, S. S. Bhawal and D. W. Armstrong, *Chem. Mater.*, 2016, **28**, 4315–4323.

42 J. Pernak, A. Skrzypczak, G. Lota and E. Frackowiak, *Chem. Eur. J.*, 2007, **13**, 3106–3112.

43 D. Mecerreyes, *Prog. Polym. Sci.*, 2011, **36**, 1629–1648.

44 F. M. Hoover, *J. Macromol. Sci. Part A - Chem.*, 1970, **4**, 1327–1418.

45 S. P. F. Costa, A. M. O. Azevedo, P. C. A. G. Pinto and L. M. F. S. Saraiva, *ChemSusChem*, 2017, **10**, 2321–2347.

46 A. J. Greer, J. Jacquemin and C. Hardacre, *Molecules*, 2020, **25**, 5207.

47 A. Jordan and N. Gathergood, *Chem. Soc. Rev.*, 2015, **44**, 8200–8237.

48 B. Gaida and A. Brzęczek-Szafran, *Molecules*, 2020, **25**, 3285.

49 J. M. Gomes, S. S. Silva and R. L. Reis, *Chem. Soc. Rev.*, 2019, **48**, 4317–4335.

50 J. Hulsbosch, D. E. De Vos, K. Binnemans and R. Ameloot, *ACS Sustain. Chem. Eng.*, 2016, **4**, 2917–2931.

51 S. T. Handy, M. Okello and G. Dickenson, *Org. Lett.*, 2003, **5**, 2513–2515.

52 L. Pellowska-Januszek, B. Dmochowska, E. Skorupa, J. Chojnacki, W. Wojnowski and A. Wiśniewski, *Carbohydr. Res.*, 2004, **339**, 1537–1544.

53 L. Poletti, C. Chiappe, L. Lay, D. Pieraccini, L. Polito and G. Russo, *Green Chem.*, 2007, **9**, 337–34.

54 M. Thomas, D. Montenegro, A. Castaño, L. Friedman, J. Leb, M. L. Huang, L. Rothman, H. Lee, C. Capodiferro, D. Ambinder, E. Cere, J. Galante, J. L. Rizzo, K. Melkonian and R. Engel, *Carbohydr. Res.*, 2009, **344**, 1620–1627.

55 A. Marra, C. Chiappe and A. Mele, *Chim. Int. J. Chem.*, 2011, **65**, 76–80.

56 K. Erfurt, I. Wandzik, K. Walczak, K. Matuszek and A. Chrobok, *Green Chem.*, 2014,

16, 3508–3514.

57 R. Yuan, Y. jiang Wang, Y. Fang, W. hui Ge, W. Lin, M. qi Li, J. biao Xu, Y. Wan, Y. Liu and H. Wu, *Chem. Eng. J.*, 2017, **316**, 1026–1034.

58 J. Schnegas and S. Jopp, *Compounds*, 2021, **1**, 154–163.

59 P. Lehmann and S. Jopp, *ChemistryOpen*, 2022, **11**, e202200135.

60 S. Jopp, T. Fleischhammer, A. Lavrentieva, S. Kara and J. Meyer, *RSC Sustain.*, , DOI:https://doi.org/10.1039/D3SU00191A.

61 R. Jayachandra and S. R. Reddy, *Trends Carbohydr. Res.*, 2015, **7**, 60–67.

62 R. Jayachandra, S. R. Reddy and Balakrishna, *ChemistrySelect*, 2016, **1**, 2341–2343.

63 N. Kaur and H. K. Chopra, *J. Mol. Liq.*, 2020, **298**, 111994.

64 R. Jayachandra and S. R. Reddy, *RSC Adv.*, 2016, **6**, 39758–39761.

65 P. G. J. Plaza, B. A. Bhongade and G. Singh, *Synlett*, 2008, **6**, 2973–2976.

66 V. Kumar, C. E. Olsen, S. J. C. Schäffer, V. S. Parmar and S. V. Malhotra, *Org. Lett.*, 2007, **9**, 3905–3908.

67 V. Kumar, C. Pei, C. E. Olsen, S. J. C. Schäffer, V. S. Parmar and S. V. Malhotra, *Tetrahedron Asymmetry*, 2008, **19**, 664–671.

68 M. D. R. Gomes Da Silva and M. M. A. Pereira, *Carbohydr. Res.*, 2011, **346**, 197–202.

69 M. Komabayashi, T. Nokami and S. Jopp, *Asian J. Org. Chem.*, 2020, **9**, 1–4.

70 M. Komabayashi, S. Okushiba, T. Nokami and S. Jopp, *Asian J. Org. Chem.*, 2023, **12**, 6–13.

71 O. N. Van Buu and G. Vo-Thanh, *Lett. Org. Chem.*, 2007, **4**, 158–167.

72 O. N. Van Buu, A. Aupoix, N. D. T. Hong and G. Vo-Thanh, *New J. Chem.*, 2009, **33**, 2060–2072.

73 B. Dmochowska, E. Skorupa, L. Pellowska-Januszek, M. Czarkowska, A. Sikorski and A. Wiśniewski, *Carbohydr. Res.*, 2006, **341**, 1916–1921.

74 C. Chiappe, A. Marra and A. Mele, in *Carbohydrates in Sustainable Development II*, 2010, pp. 177–195.

75 N. Kaur, A. Singh and H. Kumar Chopra, *Mini. Rev. Org. Chem.*, 2018, **15**, 208–219.

76 S. Jopp, *European J. Org. Chem.*, 2020, **2020**, 6418–6428.

77 P. Muthukuru, K. P., J. Rayadurgam and S. Rajasekhara Reddy, *New J. Chem.*, 2021, **45**, 20075–20090.

78 V. Zullo, A. Iuliano and L. Guazzelli, *Molecules*, 2021, 26, 1–80.

79 A. Brzęczek-Szafran, K. Erfurt, A. Blacha-Grzechnik, M. Krzywiecki, S. Boncel and A. Chrobok, *ACS Sustain. Chem. Eng.*, 2019, **7**, 19880–19888.

80 N. Ferlin, M. Courty, S. Gatard, M. Spulak, B. Quilty, I. Beadham, M. Ghavre, A. Haiß, K. Kümmerer, N. Gathergood and S. Bouquillon, *Tetrahedron*, 2013, **69**, 6150–6161.

81 A. Costa, A. Forte, K. Zalewska, G. Tiago, Z. Petrovski and L. C. Branco, *Green Chem. Lett. Rev.*, 2015, **8**, 8–12.

82 Y. Chen, Q. Yang, J. Chen, G. Bai and K. Zhuo, *J. Mol. Liq.*, 2016, **223**, 1013–1020.

83 A. Szelwicka, K. Erfurt, S. Jurczyk, S. Boncel and A. Chrobok, *Materials (Basel).*, , DOI:10.3390/ma14113090.

84 S. Lambrecht, H. Schröter, H. Pohle and S. Jopp, *ACS Omega*, 2024, **9**, 5418–5428.

85 M. Reiß, A. Brietzke, T. Eickner, F. Stein, A. Villinger, C. Vogel, U. Kragl and S. Jopp, *RSC Adv.*, 2020, **10**, 14299–14304.

86 J. Pernak, K. Czerniak, A. Biedziak, K. Marcinkowska, T. Praczyk, K. Erfurt and A. Chrobok, *RSC Adv.*, 2016, **6**, 52781–52789.

87 A. Brzęczek-Szafran, P. Więcek, M. Guzik and A. Chrobok, *RSC Adv.*, 2020, **10**, 18355–18359.

88 K. Erfurt, M. Markiewicz, A. Siewniak, D. Lisicki, M. Zalewski, S. Stolte and A. Chrobok, *ACS Sustain. Chem. Eng.*, 2020, **8**, 10911–10919.

89 N. Barteczko, M. Grymel, K. Erfurt, A. Jakóbik-Kolon, A. Brzęczek-Szafran and A. Chrobok, *J. Mol. Liq.*, 2023, **386**, 122484.

90 N. Ferlin, S. Gatard, A. N. Van Nhien, M. Courty and S. Bouquillon, *Molecules*, 2013, **18**, 11512–11525.

91 A. K. Jha and N. Jain, *Tetrahedron Lett.*, 2013, **54**, 4738–4741.

92 F. Billeci, H. Q. N. Gunaratne, F. D'Anna, G. G. Morgan, K. R. Seddon and N. V. Plechkova, *Green Chem.*, 2019, **21**, 1412–1416.

93 F. Billeci, F. D'Anna, M. Feroci, P. Cancemi, S. Feo, A. Forlino, F. Tonnelli, K. R. Seddon, H. Q. N. Gunaratne and N. V. Plechkova, *ACS Sustain. Chem. Eng.*, 2020, **8**, 926–938.

94 C. R. McElroy, A. Constantinou, L. C. Jones, L. Summerton and J. H. Clark, *Green Chem.*, 2015, **17**, 3111–3121.

95 S. Gatard, R. Plantier-Royon, C. Remond, M. Muzard and C. Kowandy, *Carbohydr. Res.*, 2017, **451**, 72–80.

96 F. Billeci, F. D'Anna, H. Q. N. Gunaratne, N. V. Plechkova and K. R. Seddon, *Green*

Chem., 2018, **20**, 4260–4276.

97 Y. Fukaya, Y. Iizuka, K. Sekikawa and H. Ohno, *Green Chem.*, 2007, **9**, 1155–1157.

98 D. J. Tao, Z. Cheng, F. F. Chen, Z. M. Li, N. Hu and X. S. Chen, *J. Chem. Eng. Data*, 2013, **58**, 1542–1548.

99 K. Marcinkowska, T. Praczyk, M. Gawlak, M. Niemczak and J. Pernak, *Crop Prot.*, 2017, **98**, 85–93.

100 S. Zhang, L. Ma, P. Wen, X. Ye, R. Dong, W. Sun, M. Fan, D. Yang, F. Zhou and W. Liu, *Tribol. Int.*, 2018, **121**, 435–441.

101 T. P. Thuy Pham, C. W. Cho and Y. S. Yun, *Water Res.*, 2010, **44**, 352–372.

102 D. Coleman and N. Gathergood, *Chem. Soc. Rev.*, 2010, **39**, 600–637.

103 M. J. Earle, J. M. S. S. Esperança, M. A. Gilea, J. N. C. Lopes, L. P. N. Rebelo, J. W. Magee, K. R. Seddon and J. A. Widegren, *Nature*, 2006, **439**, 831–834.

104 S. Wu, F. Li, L. Zeng, C. Wang, Y. Yang and Z. Tan, *RSC Adv.*, 2019, **9**, 10100–10108.

105 M. Markiewicz, J. Maszkowska, V. Nardello-Rataj and S. Stolte, *RSC Adv.*, 2016, **6**, 87325–87331.

106 M. K. Ali, R. M. Moshikur, R. Wakabayashi, Y. Tahara, M. Moniruzzaman, N. Kamiya and M. Goto, *J. Colloid Interface Sci.*, 2019, **551**, 72–80.

107 I. F. Mena, E. Diaz, J. Palomar, J. J. Rodriguez and A. F. Mohedano, *Chemosphere*, 2020, **240**, 124947.

108 M. Hong, Z. Miao, X. X. Xu and Q. Zhang, *ACS Appl. Bio Mater.*, 2020, **3**, 3664–3672.

109 J. Ranke, A. Müller, U. Bottin-Weber, F. Stock, S. Stolte, J. Arning, R. Störmann and B. Jastorff, *Ecotoxicol. Environ. Saf.*, 2007, **67**, 430–438.

110 C. Pretti, M. Renzi, S. Ettore Focardi, A. Giovani, G. Monni, B. Melai, S. Rajamani and C. Chiappe, *Ecotoxicol. Environ. Saf.*, 2011, **74**, 748–753.

111 R. F. M. Frade, A. A. Rosatella, C. S. Marques, L. C. Branco, P. S. Kulkarni, N. M. M. Mateus, C. A. M. Afonso and C. M. M. Duarte, *Green Chem.*, 2009, **11**, 1660–1665.

112 R. E. Del Sesto, T. M. McCleskey, C. Macomber, K. C. Ott, A. T. Koppisch, G. A. Baker and A. K. Burrell, *Thermochim. Acta*, 2009, **491**, 118–120.

113 Z. Xue, L. Qin, J. Jiang, T. Mu and G. Gao, *Phys. Chem. Chem. Phys.*, 2018, **20**, 8382–8402.

114 P. Tomasik, M. Pałasiński and S. Wiejak, *Adv. Carbohydr. Chem. Biochem.*, 1989, **47**, 203–278.

115 C. Maton, N. De Vos and C. V. Stevens, *Chem. Soc. Rev.*, 2013, **42**, 5963–5977.

116 R. Jayachandra, R. Lakshmipathy and S. R. Reddy, *J. Mol. Liq.*, 2016, **219**, 1172–1178.

117 I. H. J. Arellano, J. G. Guarino, F. U. Paredes and S. D. Arco, *J. Therm. Anal. Calorim.*, 2011, **103**, 725–730.

118 M. Montanino, M. Carewska, F. Alessandrini, S. Passerini and G. B. Appetecchi, *Electrochim. Acta*, 2011, **57**, 153–159.

119 Y. Cao and T. Mu, *Ind. Eng. Chem. Res.*, 2014, **53**, 8651–8664.

120 Y. Song, Y. Xia and Z. Liu, *Tribol. Trans.*, 2012, **55**, 738–746.

121 M. Petkovic, K. R. Seddon, N. Rebelo and C. Silva, *Chem. Soc. Rev.*, 2011, **40**, 1383–1403.

122 P. Garg and S. R. Reddy, *Asian J. Org. Chem.*, 2022, **11**, 1–6.

123 S. Kang, Y. G. Chung, J. H. Kang and H. Song, *J. Mol. Liq.*, 2020, **297**, 111825.

124 R. Santiago, J. Lemus, C. Moya, D. Moreno, N. Alonso-Morales and J. Palomar, *ACS Sustain. Chem. Eng.*, 2018, **6**, 14178–14187.

125 J. Guzmán, C. Ortega-Guevara, R. G. de León and R. Martínez-Palou, *Chem. Eng. Technol.*, 2017, **40**, 2339–2345.

126 B. Wang, K. Zhang, S. Ren, Y. Hou and W. Wu, *RSC Adv.*, 2016, **6**, 101462–101469.

127 Y. Sun, S. Ren, Y. Hou, K. Zhang, Q. Zhang and W. Wu, *ACS Sustain. Chem. Eng.*, 2020, **8**, 3283–3290.

128 Z. Zhou, J. Li, Y. Wu, Y. Yuan, L. Kong, J. Xue and Z. Huang, *J. Carbohydr. Chem.*, 2020, **0**, 288–299.

129 H. Ziems, M. Komabayashi, P. Lehmann, A. Villinger and S. Jopp, *European J. Org. Chem.*, 2024, **27**, 1–9.

130 P. Lehmann and S. Jopp, *Chem. - An Asian J.*, , DOI:10.1002/asia.202300918.

131 J. Chen, D. Li, C. Bao and Q. Zhang, *Chem. Commun.*, 2020, **56**, 3665–3668.

132 K. Krukiewicz, D. Kobus, R. Turczyn, K. Erfurt, A. Chrobok and M. J. P. Biggs, *Electrochem. commun.*, 2020, **110**, 106616.

133 F. Javed, F. Ullah and H. M. Akil, in *Pure and Applied Chemistry*, 2017, vol. 90, pp. 1019–1034.

134 J. Zhang, J. Wu, J. Yu, X. Zhang, J. He and J. Zhang, *Mater. Chem. Front.*, 2017, **1**, 1273–1290.

135 R. Jayachandra, S. R. Reddy and R. Lakshmipathy, *Environ. Prog. Sustain. Energy*, 2019, **38**, S139–S145.

136 E. M. Ahmed, *J. Adv. Res.*, 2015, **6**, 105–121.

137 M. Watanabe, M. L. Thomas, S. Zhang, K. Ueno, T. Yasuda and K. Dokko, *Chem. Rev.*, 2017, **117**, 7190–7239.

138 S. Zhang, K. Dokko and M. Watanabe, *Mater. Horizons*, 2015, **2**, 168–197.

139 H. Nazir, M. Batool, F. J. Bolivar Osorio, M. Isaza-Ruiz, X. Xu, K. Vignarooban, P. Phelan, Inamuddin and A. M. Kannan, *Int. J. Heat Mass Transf.*, 2019, **129**, 491–523.

140 M. M. Farid, A. M. Khudhair, S. A. K. Razack and S. Al-Hallaj, *Energy Convers. Manag.*, 2004, **45**, 1597–1615.

141 E. M. Shchukina, M. Graham, Z. Zheng and D. G. Shchukin, *Chem. Soc. Rev.*, 2018, **47**, 4156–4175.

142 O. Dumont, G. F. Frate, A. Pillai, S. Lecompte, M. De paepe and V. Lemort, *J. Energy Storage*, 2020, **32**, 101756.

143 S. N. Gunasekara, R. Pan, J. N. Chiu and V. Martin, *Appl. Energy*, 2016, **162**, 1439–1452.

144 M. Kenisarin and K. Mahkamov, *Sol. Energy Mater. Sol. Cells*, 2016, **145**, 255–286.

145 B. K. Purohit and V. S. Sistla, *Energy Storage*, 2021, **3**, 1–26.

146 K. Matuszek, R. Vijayaraghavan, C. M. Forsyth, S. Mahadevan, M. Kar and D. R. MacFarlane, *ChemSusChem*, 2019, **12**, 1–7.

147 K. Matuszek, R. Vijayaraghavan, M. Kar and D. R. Macfarlane, *Cryst. Growth Des.*, 2020, **20**, 1285–1291.

148 K. Matuszek, C. Hatton, M. Kar, J. M. Pringle and D. R. MacFarlane, *J. Non-Crystalline Solids X*, 2022, **15**, 100108.

149 S. L. Piper, C. M. Forsyth, M. Kar, D. R. Macfarlane, K. Matuszek and J. M. Pringle, *Mater. Adv.*, 2021, **2**, 7650–7661.

150 M. C. Floros, K. L. C. Kaller, K. D. Poopalam and S. S. Narine, *Sol. Energy*, 2016, **139**, 23–28.

151 K. D. Poopalam, L. Raghunanan, L. Bouzidi, S. K. Yeong and S. S. Narine, *Sol. Energy Mater. Sol. Cells*, 2019, **201**, 110056.

152 K. Pielichowska and K. Pielichowski, *Prog. Mater. Sci.*, 2014, **65**, 67–123.

153 K. Matuszek, M. Kar, J. M. Pringle and D. R. MacFarlane, *Chem. Rev.*, 2022, **123**, 491–514.

154 X. F. Shao, S. Yang, C. Wang, W. J. Wang, Y. Zeng and L. W. Fan, *Energy*, 2018, **160**, 1078–1090.

155 E. P. del Barrio, A. Godin, M. Duquesne, J. Daranlot, J. Jolly, W. Alshaer, T. Kouadio and A. Sommier, *Sol. Energy Mater. Sol. Cells*, 2017, **159**, 560–569.

156 R. A. Talja and Y. H. Roos, *Thermochim. Acta*, 2001, **380**, 109–121.

157 X. F. Shao, C. L. Chen, Y. J. Yang, X. K. Ku and L. W. Fan, *Sol. Energy Mater. Sol. Cells*, 2019, **195**, 142–154.

158 R. Jia, K. Sun, R. Li, Y. Zhang, W. Wang, H. Yin, D. Fang, Q. Shi and Z. Tan, *J. Chem. Thermodyn.*, 2017, **115**, 233–248.

159 A. Kaizawa, N. Maruoka, A. Kawai, H. Kamano, T. Jozuka, T. Senda and T. Akiyama, *Heat Mass Transf.*, 2008, **44**, 763–769.

160 S. Höhlein, A. König-Haagen and D. Brüggemann, *Materials (Basel).*, 2017, **10**, 444.

161 H. Neumann, D. Burger, Y. Taftanazi, M. P. Alferez Luna, T. Haussmann, G. Hagelstein and S. Gschwander, *Sol. Energy Mater. Sol. Cells*, 2019, **200**, 109913.

162 J. M. Maldonado, Á. G. Fernández and L. F. Cabeza, *Molecules*, 2019, 24.

163 M. Delgado, M. Navarro, A. Lázaro, S. A. E. Boyer and E. Peuvrel-Disdier, *J. Phys. Conf. Ser.*, 2021, **2116**, 012046.

164 L. Piquard, E. Gagnière, G. Largiller, D. Mangin and F. Bentivoglio, *J. Energy Storage*, 2022, **48**, 103922.

165 M. Titirici, S. G. Baird, T. D. Sparks, S. M. Yang, A. Brandt-Talbot, O. Hosseinaei, D. P. Harper, R. M. Parker, S. Vignolini, L. A. Berglund, Y. Li, H. L. Gao, L. B. Mao, S. H. Yu, N. Díez, G. A. Ferrero, M. Sevilla, P. Á. Szilágyi, C. J. Stubbs, J. C. Worch, Y. Huang, C. K. Luscombe, K. Y. Lee, H. Luo, M. J. Platts, D. Tiwari, D. Kovalevskiy, D. J. Fermin, H. Au, H. Alptekin, M. Crespo-Ribadeneyra, V. P. Ting, T. P. Fellinger, J. Barrio, O. Westhead, C. Roy, I. E. L. Stephens, S. A. Nicolae, S. C. Sarma, R. P. Oates, C. G. Wang, Z. Li, X. J. Loh, R. J. Myers, N. Heeren, A. Grégoire, C. Périssé, X. Zhao, Y. Vodovotz, B. Earley, G. Finnveden, A. Björklund, G. D. J. Harper, A. Walton and P. A. Anderson, *J. Phys. Mater.*, 2022, **5**, 032001.

166 S. L. Piper, M. Kar, D. R. MacFarlane, K. Matuszek and J. M. Pringle, *Green Chem.*, 2021, **24**, 102–117.

167 G. Diarce, I. Gandarias, Campos-Celador, A. García-Romero and U. J. Griesser, *Sol. Energy Mater. Sol. Cells*, 2015, 134, 215–226.

168 E. Palomo Del Barrio, R. Cadoret, J. Daranlot and F. Achchaq, *Sol. Energy Mater. Sol. Cells*, 2016, **155**, 454–468.

169 Y. H. Chen, L. M. Jiang, Y. Fang, L. Shu, Y. X. Zhang, T. Xie, K. Y. Li, N. Tan, L. Zhu, Z. Cao and J. L. Zeng, *Sol. Energy Mater. Sol. Cells*, 2019, **200**, 109989.

170 L. M. Jiang, Y. H. Chen, L. Shu, Y. X. Zhang, T. Xie, N. Tan, Y. Fang, S. F. Wang, L. Zhang and J. L. Zeng, *Int. J. Energy Res.*, 2019, **43**, 8385–8397.

171 M. R. Yazdani, J. Etula, J. B. Zimmerman and A. Seppälä, *Green Chem.*, 2020, **22**,

5447–5462.

172 H. Liu, Z. Qian, Q. Wang, D. Wu and X. Wang, *ACS Appl. Energy Mater.*, 2021, **4**, 1714–1730.

173 T. Wang, Y. Liu, R. Meng and M. Zhang, *J. Energy Storage*, 2021, **34**, 101997.

174 C. Dames, J. J. Urban and H. Kang, *J. Phys. Chem. C*, 2021, **125**, 10001–10010.

175 L. Hackl, C. H. Hsu, M. P. Gordon, K. Chou, C. Ma, M. Kolaczkowski, C. L. Anderson, Y. S. Liu, J. Guo, P. Ercius and J. J. Urban, *J. Mater. Chem. A*, 2020, **8**, 23795–23802.

176 T. Nomura, N. Okinaka and T. Akiyama, *Mater. Chem. Phys.*, 2009, **115**, 846–850.

177 T. Oya, T. Nomura, N. Okinaka and T. Akiyama, *Appl. Therm. Eng.*, 2012, **40**, 373–377.

178 L. He, S. Mo, P. Lin, L. Jia, Y. Chen and Z. Cheng, *Sol. Energy Mater. Sol. Cells*, 2020, **209**, 110473.

179 Y. Wang, Z. Qin, T. Zhang, Z. Zhang and Y. Li, *J. Renew. Sustain. Energy*, 2020, **12**, 024103.

180 S. Mo, S. Shan, L. He, L. Jia and Y. Chen, *J. Clust. Sci.*, 2023, **34**, 547–556.

181 M. Pramothraj, R. Santosh, M. R. Swaminathan and G. Kumaresan, *J. Therm. Anal. Calorim.*, 2020, 139, 895–904.

182 A. Sari, A. Biçer, Ö. Lafçi and M. Ceylan, *Sol. Energy*, 2011, **85**, 2061–2071.

183 A. Sari, *Energy Convers. Manag.*, 2012, **64**, 68–78.

184 H. Huang, C. Li, S. Zhu, H. Wang, C. Chen, Z. Wang, T. Bai, Z. Shi and S. Feng, *Langmuir*, 2014, **30**, 13542–13548.

185 M. Biswas, M. Dule, P. N. Samanta, S. Ghosh and T. K. Mandal, *Phys. Chem. Chem. Phys.*, 2014, **16**, 16255–16263.

186 H. Shi, X. Zhang, K. Sundmacher and T. Zhou, *Green Energy Environ.*, 2021, **6**, 392–404.

187 Z. Zhang, A. A. M. Salih, M. Li and B. Yang, *Energy and Fuels*, 2014, **28**, 2802–2810.

188 H. Zhang, W. Xu, J. Liu, M. Li and B. Yang, *J. Mol. Liq.*, 2019, **282**, 474–483.

189 J. Liu, W. Yang, Z. Li, F. Ren and H. Hao, *J. Mol. Liq.*, 2020, **307**, 112994.

190 H. Zhang, J. Liu, M. Li and B. Yang, *J. Mol. Liq.*, 2018, **269**, 738–745.

191 B. D. Rabideau, M. Soltani, R. A. Parker, B. Siu, E. A. Salter, A. Wierzbicki, K. N. West and J. H. Davis, *Phys. Chem. Chem. Phys.*, 2020, **22**, 12301–12311.

192 R. Vijayraghavan, U. A. Rana, G. D. Elliott and D. R. MacFarlane, *Energy Technol.*, 2013, **1**, 609–612.

193 J. J. Parajó, M. Villanueva, J. Troncoso and J. Salgado, *J. Chem. Thermodyn.*, 2020, **141**, 105947.

194 C. Castillo, E. Chenard, M. Zeller, N. Hatab, P. F. Fulvio and P. C. Hillesheim, *J. Mol. Liq.*, 2021, **327**, 114800.

195 C. Alkan, E. Günther, S. Hiebler, Ö. F. Ensari and D. Kahraman, *Polym. Compos.*, 2012, **33**, 1728–1736.

196 G. M. Kumar, M. Mutharayappa, D. H. Rajappa and B. A. Anand, *J. Food Process Eng.*, 2022, **45**, 1–12.

197 F. W. Schenck, in *Ullmann's Encyclopedia of Industrial Chemistry*, Wiley-VCH Verlag GmbH & Co. KGaA, Weinheim, 7th ed., 2012, pp. 45–66.

198 A. E. Koklin, T. A. Klimenko, A. V. Kondratyuk, V. V. Lunin and V. I. Bogdan, *Kinet. Catal.*, 2015, **56**, 84–88.

199 A. Aho, S. Engblom, K. Eränen, V. Russo, P. Mäki-Arvela, N. Kumar, J. Wärnå, T. Salmi and D. Y. Murzin, *Chem. Eng. J.*, 2021, **405**, 126945.

200 H. Xu, Z. Wang, J. Huang and Y. Jiang, *Energy and Fuels*, 2021, **35**, 8602–8616.

201 A. Galadima, A. Masudi and O. Muraza, *Microporous Mesoporous Mater.*, 2022, **336**, 111846.

202 B. Gaida, J. Kondratowicz, S. L. Piper, C. M. Forsyth, A. Chrobok, D. R. Macfarlane, K. Matuszek and A. Brzeczek-Szafran, *ACS Sustain. Chem. Eng.*, 2024, **12**, 623–632.

203 I. Gutzow, D. Kashchiev and I. Avramov, *J. Non. Cryst. Solids*, 1985, **73**, 477–499.

204 E. S. Feldblum and I. T. Arkin, *Proc. Natl. Acad. Sci. U. S. A.*, 2014, **111**, 4085–4090.

205 H. M. Berman and S. H. Kim, *Acta Crystallogr. Sect. B Struct. Crystallogr. Cryst. Chem.*, 1968, **24**, 897–904.

206 T. Steiner, *Angew. Chemie - Int. Ed.*, 2002, **41**, 48–76.

207 J. J. McKinnon, M. A. Spackman and A. S. Mitchell, *Acta Crystallogr. Sect. B Struct. Sci.*, 2004, **60**, 627–668.

208 M. A. Spackman and D. Jayatilaka, *CrystEngComm*, 2009, **11**, 19–32.

209 J. Schröder and K. Gawron, *Int. J. Energy Res.*, 1981, **5**, 103–109.

210 Z. Khan, Z. Khan and A. Ghafoor, *Energy Convers. Manag.*, 2016, **115**, 132–158.

211 Y. M. Choo and W. Wei, *Energy Sci. Eng.*, 2022, **10**, 1630–1642.

212 N. Xie, Z. Huang, Z. Luo, X. Gao, Y. Fang and Z. Zhang, *Appl. Sci.*, 2017, **7**, 1317.

213 W. Zhang, X. Du, K. Guo, R. Chen and J. Chen, *J. Mol. Liq.*, 2022, **368**, 120643.

214 T. Suginaka, H. Sakamoto, K. Iino, S. Takeya, M. Nakajima and R. Ohmura, *Fluid Phase Equilib.*, 2012, **317**, 25–28.

215

216 H. Sakamoto, K. Sato, K. Shiraiwa, S. Takeya, M. Nakajima and R. Ohmura, *RSC Adv.*, 2011, **1**, 315–322.

217 R. Koyama and R. Ohmura, *Int. J. Mater. Sci. Eng.*, 2019, **7**, 102–108.

218 Y. Arai, R. Koyama, F. Endo, A. Hotta and R. Ohmura, *J. Chem. Thermodyn.*, 2019, **131**, 330–335.

219 T. Iwai, T. Miyamoto, N. Kurokawa, A. Hotta and R. Ohmura, *J. Energy Storage*, 2022, **52**, 104801.

220 J. Shimada, M. Shimada, T. Sugahara, K. Tsunashima, A. Tani, Y. Tsuchida and M. Matsumiya, *J. Chem. Eng. Data*, 2018, **63**, 3615–3620.

221 Y. Arai, Y. Yamauchi, H. Tokutomi, F. Endo, A. Hotta, S. Alavi and R. Ohmura, *Int. J. Refrig.*, 2018, **88**, 102–107.

222 J. Shimada, M. Shimada, T. Sugahara and K. Tsunashima, *Fluid Phase Equilib.*, 2019, **485**, 61–66.

223 T. Miyamoto, R. Koyama, N. Kurokawa, A. Hotta, S. Alavi and R. Ohmura, *Front. Chem.*, 2020, **8**, 1–10.

224 A. Erfani, S. Taghizadeh, M. Karamoddin and F. Varaminian, *Int. J. Refrig.*, 2015, **59**, 84–90.

225 Z. Sun, M. Dai, M. Zhu and J. Li, *J. Mol. Liq.*, 2020, **299**, 112188.

226 A. Hassanpouryouzband, E. Joonaki, M. Vasheghani Farahani, S. Takeya, C. Ruppel, J. Yang, N. J. English, J. M. Schicks, K. Edlmann, H. Mehrabian, Z. M. Aman

and B. Tohidi, *Chem. Soc. Rev.*, 2020, **49**, 5225–5309.

227 L. Zhang, X. Xia, Y. Lv, F. Wang, C. Cheng, S. Shen, L. Yang, H. Dong, J. Zhao and Y. Song, *J. Energy Storage*, 2023, **72**, 108279.

228 A. Erfani and F. Varaminian, *J. Mol. Liq.*, 2016, **221**, 963–971.

229 L. Han, S. Xie, S. Liu, J. Sun, Y. Jia and Y. Jing, *Appl. Energy*, 2017, **185**, 762–767.

230 H. Kim, J. Zheng, Z. Yin, S. Kumar, J. Tee, Y. Seo and P. Linga, *Appl. Energy*, 2022, **308**, 118397.

231 G. Lu, M. Li, Y. Liu, Y. Zhang, L. Zhao, G. Li, J. Li, Z. Deng and X. Ma, *Appl. Therm. Eng.*, 2022, **215**, 118974.

232 H. Kim, J. Zheng, Z. Yin, P. Babu, S. Kumar, J. Tee and P. Linga, *Energy*, 2023, **264**, 126226.

233 S. Takeya, S. Muromachi, T. Maekawa, Y. Yamamoto, H. Mimachi, T. Kinoshita, T. Murayama, H. Umeda, D. H. Ahn, Y. Iwasaki, H. Hashimoto, T. Yamaguchi, K. Okaya and S. Matsuo, *Energies*, , DOI:10.3390/en10070927.

234 A. Stoporev, R. Mendgaziev, M. Artemova, A. Semenov, A. Novikov, A. Kiiamov, D. Emelianov, T. Rodionova, R. Fakhrullin and D. Shchukin, *Appl. Clay Sci.*, 2020, **191**, 105618.

235 T. Zou, W. Fu, X. Liang, S. Wang, X. Gao, Z. Zhang and Y. Fang, *Int. J. Refrig.*, 2019, **101**, 117–124.

236 F. Wang, X. Xia, Y. Lv, C. Cheng, L. Yang, L. Zhang, J. Zhao and Y. Song, *J. Energy Storage*, 2022, **48**, 103980.

237 X. J. Shi and P. Zhang, *Energy*, 2016, **99**, 58–68.

238 K. Yamamoto, T. Iwai, K. Hiraga, T. Miyamoto, A. Hotta and R. Ohmura, *J. Energy*

Storage, 2022, **55**, 105812.

239 T. Sugahara, H. Machida, S. Muromachi and N. Tenma, *Int. J. Refrig.*, 2019, **106**, 113–119.

240 A. Mohammadi, A. Kamran-Pirzaman and N. Rahmati, *Pet. Sci. Technol.*, 2021, **39**, 647–665.

241 T. Kobori, S. Muromachi, T. Yamasaki, S. Takeya, Y. Yamamoto, S. Alavi and R. Ohmura, *Cryst. Growth Des.*, 2015, **15**, 3862–3867.

242 R. Koyama, A. Hotta and R. Ohmura, *J. Chem. Thermodyn.*, 2020, **144**, 106088.

243 T. Iwai, I. Ohta, K. Hiraga, K. Kashima, A. Hotta and R. Ohmura, *Fluid Phase Equilib.*, 2022, **562**, 113561.

244 T. Miyamoto, N. Kurokawa, I. Ota, A. Hotta and R. Ohmura, *J. Energy Storage*, 2022, **45**, 103773.

245 H. Kiyokawa, Y. Kondo, R. Koyama, N. Kurokawa, H. Atsushi, S. Alavi, I. Ota and R. Ohmura, *J. Energy Storage*, 2022, **51**, 104404.

246 D. Li, D. Liang, H. Peng and L. Wan, *J. Therm. Anal. Calorim.*, 2016, **123**, 1391–1397.

247 H. Kakiuchi, M. Yabe and M. Yamazaki, *J. Chem. Eng. Japan*, 2003, **36**, 788–793.

248 T. Liao, F. Luo, X. Liang, S. Wang, X. Gao, Z. Zhang and Y. Fang, *J. Energy Storage*, 2023, 59.

249 S. Xie, J. Sun, Z. Wang, S. Liu, L. Han, G. Ma, Y. Jing and Y. Jia, *Sol. Energy Mater. Sol. Cells*, 2017, **168**, 38–44.

250 J. Wang, W. Han, C. Ge, H. Guan, H. Yang and X. Zhang, *Renew. Energy*, 2019, **136**, 657–663.

251 K. Matuszek, R. Vijayaraghavan, M. Kar, S. Mahadevan and D. R. MacFarlane, *ChemSusChem*, 2021, **14**, 2757–2762.

252 H. Schiweck, A. Bär, R. Vogel, E. Schwarz, M. Kunz, C. Dusautois, A. Clement, C. Lefranc, B. Lüssem, M. Moser and S. Peters, in *Ullmann's Encyclopedia of Industrial Chemistry*, Wiley-VCH Verlag GmbH & Co. KGaA, Weinheim, 7th ed., 2012, pp. 1–37.

253 C. Crombez-Robert, M. Benazza, C. Frechou and G. Demailly, *Carbohydr. Res.*, 1997, **303**, 359–365.

254 A. Solé, H. Neumann, S. Niedermaier, L. F. Cabeza and E. Palomo, *Energy Procedia*, 2014, **48**, 436–439.

255 F. R. Fronczek, H. N. Kamel and M. Slattery, *Acta Crystallogr. Sect. C Cryst. Struct. Commun.*, 2003, **59**, 567–570.

256 J. Pernak, K. Czerniak, M. Niemczak, Ł. Ławniczak, D. K. Kaczmarek, A. Borkowski and T. Praczyk, *ACS Sustain. Chem. Eng.*, 2018, **6**, 2741–2750.

257 S. L. Piper, C. M. Forsyth, M. Kar, C. Gassner, R. Vijayaraghavan, S. Mahadevan, K. Matuszek, J. M. Pringle and D. R. MacFarlane, *RSC Sustain.*, 2023, **1**, 470–480.

258 T. Y. Ma, L. Liu and Z. Y. Yuan, *Chem. Soc. Rev.*, 2013, **42**, 3977–4003.

259 D. Jariwala, V. K. Sangwan, L. J. Lauhon, T. J. Marks and M. C. Hersam, *Chem. Soc. Rev.*, 2013, **42**, 2824–2860.

260 M. M. Titirici and M. Antonietti, *Chem. Soc. Rev.*, 2010, **39**, 103–116.

261 J. Deng, M. Li and Y. Wang, *Green Chem.*, 2016, **18**, 4824–4854.

262 Y. Zhai, Y. Wan, Y. Cheng, Y. Shi, F. Zhang, B. Tu and D. Zhao, *J. Porous Mater.*, 2008, **15**, 601–611.

263 D. P. Yang, Z. Li, M. Liu, X. Zhang, Y. Chen, H. Xue, E. Ye and R. Luque, *ACS Sustain. Chem. Eng.*, 2019, **7**, 4564–4585.

264 P. F. Zhang, Y. T. Gong, Z. Z. Wei, J. Wang, Z. Y. Zhang, H. R. Li, S. Dai and Y. Wang, *ACS Appl. Mater. Interfaces*, 2014, **6**, 12515–12522.

265 J. S. Lee, R. T. Mayes, H. Luo and S. Dai, *Carbon N. Y.*, 2010, **48**, 3364–3368.

266 M. Zhao, T. Li, L. Jia, H. Li, W. Yuan and C. M. Li, *ChemSusChem*, 2019, **12**, 5041–5050.

267 H. Zhou, Y. Zhou, L. Li, Y. Li, X. Liu, P. Zhao and B. Gao, *ACS Sustain. Chem. Eng.*, 2019, **7**, 9281–9290.

268 H. Zhou, Y. Zhou, S. Wu, L. Li, Y. Li, M. Guo, Z. Qi and C. Feng, *J. Alloys Compd.*, 2020, **829**, 154549.

269 H. Zhou, S. Wu, H. Wang, Y. Li, X. Liu and Y. Zhou, *J. Hazard. Mater.*, 2021, **402**, 124023.

270 J. Cheng, Q. Xu, J. Lu, J. Du, Q. Chen, Y. Zhang, Z. Li, F. He, F. Wu and H. Xie, *Energy Technol.*, 2019, **7**, 1–14.

271 E. H. Fragal, V. H. Fragal, X. Huang, A. C. Martins, T. S. P. Cellet, G. M. Pereira, E. Mikmeková, A. F. Rubira, R. Silva and T. Asefa, *J. Mater. Chem. A*, 2017, **5**, 1066–1077.

272 Y. Zhang, J. Wang, G. Shen, J. Duan and S. Zhang, *Front. Chem.*, 2020, **8**, 1–12.

273 J. S. Lee, S. M. Mahurin, X. Wang, R. T. Mayes, P. F. Fulvio and S. Dai, *Phys. Chem. Chem. Phys.*, 2011, **13**, 13486.

274 A. Brzęczek-szafran, B. Gaida, A. Blacha-grzechnik, K. Matuszek and A. Chrobok, *Int. J. Mol. Sci.*, 2021, **22**, 10426.

275 J. S. Lee, X. Wang, H. Luo, G. A. Baker and S. Dai, *J. Am. Chem. Soc.*, 2009, **131**, 4596–4597.

276 J. P. Paraknowitsch, J. Zhang, D. Su, A. Thomas and M. Antonietti, *Adv. Mater.*, 2010, **22**, 87–92.

277 J. P. Paraknowitsch, A. Thomas and M. Antonietti, *J. Mater. Chem.*, 2010, **20**, 6746–6758.

278 J. P. Paraknowitsch, B. Wienert, Y. Zhang and A. Thomas, *Chem. - A Eur. J.*, 2012, **18**, 15416–15423.

279 J. S. Lee, H. Luo, G. A. Baker and S. Dai, *Chem. Mater.*, 2009, **21**, 4756–4758.

280 T. P. Fellinger, D. S. Su, M. Engenhorst, D. Gautam, R. Schlögl and M. Antonietti, *J. Mater. Chem.*, 2012, **22**, 23996–24005.

281 N. Fechler, T. P. Fellinger and M. Antonietti, *J. Mater. Chem. A*, 2013, **1**, 14097–14102.

282 P. Navarro, M. Larriba, E. Rojo, J. García and F. Rodríguez, *J. Chem. Eng. Data*, 2013, **58**, 2187–2193.

283 J. Liang, Y. Jiao, M. Jaroniec and S. Z. Qiao, *Angew. Chemie - Int. Ed.*, 2012, **51**, 11496–11500.

284 S. De, S. Malik, A. Ghosh, R. Saha and B. Saha, *RSC Adv.*, 2015, **5**, 65757–65767.

285 N. M. P. Rocha e Silva, H. M. Meira, F. C. G. Almeida, R. de C. F. Soares da Silva, D. G. Almeida, J. M. Luna, R. D. Rufino, V. A. Santos and L. A. Sarubbo, *Sep. Purif. Rev.*, 2019, **48**, 267–281.

286 I. Kralova and J. Sjöblom, *J. Dispers. Sci. Technol.*, 2009, **30**, 1363–1383.

287 M. J. L. Castro, C. Ojeda and A. F. Cirelli, *Environ. Chem. Lett.*, 2014, **12**, 85–95.

288 N. Lourith and M. Kanlayavattanakul, *Int. J. Cosmet. Sci.*, 2009, **31**, 255–261.

289 C. Ceresa, L. Fracchia, E. Fedeli, C. Porta and I. M. Banat, *Pharmaceutics*, , DOI:10.3390/pharmaceutics13040466.

290 N. Esmaeilian, B. Dabir, R. M. A. Malek, M. Arami and F. M. Mazaheri, *J. Mol. Liq.*, 2020, **318**, 114269.

291 K. Holmberg, B. Jönsson, B. Kronberg and B. Lindman, *Surfactants and Polymers in Aqueous Solution*, John Wiley & Sons, Ltd, Chichester, 2 ed., 2003.

292 K. Holmberg, *Curr. Opin. Colloid Interface Sci. 6*, 2001, **6**, 148–159.

293 K. Hill and O. Rhode, *Lipid - Fett*, 1999, **101**, 25–33.

294 T. Gaudin, H. Lu, G. Fayet, A. Berthauld-Drelich, P. Rotureau, G. Pourceau, A. Wadouachi, E. Van Hecke, A. Nesterenko and I. Pezron, *Adv. Colloid Interface Sci.*, 2019, **270**, 87–100.

295 T. H. Zhao, J. Y. Gu, W. F. Pu, Z. M. Dong and R. Liu, *RSC Adv.*, 2016, **6**, 70165–70173.

296 B. Abdellahi, R. Bois, S. Golonu, G. Pourceau, D. Lesur, V. Chagnault, A. Drelich, I. Pezron, A. Nesterenko and A. Wadouachi, *Tetrahedron Lett.*, 2021, **74**, 153113.

297 C. F. Jesus, A. A. S. Alves, S. M. Fiuza, D. Murtinho and F. E. Antunes, *J. Mol. Liq.*, 2021, **342**, 117389.

298 H. Li, C. M. Sims, R. Kang, F. Biedermann, J. A. Fagan and B. S. Flavel, *Carbon N. Y.*, 2023, **204**, 475–483.

299 M. Avramenko, J. Defillet, M. Á. López Carrillo, M. Martinati, W. Wenseleers and S. Cambré, *Nanoscale*, 2022, **14**, 15484–15497.

300 C. M. Sims and J. A. Fagan, *Carbon N. Y.*, 2022, **191**, 215–226.

301 B. Podlesny, B. Gaida, A. Brzeczek-Szafran, A. Chrobok and D. Janas, *Sep. Purif. Technol.*, 2024, **343**, 127120.

302 C. S. Buettner, A. Cognigni, C. Schröder and K. Bica-Schröder, *J. Mol. Liq.*, 2022, **347**, 118160.

303 D. M. Ćirin, M. M. Poša and V. S. Krstonošić, *Ind. Eng. Chem. Res.*, 2012, **51**, 3670–3676.

304 L. Dommett, *Biofuels, Bioprod. Biorefining*, 2009, **3**, 496–499.

305 Deaprtment for Energy Secrurity and Net Zero, *UK Parliment*, 2023, 204.

306 D. Aragão, J. Aishima, H. Cherukuvada, R. Clarken, M. Clift, N. P. Cowieson, D. J. Ericsson, C. L. Gee, S. Macedo, N. Mudie, S. Panjikar, J. R. Price, A. Riboldi-Tunnicliffe, R. Rostan, R. Williamson and T. T. Caradoc-Davies, *J. Synchrotron Radiat.*, 2018, **25**, 885–891.

307 T. M. McPhillips, S. E. McPhillips, H. J. Chiu, A. E. Cohen, A. M. Deacon, P. J. Ellis, E. Garman, A. Gonzalez, N. K. Sauter, R. P. Phizackerley, S. M. Soltis and P. Kuhn, *J. Synchrotron Radiat.*, 2002, **9**, 401–406.

308 W. Kabsch, *J. Appl. Crystallogr.*, 1993, **26**, 795–800.

309 2014.

310 G. M. Sheldrick, *Acta Crystallogr. Sect. C Struct. Chem.*, 2015, **71**, 3–8.

311 G. M. Sheldrick, *Acta Crystallogr. Sect. A Found. Crystallogr.*, 2015, **71**, 3–8.

312 O. V. Dolomanov, L. J. Bourhis, R. J. Gildea, J. A. K. Howard and H. Puschmann, *J. Appl. Crystallogr.*, 2009, **42**, 339–341.

8. List of figures

9. List of tables

10. List of scientific achievements

Publications related to doctoral dissertation:

1. B. Gaida, A. Brzęczek-Szafran, Insights into the properties and potential applications of renewable carbohydrate-based ionic liquids: a review. *Molecules* **2020**, *25*, 3285. (IF = 4.412 / 2021, MNiSW = 100)
2. A. Brzęczek-Szafran, B. Gaida, A. Blacha-Grzechnik, K. Matuszek, A. Chrobok, Bio-derived ionic liquids and salts with various cyano anions as precursors for doped carbon materials. *Int. J. Mol. Sci.* **2021**, *22*, 10426. (IF = 6.208 / 2021, MNiSW = 140)
3. B. Gaida, J. Kondratowicz, S.L. Piper, C.M. Forsyth, A. Chrobok, D.R. MacFarlane, K. Matuszek, A. Brzęczek-Szafran, Transforming sugars into salts–a novel strategy to reduce supercooling in polyol phase-change materials, *ACS Sustain. Chem. Eng.*, **2024**, 12, 623–632. (IF = 7.170 / 2023, MNiSW = 140)
4. B. Podleśny, B. Gaida, A. Brzęczek-Szafran, A. Chrobok, D. Janas, Partitioning of SWCNT mixtures using amphiphilic carbohydrate-based surfactants, *Sep. Purif. Technol.*, **2024**, 343, 127120. (IF = 8.100 / 2023, MNiSW = 140)

Publications not related to doctoral dissertation:

1. A. Brzęczek-Szafran, M. Gwóźdź, B. Gaida, M. Krzywiecki, M. Pawlyta, A. Blacha-Grzechnik, A. Kolanowska, A. Chrobok, D. Janas, Bio-based protic salts as precursors for sustainable free-standing film electrodes, *Sci. Rep.*, **2024**, 14, 1–13. (IF = 3.800 / 2023, MNiSW = 140)

Internships:

1. Monash University, Clayton, Australia. 15.04.-28.06.2022
2. Queen's University Ionic Liquid Laboratories (QUILL) Research Centre, Belfast, Northern Ireland. 18.10.-27.12.2021
3. Institute Charles Gerhardt, Department of Porous and Hybrid Materials, Montpellier, France. 17-28.07.2023

Conferences – oral presentation:

1. B. Gaida, A. Brzęczek-Szafran, K. Matuszek, J. Kondratowicz, D.R. MacFarlane, A. Chrobok, *Carbohydrate-derived ionic compounds as candidates for phase change materials*, **6th International Conference on Ionic Liquid-Based Materials (ILMAT VI)** 22-26.11.2021, Obernai, France
2. B. Gaida, A. Brzęczek-Szafran, K. Matuszek, J. Kondratowicz, D.R. MacFarlane, A. Chrobok, *Transforming sugars into salts – the first step towards ionic carbohydrate-based phase change materials*, **10th Australasian Symposium on Ionic Liquids (ASIL10)**, 23-25.05.2022, Melbourne, Australia
3. B. Gaida, J. Kondratowicz, S.L. Piper, A. Chrobok, D.R. MacFarlane, K. Matuszek, A. Brzęczek-Szafran, *A closer look at hydrogen bonding in ionic bio-derived salts – towards sustainable phase change materials for thermal energy storage*, **9th Congress on Ionic Liquids (COIL9)**, 24-28.04.2023, Lyon, France
4. B. Gaida, A. Brzęczek-Szafran, K. Matuszek, J. Kondratowicz, D.R. MacFarlane, A. Chrobok, *Ionic compounds derived from natural precursors – in pursuit of sustainable phase change materials for solar energy storage*,

3rd Advances in Green Chemistry Conference (3rd AGChem), 26-30.09.2022, Poznań, Poland

5. B. Gaida, A. Brzęczek-Szafran, A. Chrobok, *Synteza oraz badanie właściwości fizycznych materiałów zmiennofazowych opartych na prekursorach pochodzenia naturalnego*, **VIII Interdyscyplinarna Konferencja Doktorantów Uczelni Technicznych (InterTechDoc'23)**, 19-20.04.2023, Ustroń, Poland
6. B. Gaida, A. Brzęczek-Szafran, K. Matuszek, J. Kondratowicz, D.R. MacFarlane, A. Chrobok, *Carbohydrate-derived ionic compounds as candidates for phase change materials*, **VI Międzynarodowa Interdyscyplinarna Konferencja Doktorantów Uczelni Technicznych (InterTechDoc'2021)**, 21-23.07.2021, Ustroń, Poland
7. B. Gaida, *W poszukiwaniu materiałów zmiennofazowych z wykorzystaniem cukrowych cieczy jonowych*, **e-Zjazd Wiosenny SSPTChem 2021**, 27-29.12.2020, online

Conferences – posters:

1. B. Gaida, A. Brzęczek-Szafran, A. Chrobok, *Sól z cukru: postęp w syntezie i zastosowaniu cukrowych cieczy jonowych*, **I Ogólnopolska Konferencja Online SSPTChem**, 10-12.09.2020, online
2. B. Gaida, A. Brzęczek-Szafran, K. Erfurt, A. Chrobok, *Metody wykorzystania biomasy do otrzymania funkcyjnych materiałów węglowych*, **III Konferencja Naukowo-Techniczna „Innowacje w Przemyśle Chemicznym"**, 29-30.10.2019, Gliwice, Poland

Projects:

1. Contractor in OPUS project (UMO-2018/29/B/ST8/01784), *N-doped carbons as catalysts for model electrochemical and chemical processes*, **National Science Centre**, 01.07.2020-01.02.2021
2. Contractor in LIDER project (LIDER/24/0100//L-9/17/NCBR/2018), *IoLacTec: Innovative method for acidic ionic liquids mediated lactams production*, **National Centre for Research and Development**, 07.07.-30.09.2021, 20.01.-30.04.2022
3. Contractor in NAWA project (BPN/BFR/2022/1/00029/U/00001), *Ionic bio-aerogels for carbon dioxide (CO_2) capture and bioconversion*, **National Agency of Academic Exchange**, 02.01.2023-31.12.2024
4. Project manager in New Research Topic project (32/014/SDU/10-22-26), *Uwodnione sole organiczne jako materiały zmiennofazowe do magazynowania energii cieplnej*, **"The Excellence Initiative - Research University" program**, 17.05.2022-16.11.2023
5. Project manager in BKM project (04/050/BKM22/0149), *Synteza cukrowych cieczy jonowych – potencjalnych materiałów zmiennofazowych*, **Silesian University of Technology grant**, 12.05.-31.12.2022

Scientific monographs:

1. B. Gaida, *Właściwości i zastosowania organicznych materiałów zmiennofazowych ciało stałe – ciecz*, InterTechDoc'2021, Gliwice-Ustroń, **2021**, 42-55, ISBN 978-83-65138-29-3 (MNiSW = 20)

2. B. Gaida, *Materiały zmiennofazowe oparte na alkoholach cukrowych*, ARCHEGRAF Wydawnictwo Naukowe, Łódź, **2022**, 77-92, ISBN 978-83-67074-74-2 (MNiSW = 20)

Awards and distinctions:

1. Grant for the best PhD students, founded by "The Excellence Initiative - Research University" program in academic years 2020/2021 and 2021/2022
2. Grant for the publication "*Transforming Sugars into Salts – A Novel Strategy to Reduce Supercooling in Polyol Phase-Change Materials*" (TOP 5), founded by "The Excellence Initiative - Research University" program, 31.01.2024
3. Grant for the publication "*Partitioning of SWCNT mixtures using amphiphilic carbohydrate-based surfactants*" (TOP 10), founded by "The Excellence Initiative - Research University" program, 29.05.2024